FINAL REPORT

ECHO II DATA REDUCTION AND ANALYSIS

VOLUME II

POST LAUNCH EFFORT

Report No. 0038-7-F(2)

Prepared For:

National Aeronautics and Space Administration

Goddard Space Flight Center

Greenbelt, Maryland

Under:

Contract No. NAS 5-3232

Conductron Corporation

343 SOUTH MAIN ST. ANN ARBOR, MICH.

Conductron Corporation

FINAL REPORT

ECHO II DATA REDUCTION AND ANALYSIS

VOLUME II

POST LAUNCH EFFORT

Report No. 0038-7-F(2)

Prepared For:

National Aeronautics and Space Administration

Goddard Space Flight Center

Greenbelt, Maryland

Under:

Contract No. NAS 5-3232

15 October 1964

CONDUCTRON CORPORATION
343 S. Main Street
Ann Arbor, Michigan

TABLE OF CONTENTS

TABLE OF CONTENTS
(Continued)

TABLE OF CONTENTS
(Continued)

1.0 INTRODUCTION

1.1 Report Content

This volume of the Final Report of work performed under contract NAS 5-3232 describes the collection, reduction, and analysis of radar and beacon data on the ECHO II communications satellite. It summarizes the work conducted on the post-launch analysis which started on 17 January 1964. Much of this material has previously been reported to NASA. The reports are listed in Table 1.1.

1.2 Project Tasks

The items of work defined by this contract were:

(a) Providing observers at three radar tracking stations and writing a Quick Look Report on radar data gathered during the first week that ECHO II was in orbit.

(b) Providing assistance to NASA in planning and developing computer programs to process radar cross-section data collected during the ECHO II and later ECHO flights.

(c) Assisting NASA in comparing data collected from the static inflation tests at Lakehurst with data collected from radar measurements while ECHO is in orbit. This study was to attempt to explain any anomalies observed in the orbital data when compared with the static data and also to attempt to determine information on the balloon geometry. Subjects of interest included:

(1) RF scintillation due to balloon structure,
(2) characteristics of balloon surface and geometry,
(3) balloon spin axis orientation and spin rate,
(4) comparison of radar returns obtained from segment and ground measurements on this contract with radar data from the orbiting balloon.

1.3 Summary of Program

The pre-launch effort, discussed in Volume I, had provided a guideline to the values of radar cross section and the nature of their scintillations

(a) Monthly Progress Reports on ECHO II Flight Test Data Reduction and Analysis

No. 1, 20 January 1964 through 21 February 1964, Report 038-1-P.
No. 2, 22 February 1964 through 22 March 1964, Report 038-2-P.
No. 3, 22 March 1964 through 30 April 1964, Report 038-3-P.
No. 4, 1 May 1964 through 31 May 1964, Report 038-4-P.
No. 5, 1 June 1964 through 31 July 1964, Report 038-5-P.
No. 6, 1 August 1964 through 31 August 1964, Report 038-6-P.
No. 7, 1 September 1964 through 30 September 1964, Report 038-7-P.
No. 8, 1 October 1964 through 31 October 1964, Report 038-8-P.

(b) Technical Reports

No. 1, "Quick Look Report on ECHO II Data," Report 038-1-T, 13 Februrary 1964.
No. 2, "Supplement to Quick Look Report on ECHO II Data (Report 0038-1-T)," Report 0038-2-T, 24 February 1964.
No. 3, "Quick Look Report on ECHO II Data," Report 0038-3-T, 4 March 1964, SECRET.
No. 4, "Data Processing and Analysis for ECHO II Data," Report 0038-4-T, 18 March 1964.
No. 5, "Digest of Quick Look Report on ECHO II Data," Report 0038-5-T, 11 May 1964.
No. 6, "Six Months Summary Report on ECHO II Data Reduction and Analysis," Report 0038-6-T, 10 August 1964.
No. 8, ECHO II Data Reduction and Analysis Computer Write-up, Report 0038-8-T, 19 October 1964

TABLE 1.1

REPORTS ISSUED ON NAS 5-3232

to be expected from the flight test balloon. It was felt in particular that if the flight test balloon inflated in a fashion similar to the test balloons, the mean value of the average cross section would be approximately 30 db > m^2 and that the peak-peak scintillations would be somewhere between 4 and 8 db, with the larger scintillations being observed at the higher frequencies. It was not expected that there would be any significant dependence of the cross section upon polarization.

Any departure from these characteristics in the radar cross section return, if observed consistently and by more than one radar site, would be taken as evidence that the shape of the flight balloon was different from the shape of the test balloons; by "anomalies" in the radar data it was meant departures in the radar data from what had been expected; by explanation of the "anomalies" was meant an explanation consistent with what was already known about the balloon and consistent with the laws of nature, which would account for the observed effect.

To this end, data was examined by visually studying analog recordings and by digitally processing taped data as it became available in suitable format. The purpose of the digital analysis was to give numerical values to the mean cross section and levels of scintillation based on agreed upon criteria and to provide statistical answers to questions about the polarization and frequency dependence of the radar cross section and about periodicities in the data.

After launch, using both the analog and digital data, it was observed and eventually concluded that with one notable exception the radar cross section, and inferentially the shape, of the flight balloon was similar to that of a test balloon which had been inflated to a pressure less than that required to achieve rigidization. The exception was a systematic drop in the radar cross section of about 10 db for an interval which varied from 6 to 13 seconds and which was repeated approximately every 100 seconds. A less noticeable but definite "drop out" also took place approximately half way in time between the major ones. A large part of the work performed and reported here was devoted to examining various hypotheses that others

had proposed to explain this effect and to provide an explanation which met the criteria that are stated above. These analyses are reported in the pages that follow.

1.4 Data Sources

The satellite was launched 25 January 1964. Various radars were assigned by the DOD and other organizations to furnish NASA/GSFC with data for analysis and interpretation. The radar data was taken at frequencies from UHF through X-band and telemetry data was collected from beacons operating at frequencies of 136.170 MC and 136.020 MC.

Observers were stationed at the following sites:

(a) The L-band radar at Millstone Hill, Massachusetts,

(b) Wallops Island, Virginia, where UHF, S, and X-band radars were used, and

(c) The S-band RAMPART radar at White Sands Missile Range.

Preliminary data from the sites listed were furnished in the form of analog pen records; additional pen recordings were received for satellite passes during the first and succeeding weeks from the C-band radars at Kwajalein and Ascension Island. Pulse-by-pulse radar data on magnetic tapes were obtained from the C-band radars at White Sands Missile Range, Kwajalein, and Ascension Island, the UHF radar at Trinidad and the Millstone and Wallops Island sites. Beacon analog records and radar cross section pen recordings taken at the Royal Radar Establishment (RRE) at Malvern, England, were made available. The several analog records formed the basis for the technical reports listed in Table 1.1. In addition, a series of data processing and statistical programs have been prepared for the computers at GSFC. These programs have been used for an analysis of the radar data stored on magnetic tape.

The data collection effort was very intensive during initial pressurization, the first continuous sunlit period of eleven days, and the initial eclipse period. Thus the balloon's behavior during the first critical two weeks could be examined carefully. Thereafter, most radar establishments

collected ECHO II data on a non-interference basis until observations were again increased during the onset of the second sunlit period. The recordings on magnetic tape were the primary data source for balloon analysis. Nevertheless, it proved possible to determine a good deal of information from the analog recordings with considerable confidence in the results.

2.0 DATA ANALYSIS AND INTERPRETATION

2.1 Objectives of the Computer Data Analysis Effort

The Quick Look Report (Technical Report No. 3) was based on analog records. Two unexpected effects were observed:

(a) A pronounced drop in average return of approximately 10 db was noted on some of the analog pen records. This effect, called a "drop out", appears intermittently with the drops in return enduring for as much as several seconds. When this effect is present it appears with a period which is a multiple of approximately 50 seconds.

(b) The return in general has a spikey appearance dipping about 20 db for very brief periods.

In connection with the "drop out", it was observed that for some of the data the 50-second intervals preceding and following each drop appeared to have significantly different fine structure.

The conclusions of the Quick Look Report were tentative. Further investigation was required to put them on a firm basis and to analyze phenomena which might be present in the data whose significance could only be discovered through formal statistical analysis. Some of the subjects which warranted digital exploration were:

(a) Whether the amplitude and frequency of the radar cross section scintillations are dependent on the radar frequency.

(b) Whether the radar cross section is dependent on the radar polarization.

(c) Whether the mean radar cross section is radar frequency dependent.

(d) Whether any of the radar cross section signatures vary with the length of time since launch.

(e) Whether regular periodic phenomena exist in the data; if so, whether these phenomena are frequency dependent.

(f) Whether the radar cross section has, for a given pass, a log-normal probability distribution.

A series of computer programs, which will be described in the next section, was designed to permit examination of items (a) through (f). Item (f) was undertaken when preliminary digital data processing suggested the hypothesis that the radar cross section data might well be log-normally distributed. If this hypothesis were correct, it could be accounted for by assuming that the radii of curvature of the balloon are normally distributed, which in turn would indicate a random, rather than a systematic perturbation of the balloon from sphericity. These programs are now at GSFC, and we are available for any future analysis by NASA.

2.2 Computer Programs

In order to investigate the questions outlined in Section 2.1, a series of computer programs for the NASA/GSFC 7094 computer was written. These programs were designed to have a maximum of generality and were carefully documented. They provide a tool which can be employed for similar future investigations. Complete program listings are available to possible interested users through the NASA/GSFC Computation Center. The programs are summarized below:

(a) A program to convert all tapes received from the various installations into radar cross section versus time. This program extracts from the data tapes the received power calibration and the range, and converts this information to radar cross section information by using the radar range equation and the parameters of the specific radar involved. It then puts the output into a uniform format suitable for further processing. To provide for automatic operation, tests for missing data, criteria for rejection of spurious values and the capability of accepting a large number of different input formats are all taken into account. Figure 2-1 illustrates a radar cross section vs. time printout for the Millstone Hill tape of 28 January.

(b) A computer program called STAT 1 which computes a mean and a standard deviation for the radar cross sections; a histogram of the radar cross sections; auto-correlations of the radar cross sections; and a frequency

```
58719.00    C.15848931E C3  XXXXXXXXXXXX
58720.00    0.44668357E C3  XXXXXXXXXXXXXXXXXXXXXXXXXXXXXXXXXXXXX
58721.00    C.56234130E 03  XXXXXXXXXXXXXXXXXXXXXXXXXXXXXXXXXXXXXXXXXXXXXX
58722.00    C.31622775E C3  XXXXXXXXXXXXXXXXXXXXXXXXX
58723.00    C.39810716E C3  XXXXXXXXXXXXXXXXXXXXXXXXXXXXXXXXX
58724.00    C.09999999E 03  XXXXXXX
58725.00    C.15848931E C3  XXXXXXXXXXXX
58726.00    C.5C118722E C3  XXXXXXXXXXXXXXXXXXXXXXXXXXXXXXXXXXXXXXXXX
58727.00    0.35481338E C3  XXXXXXXXXXXXXXXXXXXXXXXXXXXXX
58728.00    0.12589253E C3  XXXXXXXXX
58729.00    C.28183828E C3  XXXXXXXXXXXXXXXXXXXXXX
58730.00    C.63095732E C2  XXXX
58731.00    C.63C95732E C2  XXXX
58732.00    0.28183828E C3  XXXXXXXXXXXXXXXXXXXXXX
58733.00    0.17782793E C3  XXXXXXXXXXXXXX
58734.00    C.09999999E C3  XXXXXXX
58735.00    C.17782793E C3  XXXXXXXXXXXXXX
58736.00    C.79432822E C2  XXXXXX
58737.00    C.19952623E C3  XXXXXXXXXXXXXXX
58738.00    C.31622775E C3  XXXXXXXXXXXXXXXXXXXXXXXXX
58739.00    C.14125375E C3  XXXXXXXXXXX
58740.00    C.22387210E C3  XXXXXXXXXXXXXXXXX
58741.00    C.35481338E 03  XXXXXXXXXXXXXXXXXXXXXXXXXXXXX
58742.00    C.44668358E C2  XXX
58743.00    C.35481338E C3  XXXXXXXXXXXXXXXXXXXXXXXXXXXXX
58744.00    C.7C794574E C2  XXXXX
58745.00    C.70794574E C2  XXXXX
58746.00    C.11220184E C3  XXXXXXXX
58747.00    0.19952623E 03  XXXXXXXXXXXXXXX
58748.00    C.14125375E C3  XXXXXXXXXXX
58749.00    C.35481338E C3  XXXXXXXXXXXXXXXXXXXXXXXXXXXXX
58750.00    C.22387210E C3  XXXXXXXXXXXXXXXXX
58751.00    0.15848931E C3  XXXXXXXXXXXX
58752.00    C.22387210E C3  XXXXXXXXXXXXXXXXX
58753.00    C.70794574E C2  XXXXX
58754.00    C.19952623E C3  XXXXXXXXXXXXXXX
58755.00    0.89125C90E 02  XXXXXX
58756.00    C.28183828E C3  XXXXXXXXXXXXXXXXXXXXXX
58757.00    C.17782793E 03  XXXXXXXXXXXXXX
58758.00    C.99999997E C3  XXXXXXXXXXXXXXXXXXXXXXXXXXXXXXXXXXXXXXXXXXXXXXXXXXXXXXXXXXXXXXXXXXXXXXXXXXXXXXXXXX
58759.00    0.99999997E 03  XXXXXXXXXXXXXXXXXXXXXXXXXXXXXXXXXXXXXXXXXXXXXXXXXXXXXXXXXXXXXXXXXXXXXXXXXXXXXXXXXX
58760.00    C.79432820E C3  XXXXXXXXXXXXXXXXXXXXXXXXXXXXXXXXXXXXXXXXXXXXXXXXXXXXXXXXXXXXXXXXX
58761.00    C.17782793E 03  XXXXXXXXXXXXXX
58762.00    C.11220184E C3  XXXXXXXX
58763.00    0.56234132E 02  XXXX
58764.00    C.28183828E C2  XX
58765.00    C.28183828E C3  XXXXXXXXXXXXXXXXXXXXXX
58766.00    C.44668357E C3  XXXXXXXXXXXXXXXXXXXXXXXXXXXXXXXXXXXXX
58767.00    0.12589253E C3  XXXXXXXXX
58768.00    C.15848931E C3  XXXXXXXXXXXX
58769.00    C.17782793E C3  XXXXXXXXXXXXXX
58770.00    0.79432820E 03  XXXXXXXXXXXXXXXXXXXXXXXXXXXXXXXXXXXXXXXXXXXXXXXXXXXXXXXXXXXXXXXXX
58771.00    0.39810716E 03  XXXXXXXXXXXXXXXXXXXXXXXXXXXXXXXXX
58772.00    C.22387210E C3  XXXXXXXXXXXXXXXXX
58773.00    C.17782793E C3  XXXXXXXXXXXXXX
58774.00    C.35481338E C3  XXXXXXXXXXXXXXXXXXXXXXXXXXXXX
58775.00    0.39810716E C3  XXXXXXXXXXXXXXXXXXXXXXXXXXXXXXXXX
58776.00    C.31622775E 03  XXXXXXXXXXXXXXXXXXXXXXXXX
58777.00    C.31622775E 03  XXXXXXXXXXXXXXXXXXXXXXXXX
58778.00    0.09999999E 03  XXXXXXX
58779.00    0.50118722E 02  XXX
58780.00    C.39810717E 02  XX
58781.00    C.15848932E 02  X
58782.00    0.25118864E 02  X
58783.00    0.15848932E 02  X
```

58783.00	0.15848932E 02	X
58784.00	0.79432822E 02	XXXXXX
58785.00	0.15848931E 03	XXXXXXXXXXXX
58786.00	0.22387210E 03	XXXXXXXXXXXXXXXXX
58787.00	0.15848931E 03	XXXXXXXXXXXX
58788.00	0.15848931E 03	XXXXXXXXXXXX
58789.00	0.12589253E 03	XXXXXXXXX
58790.00	0.28183828E 03	XXXXXXXXXXXXXXXXXXXXXX
58791.00	0.09999999E 03	XXXXXXX
58792.00	0.17782793E 03	XXXXXXXXXXXXXX
58793.00	0.63095734E 03	XXXXXXXXXXXXXXXXXXXXXXXXXXXXXXXXXXXXXXXXXXXXXXXXXXX
58794.00	0.17782793E 03	XXXXXXXXXXXXXX
58795.00	0.28183828E 03	XXXXXXXXXXXXXXXXXXXXXX
58796.00	0.31622775E 03	XXXXXXXXXXXXXXXXXXXXXXXXX
58797.00	0.22387210E 03	XXXXXXXXXXXXXXXXX
58798.00	0.28183828E 03	XXXXXXXXXXXXXXXXXXXXXX
58799.00	0.15848931E 03	XXXXXXXXXXXX
58800.00	0.17782793E 03	XXXXXXXXXXXXXX
58801.00	0.15848931E 03	XXXXXXXXXXXX
58802.00	0.35481338E 03	XXXXXXXXXXXXXXXXXXXXXXXXXXXX
58803.00	0.89125093E 03	XXXXXXXXXXXXXXXXXXXXXXXXXXXXXXXXXXXXXXXXXXXXXXXXXXXXXXXXXXXXXXXXXXXXXXXXX
58804.00	0.39810716E 03	XXXXXXXXXXXXXXXXXXXXXXXXXXXXXXXX
58805.00	0.22387210E 03	XXXXXXXXXXXXXXXXX
58806.00	0.15848931E 03	XXXXXXXXXXXX
58807.00	0.15848931E 03	XXXXXXXXXXXX
58808.00	0.35481338E 03	XXXXXXXXXXXXXXXXXXXXXXXXXXXX
58809.00	0.28183828E 03	XXXXXXXXXXXXXXXXXXXXXX
58810.00	0.19952623E 03	XXXXXXXXXXXXXXX
58811.00	0.19952623E 03	XXXXXXXXXXXXXXX
58812.00	0.17782793E 03	XXXXXXXXXXXXXX
58813.00	0.17782793E 03	XXXXXXXXXXXXXX
58814.00	0.25118864E 03	XXXXXXXXXXXXXXXXXXXX
58815.00	0.35481338E 03	XXXXXXXXXXXXXXXXXXXXXXXXXXXX
58816.00	0.28183828E 03	XXXXXXXXXXXXXXXXXXXXXX
58817.00	0.22387210E 03	XXXXXXXXXXXXXXXXX
58818.00	0.14125375E 03	XXXXXXXXXXX
58819.00	0.25118864E 03	XXXXXXXXXXXXXXXXXXXX
58820.00	0.70794577E 03	XXXXXXXXXXXXXXXXXXXXXXXXXXXXXXXXXXXXXXXXXXXXXXXXXXXXXXXXXX
58821.00	0.25118864E 03	XXXXXXXXXXXXXXXXXXXX
58822.00	0.19952623E 03	XXXXXXXXXXXXXXX
58823.00	0.14125375E 03	XXXXXXXXXXX
58824.00	0.09999999E 03	XXXXXXX
58825.00	0.44668357E 03	XXXXXXXXXXXXXXXXXXXXXXXXXXXXXXXXXXXX
58826.00	0.14125375E 03	XXXXXXXXXXX
58827.00	0.14125375E 03	XXXXXXXXXXX
58828.00	0.39810716E 03	XXXXXXXXXXXXXXXXXXXXXXXXXXXXXXXX
58829.00	0.12589253E 03	XXXXXXXXX
58830.00	0.63095732E 02	XXXX
58831.00	0.50118722E 02	XXX
58832.00	0.12589253E 03	XXXXXXXXX
58833.00	0.79432822E 02	XXXXXX
58834.00	0.31622776E 02	XX
58835.00	0.17782793E 03	XXXXXXXXXXXXXX
58836.00	0.19952623E 03	XXXXXXXXXXXXXXX
58837.00	0.19952623E 03	XXXXXXXXXXXXXXX
58838.00	0.19952623E 03	XXXXXXXXXXXXXXX
58839.00	0.15848931E 03	XXXXXXXXXXXX
58840.00	0.12589253E 04	XXXXXXXXXXXXXXXXXXXXXXXXXXXXXXXXXXXXXXXXXXXXXXXXXXXXXXXXXXXXXXXXXXXXXXXXXXXXXXXXXXXXXXXXXXXXXXXXXXXXXXXX
58841.00	0.99999997E 03	XXXXXXXXXXXXXXXXXXXXXXXXXXXXXXXXXXXXXXXXXXXXXXXXXXXXXXXXXXXXXXXXXXXXXXXXXXXXXXXXX
58842.00	0.39810716E 03	XXXXXXXXXXXXXXXXXXXXXXXXXXXXXXXX
58843.00	0.50118722E 02	XXX
58844.00	0.09999999E 03	XXXXXXX
58845.00	0.12589253E 03	XXXXXXXXX

FIGURE 2-1

PLOT OF MEDIAN CROSS SECTION (m^2) OF ECHO II VS. TIME MILLSTONE HILL - 28 JAN. 1964

The first column indicates the starting time (secs relative to GMT) of the 1-second interval over which the median cross section indicated in column 2 is plotted.

analysis of the auto-correlations. The input to STAT 1 is the output of the program described above. Definitions of each of these terms will be found in the Glossary. The standard deviation of the observations provides a measure of the magnitude of the amplitude scintillations. The mean is a measure of the size of the balloon; its usefulness is limited by errors in the radar's absolute calibration. The histogram printout shows how symmetric the data is and, to a lesser extent, whether it is log-normally distributed. The auto-correlations and their frequency or power spectrum analysis detect periods in the data. This program operates on the data expressed in square meters or in db > m^2. Figures 2-2 and 2-3 illustrate the auto-correlation and power spectrum analysis for the Millstone Hill tape of 28 January. Figure 2-4 illustrates a histogram for the C-band data from Ascension/Kwajelein on 26 February 1964.

(c) A program called STAT 2 to perform a chi-squared Goodness-of-Fit Test on the pulse-by-pulse radar cross section data. This provides a good test of the hypothesis that the data is normally distributed. The chi-squared test is a standard statistical tool for testing one distribution against another. In this case the mean and standard deviation of the data to be tested are determined; then the data are subdivided into one hundred intervals each of which has equal probability, i.e., each of which would contain the same number of points in a Gaussian distribution having the calculated mean and standard deviation. The number of data points falling in each such interval is then compared with the number which would occur in the Gaussian distribution. The output of the program consists of a printout of the above information and a graph showing the percentage departure from the Gaussian distribution interval by interval. A printout for the 28 January Millstone Hill tape is illustrated in Figure 2-5 and the graph in Figure 2-6.

(d) A program to fit an expression of the form,

$$\sigma = A\lambda^{-1} + B + C\lambda,$$

AUTO-CORRELATIONS...

X = N * DELTA-T

X	R(X)	MIN = -0.24200596E-00 / MAX = 0.38724188E-00
1.00	0.38724188E-00	
2.00	0.60958467E-01	
3.00	-0.12025627E-00	
4.00	-0.13048353E-00	
5.00	-0.26590964E-01	
6.00	0.73751815E-02	
7.00	-0.46055702E-01	
8.00	-0.27146998E-01	
9.00	-0.11233266E-00	
10.00	-0.90156880E-01	
11.00	-0.21602876E-01	
12.00	-0.17686868E-01	
13.00	-0.44007674E-01	
14.00	-0.63817524E-01	
15.00	0.90308451E-01	
16.00	0.13151569E-00	
17.00	0.68171327E-01	
18.00	-0.34759086E-01	
19.00	-0.11750037E-00	
20.00	-0.45751262E-01	
21.00	-0.59111095E-01	
22.00	-0.86827469E-01	
23.00	-0.12693916E-00	
24.00	-0.85992930E-01	
25.00	-0.10368107E-00	
26.00	-0.67639070E-01	
27.00	-0.73870002E-01	
28.00	-0.97589228E-01	
29.00	-0.86054660E-01	
30.00	-0.61394114E-01	
31.00	-0.47472893E-01	
32.00	0.10664346E-00	
33.00	0.11218552E-00	
34.00	-0.10009551E-01	
35.00	0.13356771E-02	
36.00	-0.94431875E-02	
37.00	0.13112300E-00	
38.00	0.88789089E-01	
39.00	-0.70224287E-02	
40.00	-0.10031056E-00	
41.00	-0.82380924E-01	
42.00	-0.60190531E-01	
43.00	0.31683464E-01	
44.00	0.10525321E-00	
45.00	0.12886276E-00	
46.00	0.51064295E-01	
47.00	0.10858466E-00	
48.00	0.91749557E-01	
49.00	0.54232859E-01	
50.00	0.82304694E-01	
51.00	0.66961394E-02	
52.00	-0.12296592E-01	

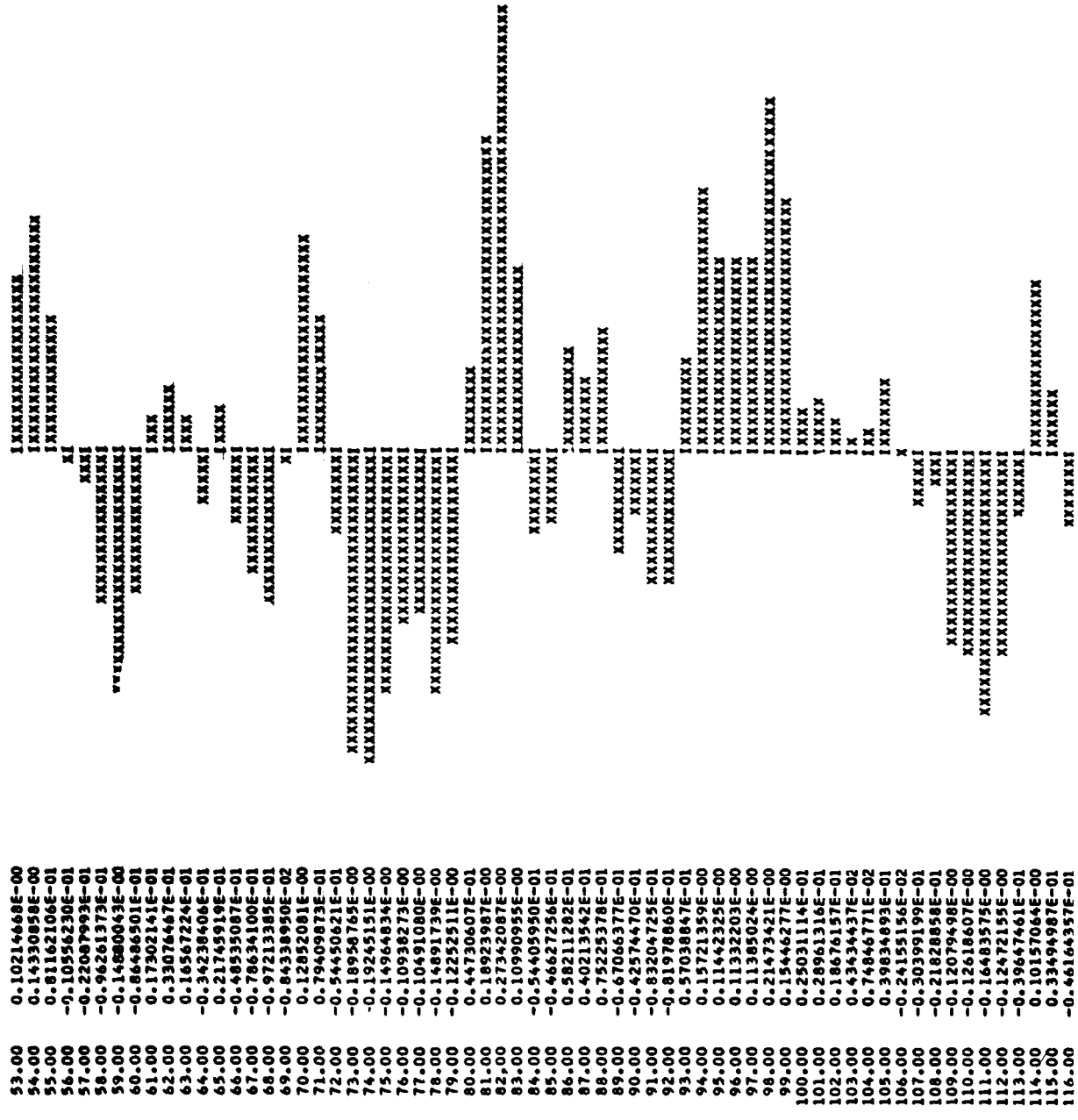

53.00	0.10214668E-00
54.00	0.14330858E-00
55.00	0.81162106E-01
56.00	-0.10556230E-01
57.00	-0.22007993E-01
58.00	-0.96261373E-01
59.00	-0.14880043E-00
60.00	-0.86486501E-01
61.00	0.17302141E-01
62.00	0.33076447E-01
63.00	0.16567224E-01
64.00	-0.34238606E-01
65.00	0.21745919E-01
66.00	-0.48535087E-01
67.00	-0.78634100E-01
68.00	-0.97213385E-01
69.00	-0.84338950E-02
70.00	0.12852081E-00
71.00	0.79409873E-01
72.00	-0.54450621E-01
73.00	-0.18958765E-00
74.00	-0.19245151E-00
75.00	-0.14964834E-00
76.00	-0.10938273E-00
77.00	-0.10491080E-00
78.00	-0.14891739E-00
79.00	-0.12252511E-00
80.00	0.44730607E-01
81.00	0.18923987E-00
82.00	0.27342087E-00
83.00	0.10990955E-00
84.00	-0.54405950E-01
85.00	-0.46627256E-01
86.00	0.58211282E-01
87.00	0.40213542E-01
88.00	0.75225378E-01
89.00	-0.67066377E-01
90.00	-0.42574470E-01
91.00	-0.83204725E-01
92.00	-0.81978860E-01
93.00	0.57038847E-01
94.00	0.15721359E-00
95.00	0.11442325E-00
96.00	0.11332203E-00
97.00	0.11385024E-00
98.00	0.21473421E-00
99.00	0.15446277E-00
100.00	0.25031114E-01
101.00	0.28961316E-01
102.00	0.18676157E-01
103.00	0.43434437E-02
104.00	0.74846771E-02
105.00	0.39834893E-01
106.00	-0.24155156E-02
107.00	-0.30399199E-01
108.00	-0.21828858E-01
109.00	-0.12079498E-00
110.00	-0.12618607E-00
111.00	-0.16483575E-00
112.00	-0.12472155E-00
113.00	-0.39647461E-01
114.00	0.10157064E-00
115.00	0.33496987E-01
116.00	-0.46164357E-01

FIGURE 2-2

POWER SPECTRUM...

X = 2 * M * DELTA-T / N

X	Y(X)	MIN = -0.67135388E 00	MAX = 0.40269174E 01
350.00	0.35001475E-00		
175.00	-0.31358151E-00		
116.67	0.41080471E-00		
87.50	-0.23393833E-00		
70.00	0.51348962E 00		
58.33	-0.67135388E 00		
50.00	0.25155935E 01		
43.75	0.21454176E 01		
38.89	-0.60524536E 00		
35.00	0.61804426E 00		
31.82	0.27505198E-00		
29.17	0.30866222E-00		
26.92	-0.46039190E-01		
25.00	0.67149934E 00		
23.33	0.29872625E-01		
21.88	0.52738648E 00		
20.59	0.24047512E-00		
19.44	0.89023898E 00		
18.42	0.24962074E-00		
17.50	0.59108878E-01		
16.67	0.40269174E 01		
15.91	0.48268559E-00		
15.22	0.57382985E 00		
14.58	-0.19860154E-01		
14.00	0.12120768E 01		
13.46	0.96137846E 00		
12.96	-0.17706039E-01		
12.50	-0.18567117E-00		
12.07	0.77984161E 00		
11.67	0.15328810E 01		
11.29	0.96636623E-01		
10.94	0.24356668E-00		
10.61	0.45939157E-00		
10.29	0.59634496E 00		
10.00	-0.16494275E-00		
9.72	0.18681158E-01		
9.46	0.35668001E-00		
9.21	0.82339477E-01		
8.97	0.21111161E 01		
9.75	0.10222128E 01		
8.54	0.10138054E-00		
8.33	-0.17027318E-00		
8.14	0.44183580E-00		
7.95	0.20509142E 01		
7.78	0.19010417E-00		
7.61	0.16783458E 01		
7.45	0.48415037E-00		
7.29	0.21744515E-00		
7.14	0.63224234E 00		
7.00	0.31917264E-00		
6.86	0.52492276E 00		
6.73	0.92608665E 00		
6.60	-0.10356533E-00		
6.48	0.30913656E-00		
6.36	0.69980527E 00		
6.25	0.21542356E 01		
6.14	-0.62258864E 00		
6.03	0.70746305E 00		
5.93	-0.30031883E-00		
5.83	0.13781083E 01		

6.25 0.21542356E 01
6.14 -0.62258864E 00
6.03 0.70746305E 00
5.93 -0.30031883E-00
5.83 0.13781083E 01
5.74 -0.44565122E-00
5.65 0.51666078E 00
5.56 -0.11869145E-00
5.47 0.24332610E 01
5.38 0.14852954E 01
5.30 -0.39996085E-01
5.22 0.44680980E-00
5.15 0.81477822E 00
5.07 0.93898956E-01
5.00 0.62620231E 00
4.93 -0.23003669E-00
4.86 0.14569063E-00
4.79 0.23351953E-00
4.73 0.85118874E 00
4.67 -0.25805835E-00
4.61 0.18608236E-00
4.55 -0.16060323E-00
4.49 0.22786515E-00
4.43 0.13864967E-00
4.38 0.31438569E-01
4.32 0.15521422E-01
4.27 0.20184289E-00
4.22 0.15562011E-00
4.17 0.26803642E-00
4.12 0.75495271E 00
4.07 0.12941054E 01
4.02 -0.63430230E 00
3.98 0.69325912E 00
3.93 -0.23166580E-00
3.89 0.84588613E 00
3.85 -0.17728373E-00
3.80 0.29371678E-00
3.76 0.20147121E-00
3.72 0.12491536E-00
3.68 0.10499186E-00
3.65 0.13781008E-00
3.61 0.47063079E-00
3.57 0.25891401E-01
3.54 0.61370537E-01
3.50 -0.45142142E-01
3.47 0.35649072E-01
3.43 -0.89344113E-01
3.40 0.29755605E-00
3.37 0.36227608E-00
3.33 0.13640962E-01
3.30 0.14611341E-00
3.27 -0.14669231E-00
3.24 0.21654799E-00
3.21 -0.96091510E-01
3.18 0.36857714E-00
3.15 0.26204576E-00
3.13 -0.93305689E-03
3.10 0.29550634E-01
3.07 0.47765634E-01
3.04 0.36332023E-01
3.02 0.11544206E-01
2.99 0.44016235E-00
2.97 0.19177673E-00

FIGURE 2-3

RADAR CROSS SECTIONS DISTRIBUTION (DBM)...

X = DBM, Y(X) = COUNT

X	Y(X)	MIN = 0.	MAX = 0.59999999E 01
		I	I
-10.00	0.	X	
-9.50	0.	X	
-9.00	0.	X	
-8.50	0.	X	
-8.00	0.	X	
-7.50	0.	X	
-7.00	0.	X	
-6.50	0.	X	
-6.00	0.	X	
-5.50	0.	X	
-5.00	0.	X	
-4.50	0.	X	
-4.00	0.	X	
-3.50	0.	X	
-3.00	0.	X	
-2.50	0.	X	
-2.00	0.	X	
-1.50	0.	X	
-1.00	0.	X	
-0.50	0.	X	
0.	0.	X	
0.50	0.	X	
1.00	0.	X	
1.50	0.	X	
2.00	0.	X	
2.50	0.	X	
3.00	0.	X	
3.50	0.	X	
4.00	0.	X	
4.50	0.	X	
5.00	0.	X	
5.50	0.	X	
6.00	0.	X	
6.50	0.	X	
7.00	0.	X	
7.50	0.	X	
8.00	0.	X	
8.50	0.	X	
9.00	0.	X	
9.50	0.	X	
10.00	0.	X	
10.50	0.	X	
11.00	0.	X	
11.50	0.	X	
12.00	0.	X	
12.50	0.	X	
13.00	0.	X	
13.50	0.	X	
14.00	0.	X	
14.50	0.	X	
15.00	0.	X	
15.50	0.	X	

HISTOGRAM OF RADAR CROSS SECTIONS (db/m²).
ASCENSION/KWAJELEIN - 26 FEB. 1964

FIGURE 2-4

CONDUCTRON CORPORATION
SECOND STATISTICAL PROGRAM

TAPE ID WORDS...

CONDUCTRON CORPORATION TAPE FILE NO. 00001 1-28-64 MILLSTONE/MIT ECHO II RADAR DATA

STATISTICAL PARAMETERS...

MEAN CROSS-SECTION = 2.4124406E 01 DB REL. TO A SQ. METER. CHI-SQUARED FOR 97 D. F. = 1.2216218E

STANDARD DEVIATION = 4.1905180E 00 DB REL. TO A SQ. METER. NORMAL DISTRIBUTION PROB. = 0 PERCENT.

DETAILS OF CHI-SQUARED ANALYSIS...

NUMBER OF DATA POINTS PROCESSED = 12693

EXPECTED FREQUENCY IN 100 EQUALLY PROBABLE RANGES = 1.2693000E 02. NO. RANGES WITH FREQ. LESS THAN 5 =

FREQUENCY DATA FOR 100 EQUALLY PROBABLE RANGES, FROM LOW VALUES TO HIGH...

NO.	FREQ.	NO.	FREQ.	NO.	FREQ.	NO.	FREQ.	NO.	FREQ.	NO.	FREQ.	NO.	FREQ.	NO.	FREQ.	NO.	FREQ.	NO.	FREQ.
1	331	2	123	3	131	4	102	5	79	6	93	7	107	8	65	9	83	10	71
11	71	12	77	13	101	14	80	15	59	16	134	17	107	18	92	19	119	20	118
21	115	22	104	23	104	24	95	25	96	26	96	27	108	28	126	29	122	30	85
31	101	32	120	33	162	34	143	35	117	36	129	37	153	38	149	39	139	40	113
41	131	42	140	43	142	44	106	45	114	46	130	47	170	48	147	49	108	50	128
51	130	52	186	53	182	54	140	55	109	56	124	57	149	58	183	59	159	60	134
61	180	62	165	63	153	64	146	65	144	66	171	67	123	68	138	69	144	70	148
71	116	72	134	73	161	74	126	75	146	76	146	77	141	78	129	79	136	80	117
81	139	82	116	83	135	84	127	85	165	86	112	87	150	88	113	89	171	90	197
91	175	92	175	93	158	94	172	95	124	96	100	97	59	98	60	99	44	100	5

FIGURE 2-5

CONDUCTRON CORPORATION
SECCND STATISTICAL PROGRAM

TAPE ID WORDS...

CONDUCTRON CORPORATION TAPE FILE NO. 00001 1-28-64 MILLSTONE/MIT ECHO II RADAR DATA

PERCENT DIFFERENCE FROM NORMAL DISTRIBUTION

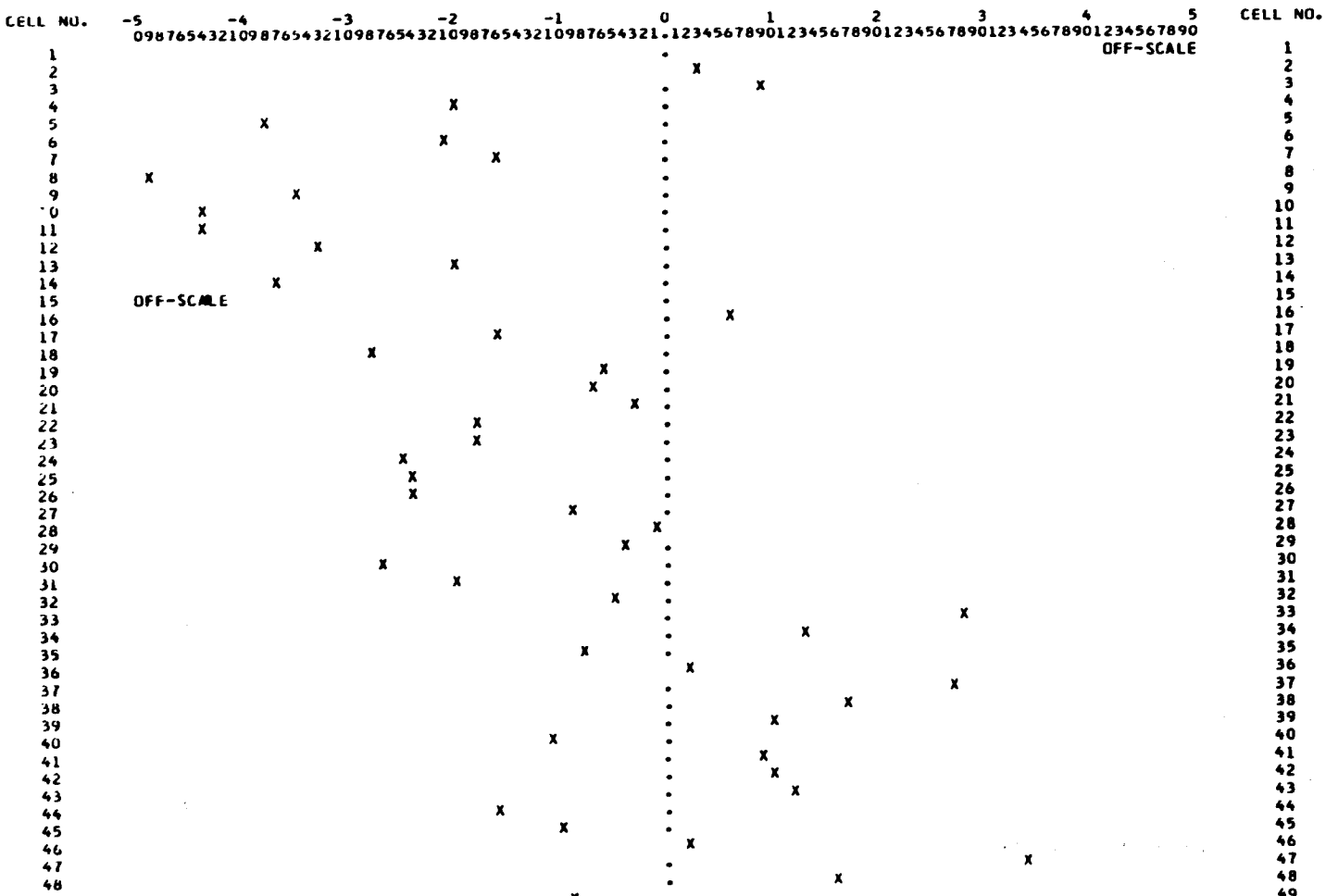

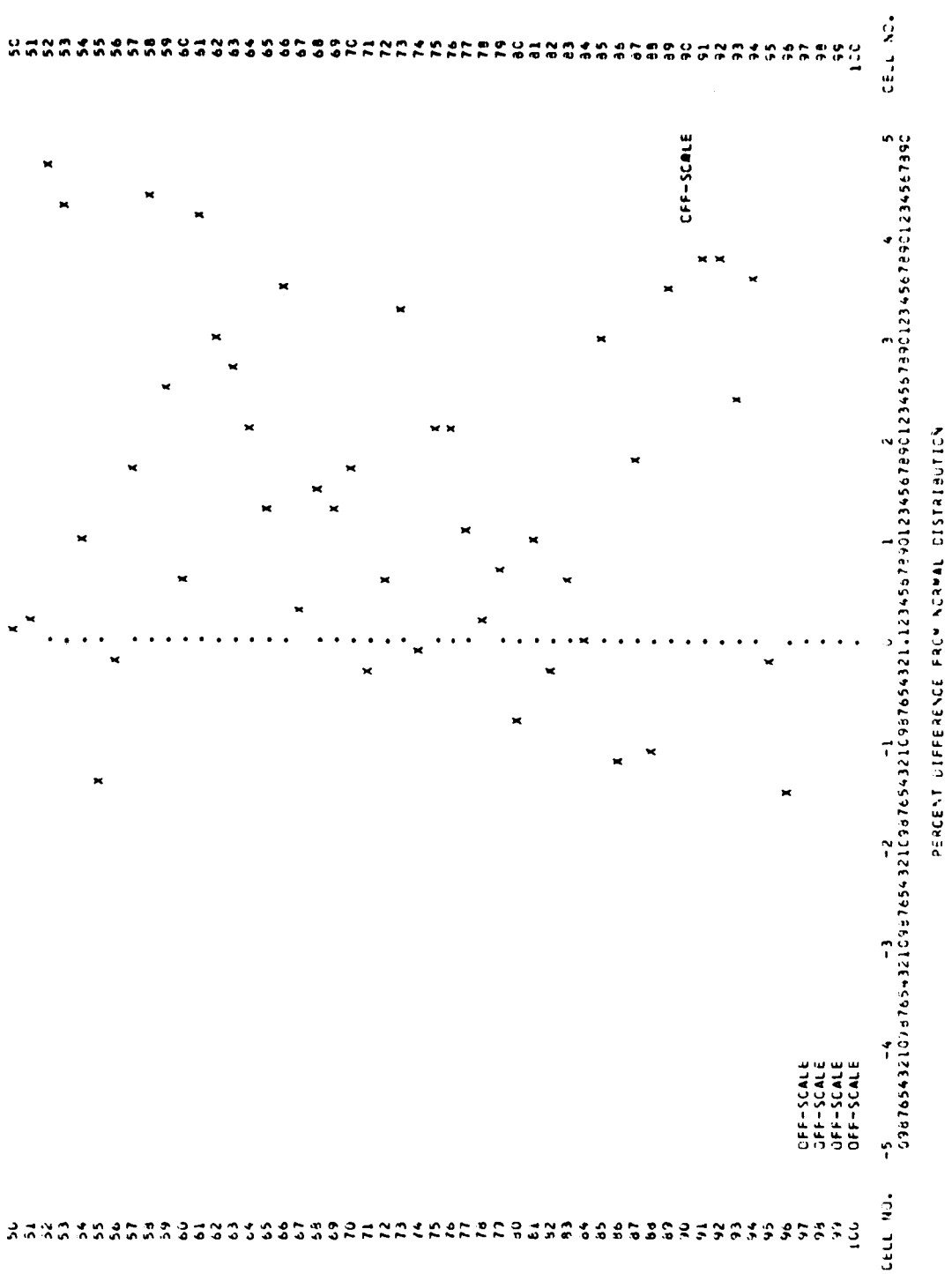
CELL NO.
OFF-SCALE
OFF-SCALE
OFF-SCALE
OFF-SCALE
PERCENT DIFFERENCE FROM NORMAL DISTRIBUTION

FIGURE 2-6

where λ is radar wavelength and σ is radar cross section, to the data in the format of that received from the three Wallops Island radars. This program determines the constants A, B, and C. B, the wavelength independent term, corresponds to the optics return from a sphere, while A and C respectively provide a measure of the relative significance of return inversely proportional to the wavelength and directly proportional to the wavelength. The relative magnitude of A, B, and C provides a measure of the wavelength dependence. It was expected that A and C would be quite small relative to B. Theoretical explanation of the role played by returns proportional to the wavelength and inversely proportional to the wavelength may be found in Reference 2.

(e) A program to study polarization effects by computing the ratio $(\sigma_H - \sigma_V)/(\sigma_H + \sigma_V)$, where σ_H and σ_V are the recorded horizontal and vertical cross sections respectively, was planned. The AMR and RAMPART radar data were expected to provide suitable input for this program. The program was not coded for reasons explained in Section 2.4.

2.3 Sources of Expected Data

It was anticipated digitalized radar data would be received from the following sources:

(a) Millstone Hill, Massachusetts, an L-band (1295 m.c.) radar which transmits a right circular pattern and records a left circular pattern.

(b) Wallops Island, Virginia, a complex of three radars; UHF, S-band and X-band. The S-band (2801 m.c.) radar and the X-band (9370 m.c.) radar transmit and record vertical polarization. The UHF (420 m.c.) radar transmits vertical and records vertical and horizontal polarizations.

(c) Rampart, WSMR (White Sands Missile Range), an S-band (3000 m.c.) radar which transmits a circular pattern and records both vertical and horizontal polarizations.

(d) AMR (Atlantic Missile Range), Trinidad, a UHF (425 m.c.) radar which transmits a linear polarization and records that polarization and the orthogonal one.

(e) TTR's (Target Tracking Radars) at Ascension Island, Kwajelein, and at WSMR. These C-band radars were developed by the Bell Telephone Laboratories for the Nike-Zeus system. No further specifications were found in unclassified literature.

2.4 Available Data

Not all the expected data was provided to NASA/GSFC in expected form. Some of the difficulties were:

(a) Millstone Hill made available significant amounts of data on 9 passes. Two passes (Nos. 136 and 137) were not processed because the tapes were not in their standard format. This format problem was discovered too late for programming modifications to be made. One pass (No. 321) was not processed because of an excessive number of parity errors. Four of the remaining passes (Nos. 6, 11, 31, and 229) had mean cross sections 4 to 10 db below the values estimated by Lincoln Laboratories for the same pass (see Reference 3). This inconsistency caused the data to be of marginal utility. The remaining two passes (Nos. 5 and 12) are in good agreement with the Lincoln Laboratory estimates.

(b) Wallops Island covered at least a dozen passes and provided, in suitable format, tapes for two of these passes. Neither tape could be used because of the excessive noise on the tapes. The FPS-6 channel on the tape made 28 January had 1/3 of the returns greater than 50 db > m^2. Additional tapes were provided for two ECHO I and two ECHO II passes. The recording was on 1-inch, 14-channel binary tapes and could not be processed.

(c) RAMPART covered approximately five passes. However, the Hollaman AFB computation facility did not convert the data to an IBM compatible format within the time constraints of the program.

(d) AMR-Trinidad provided tapes for 23 passes. Only eight of the passes were in the agreed format and arrived too late to determine new formats and reprogram. Evidence, which is discussed in the next section, suggests that only one of these tapes is valid.

(e) TTR tapes for sixteen passes from Bell Telephone Laboratories facilities were provided. Each of these tapes is good.

Since the Wallops Island and RAMPART tapes could not be used, it was impossible to make a computer analysis of the polarization dependency of the balloon's radar cross section. The lack of Wallops tapes also reduced greatly the sophistication of the radar frequency dependency analysis, since simultaneous cross section measurements at more than one radar frequency were not obtained.

2.5 Summary of Output

Each tape which could be read was put through the STAT 1 program. Table 2.1 summarizes the means and standard deviations of the pulse-by-pulse histories. The median cross section measurement is also included for those runs which are regarded as valid. (The median is presented because it does not depend upon whether the data is in the units of db > m^2 or in m^2. The mean obtained when working in db > m^2 is a geometric mean because it is an average of logarithms; when the data in m^2 is used, then an arithmetic mean is computed. No median is given for the AMR tape of 4 March, since it contains only 30 seconds of data within a 600-second run. Each of the other invalid runs summarized in Table 2.1 has an implausible mean, an implausible standard deviation, or, in the case of Millstone Hill data, disagrees with Reference 3. A possible error source is in radar calibration. The BTL cross-section data indicates strongly that the standard deviation should be about 5 to 6 db/m^2 at C-band during valid runs. The transmitted power may have been changed during questionable runs; such a power change would cause the points to cluster about two or more means and, consequently, give a large standard deviation. Other runs show mean radar cross sections approximately 10 db different from what was expected; perhaps an incorrect calibration constant was provided for data reduction. Another possible error source is that the data was taken while the radar was not in an automatic track mode; such cross section data is inherently noisy and should not be used in cross section analyses inasmuch as the operator is trying manually to acquire the target.

Date		Source	Average Cross Section in db/m^2	Median Cross Section in db/m^2	Standard Deviation in db/m^2
Day	Month				
25	Jan.	BTL	26.4	27.5	6.25
25		MIT	31.7	32.7	4.80
25		MIT	29.0	28.5	6.56
26		MIT	22.1	--	4.91
27		BTL	29.6	30.3	5.83
27		BTL	29.9	30.6	5.85
27		BTL	28.8	30.2	7.08
27		MIT	22.5	--	4.26
28		MIT	24.1	24.5	4.19
31		BTL	27.0	27.7	5.41
11	Feb.	MIT	17.9	--	5.55
12		AMR	25.6	--	13.2
12		AMR	26.4	--	13.2
13		BTL	27.0	27.5	5.38
15		BTL	27.6	28.0	5.35
16		AMR	37.4	--	8.21
16		AMR	32.0	--	11.9
19		BTL	26.3	27.1	5.97
26		BTL	28.6	29.4	5.45
27		BTL	29.1	29.8	5.37
4	Mar.	AMR	30.2	--	6.24
5		AMR	39.1	--	5.67
6		AMR	42.4	--	5.49
14		BTL	27.0	27.7	5.55
14		BTL	27.0	27.6	5.71
17		BTL	25.2	26.0	5.49
17		BTL	28.0	28.7	5.69
27		AMR	28.3	--	13.1
31		AMR	34.3	--	13.8
27	April	BTL	25.9	26.6	5.83
29		BTL	29.9	30.6	5.42

TABLE 2.1 Means and Standard Deviations of Computer Processed Data
BTL - Bell Telephone Lab., C-band tracking radars at Ascension, Kwajelein and WSMR. MIT - Millstone Hill L-band radar.
AMR - Atlantic Missile Range UHF radar.

The hypothesis that the pulse-by-pulse radar cross section data is log-normally distributed was rejected for every tape processed with STAT 2. A comparison of the means and medians gives insight into why the hypothesis was rejected. For 18 of the 19 runs, the median is larger than the mean. If the data were log-normal, then the sample mean and sample median should be very nearly coincident, cf. p. 369, Reference 4, and the median should be less than the mean about 50 percent of the time. The obvious interpretation is that the "drop out" tends to distort the distribution by making some low values lower than would be expected if the data were log-normal. Unsuccessful efforts were made to isolate the "drop out" portion of the data, so that the rest could be tested for a log-normal distribution. No method could be found for satisfactorily dividing the data without prejudging the log-normal hypothesis. For the one run with the median less than the mean, the computed mean differs by 4 db from the value in Reference 3; the histogram for this run suggests that an uncompensated power change occurred during the run.

The STAT 1 programs have been used to process the Millstone Hill tape for January 28. The most prominent period (time intervals which contain repetitive data characteristics) in this tape were approximately 17 seconds and 50 seconds. The 50-second period was expected since drop-outs occurred in multiples of approximately 50 seconds; the 17-second period was unexpected. No explanation has been found for the 17-second period.

These programs have also been used to process a BTL tape recorded on March 17. This tape is considerably shorter than the Millstone Hill tape--345 seconds vs. 846 seconds. The 50-second period was evident, but not as dominant as visual interpretation of pen recordings would have suggested. Twelve- and 8-second periods are also noticeable in this tape. Processing of the other tapes yielded additional support for the existence of the 50-second period together with other periods, which change from tape to tape.

2.6 Interpretation of Output

2.6.1 General Comments

Due to the very limited quantities of good data and the fact that almost without exception good data came from the C-band radars, definitive answers to some of the questions raised in Section 2.1 are not possible. The first three questions, (a), (b), and (c), for detailed digital analysis require data over a reasonably wide bandwidth or for a range of polarizations. This data was not received as explained above.

As to whether or not the radar cross section varies in a systematic way as a function of time from launch, Figure 2-7 displays those cross section results meriting high confidence plotted as a function of days after launch.

Analogue data obtained at UHF from a DOD Radar, on the other hand, indicates a qualitative change in the appearance of the data as the time from launch varies. Although it is difficult to pinpoint a transition, the data obtained after March 4, 1964 is noticeably "rougher" than data obtained before February 15, 1964. The "rougher" data is typical of an interference pattern, as though an additional scattering center had appeared, acting in and out of phase with the main return.

Standard deviation has been chosen as a statistical measure of the magnitude of scintillation. It is to be noted that this number is well defined and gives a good measure of the excursion of the data from the mean value independently of data being normally distributed. Another possible measure of the scintillation is the peak-to-peak difference of the cross section. Characterization of the data on this basis suffers from the difficulty in obtaining objective criteria for assigning numerical values.

As may be seen from Table 2.1, the average standard deviation for the 16 C-band ditigal tapes processed is 5.7 db. The three L-band digital tapes accepted as reliable gave standard deviations of 4.80, 6.0 and 4.2 db. The fact that two of these three values are smaller than any C-band standard divation recorded might be taken as evidence supporting expectation of greater scintillation at C-band than at the lower frequency. This observation should be regarded as highly tentative but is relevant because more scintillation arising from irregularities in the surface of the balloon at shorter wavelengths had been predicted. (See Volume I.)

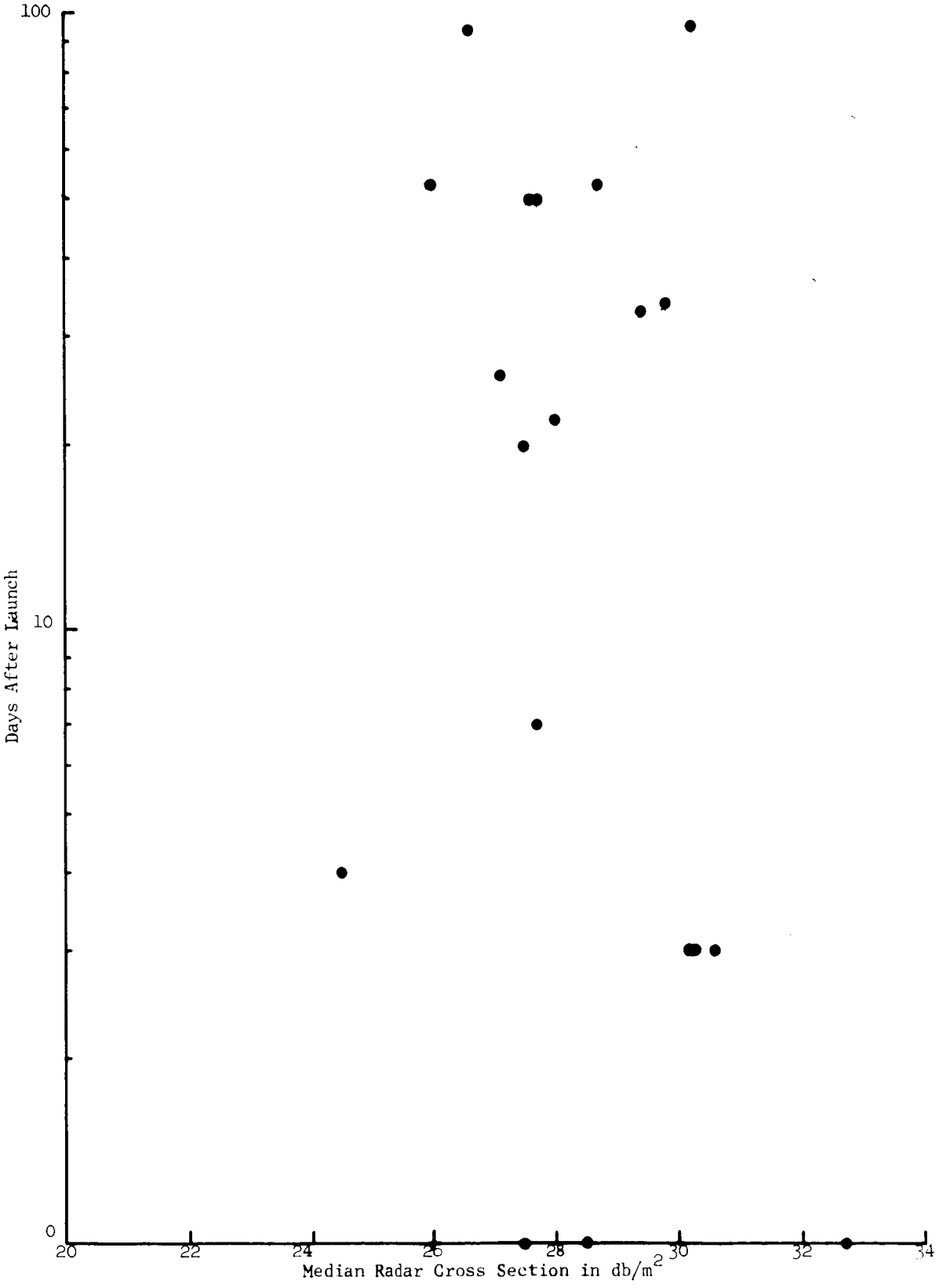

Figure 2-7 Variation Of Echo II Cross Section From Launch Time

As far as peak-to-peak measurements are concerned, further support for the expected greater scintillation at higher frequencies was provided by examination of digitalized data produced manually from Wallops Island UHF, S- and X-band AGC records. A slight but definite trend was found in this data indicating greater total excursions as frequency increased.

Concerning periodicities in the data, the original expectation based upon visual examination of the returns was that the programs which perform auto-correlation and frequency analysis would exhibit strong periodicities. As reported in Section 2.5 which summarized the output, this did not prove to be the case.

Subsequent scrutiny of the cross section pen recordings for these runs has shown that the spacing between "drop outs" is not as regular as initial visual inspection had suggested. For example, there are sections of each pass which show only slight signs of "drop-outs". A reasonable explanation for this lack of true periodicity in the radar cross section data is that the magnitude of change in orientation of the balloon spin axis with respect to the radar is sufficient to keep the radar from illuminating the same portion of the balloon on successive spins. This means that the locus of points illuminated on the balloon during a pass will be, for example, more nearly a spiral than a circle. This point is illustrated by the following analysis.

2.6.2 Migration of the Specular Point

During a particular pass the specular point on the balloon does not retrace its path on successive rotations of the balloon. The distance between the specular points at times which are one period of the balloon roation apart is calculated below. From these calculations it can be seen that periodic (in time) repetition of RCS characteristics are not to be expected.

The situation analyzed is a pass of ECHO II over the Millstone tracking station on 28 January 1964. This was a "low" pass, the maximum elevation above the horizon being 12.65°. A low pass was chosen because the low maximum elevation results in a minimal migration of the specular point during one rotation of the balloon. In other words the migration distances calculated for the lowest available pass would be the best possible case.

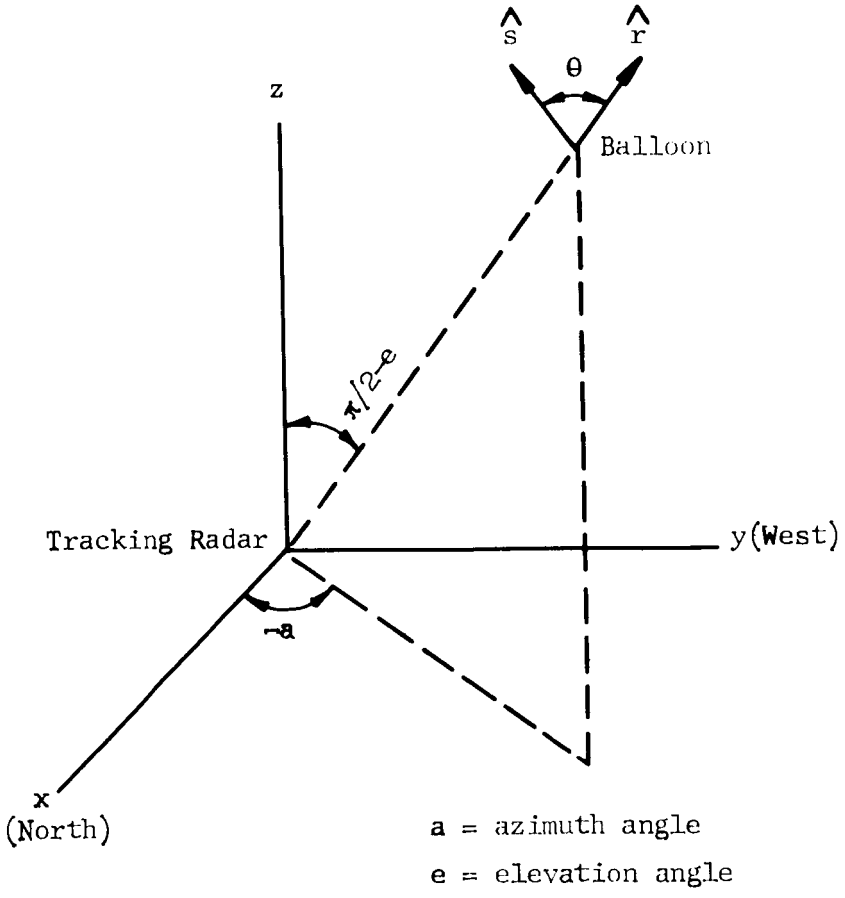

Figure 2-8 Radar - Balloon Geometry

The following data was necessary for the calculation of the vecotr $\hat{s}(t)$ to determine the navigation of the specular point.

Latitude of Millstone Tracking Station - 42.617^{o} N

Longitude of Millstone Tracking Station - 71.492^{o} W

Approximate Orientation of Spin Axis of Balloon:

Right Ascension - $137^{o}22'$

Declination - $54^{o}53'$

The components of $\hat{r}(t)$ were computed from the formulas

$$r_x = \cos e \cos a$$

$$r_y = -\cos e \sin a$$

$$r_z = \sin e$$

where a(t) and e(t) are the azimuth and elevation of the balloon at the times mentioned above. The values of a and e are obtained directly from the Millstone tracking data. The computations are summarized in Table 2-3.

TABLE 2-3

Summary of Calculations

Time (hrs/min/sec)		16-16-43	16-18-19	16-19-55	16-21-31	16-23-08
Spin-Axis Components	s_x	-.59072	-.59348	-.59617	-.59885	-.60163
	s_y	-.40553	-.40424	-.40303	-.40181	-.40048
	s_z	-.69755	-.69597	.69437	.69277	.69113
Azimuth and Elevation	a	127.81^{o}	119.83^{o}	109.77^{o}	97.42^{o}	83.01^{o}
Line of Sight:	e	$.96^{o}$	4.83^{o}	8.43^{o}	11.23^{o}	12.61^{o}
Line of Sight Vector:	r_x	-.61294	-.49566	-.33460	-.12667	.11876
Components:	r_y	-.78994	-.86442	-.93090	-.97264	-96863
	r_z	+.016754	.084200	.14660	.19475	.21831
$\cos\theta$ =	$\hat{r}\cdot\hat{s}$	.69411	.7022	.67645	.60159	.46864
	θ	46.04^{o}	45.39^{o}	47.43^{o}	53.02^{o}	62.05^{o}

2.6.3 Balloon Radii of Curvature

We now turn to the question whether the radar cross section of the balloon is in fact log-normally distributed and what conclusions may be drawn from a study of the cross section distributions. As has been indicated above, a visual examination of the AGC records and the preliminary digital data processing results suggested that the radar data was log-normally distributed; that is, distributions of the radar cross section in db > m^2 were normal (Gaussian). A measure of the validity of this hypothesis is provided by plotting the cumulative distribution of the data on probability paper. A normal distribution gives a linear plot on probability paper. The slope of this straight line is the inverse of the standard deviation of the distribution. The horizontal scale on such a plot is the radar cross section in db, the vertical scale is the percentage of the data points having cross section less than or equal to the corresponding abscissa. This provides a convenient method of comparing two or more distributions.

It was reasoned that if, in fact, the cross section data were normally distriubted, the validity of using the simple formula, $\sigma = \pi\rho_H\rho_V$, to predict the cross section could be tested by examining the distributions of the logs of the radii of curvature (in orthogonal directions--latitudinal and longitudinal) ρ_H and ρ_V. Furthermore, it is possible by this technique to compare the distributions of the radar cross section resulting from the static inflation tests (discussed in Volume I) with the distributions of the flight test data. Thus, cumulative distributions of all three of these sets of data were constructed and examined.

As has been reported above in the summary of flight test data (Section 2.5), in no case was the flight test data normally distributed on the basis of the rigorous statistical tests programmed for the NASA/GSFC computer. This may reasonably be attributed to the presence of the "drop-outs", and for comparative purposes the approximately linear portions of the flight test data which occur between the 5th and 98th percentiles have been used. In what follows we present graphically the cumulative distributions generated for comparative purposes and discuss the comparisons which have been made. Briefly, the conclusions arrived at are as follows:

(a) The optics formula $\sigma = \pi\rho_H\rho_V$ cannot adequately describe the cross section of ECHO II consistency with pre-launch. A feasible explanation based on a comparison of the distributions is that it is necessary to assume more than one specular point contributing with random phase to the return from the balloon.

(b) The cumulative distributions arising from the static inflation tests agree well with the flight test data distributions only for the case in which the static test distributions are taken from data at low pressure levels.

(c) In all cases examined the static L-band data varies over a narrower range of cross section values than does the static C-band data. This is expected behavior. On the other hand, the L-band flight test data exhibits an anomaly in showing a smaller standard deviation from its mean than the C-band flight test data. [We cannot explain this anomoly].

As is well known, for a sufficiently smooth body which is large with respect to the wavelength, the radar cross section can be predicted from the optics formula $\sigma = \pi R_1 R_2$ where R_1 and R_2 are the principal radii of curvature. The ECHO II balloon however should be regarded as a body which presents to the radar a statistical distribution of radii of curvature in both the longitudinal and the latitudinal directions. If simple optical scattering sufficed to explain the cross section return from the balloon, then the distribution of the sum of the logarithms of these radii might be expected to predict the distribution of the static inflation test cross section data. To this end distributions of the logarithm of $\rho_H\rho_V$ were determined from the photogrammetric data obtained during the static inflation tests (Volume I).

Figure 2-9 shows these distributions for three balloon pressures. The nominal value of the radius of curvature is indicated in Figure 2-9 and as should be expected, occurs very near the median--i.e., about half the radii of curvature are smaller than the design radius and about half are larger.

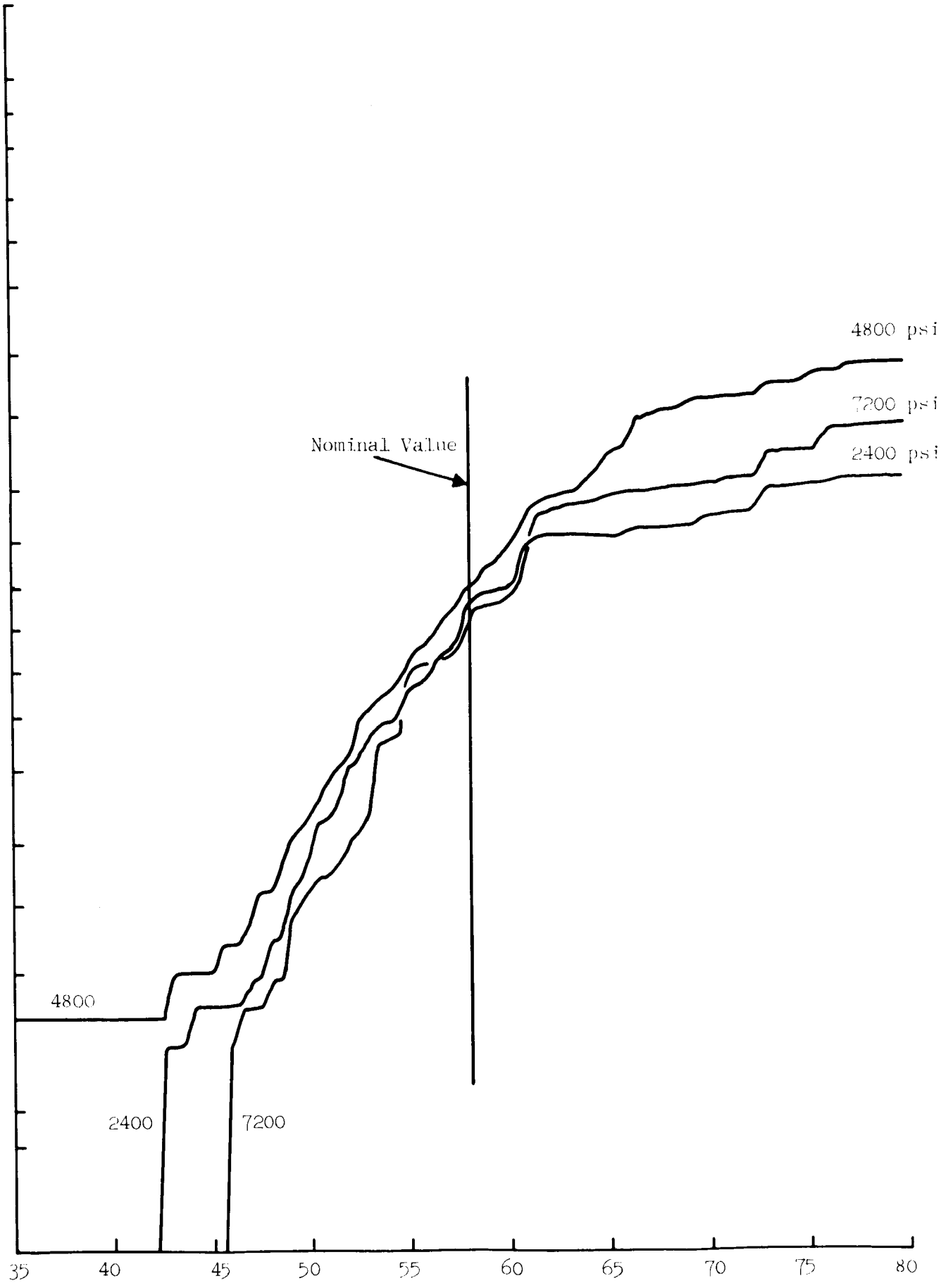

Figure 2-9 Product Of Radii Of Curvature (In db relative to 1 inch^2)

Next consider the cumulative distributions of the static test data. This data was the result of a series of experiments performed on the ground at various inflation levels. The experiments are described and the data is discussed in Volume I of this report. Figures 2-10 through 2-13 present cumulative distributions of this data. Each figure gives a cumulative distribution for C-band data and one for L-band data. Three successive figures show the effect of increasing pressure; the fourth gives a distribution for data taken at 560 psi after relaxation from 4800 psi. Since only comparing shapes of the distributions is of interest here, the C-band data have been adjusted by the addition of a constant 3.5 db to match the L-band distributions.

Comparing of these figures with the radii of curvature distributions show that it is not possible to predict the cross section of the balloon by the simple optics formula $\sigma = \pi\rho_H\rho_V$. There are two possible mechanisms which can provide an explanation for the fact that the range of the cross section value is much lower than would be predicted from the radius of curvature data and this simple optics formula. First, the lower values of the product of the radii of curvature represent bumps on the balloon surface. The smaller of these bumps will not contribute to the L-band scattering if their size is small compared to a wavelength. Further, at both L-band and C-band it is probable that a specular point exists on more than one bump. In fact, if four specular points exist, then the low end of the C-band data is explained. Assuming a random phase relationship between the scattered fields of the specular points, four specular points would yield a cross section which is on the average four times greater than that due to one specular point, and an increase of 6 db in the lower values of cross section would result. On the other hand, the high values of the product of the radii of curvature correspond to "flat" spots on the balloon surface. But the formula $\sigma = \pi\rho_h\rho_v$ cannot be used to calculate the cross section since this formula is only accurate if the "flat" spot is as large as the first Fresnel zone on a spheroid with the same radii (refer to previous report). A crude estimate of the diameter of such a Fresnel zone is 200 inches at L-band and 60 inches at C-band. But the radii of curvature data shows that the flat spots on the balloon are almost never wide than 12 inches. This argument predicts correctly that the actual radar cross section never approaches $\pi_{h\,v}$ for the larger values of ρ_h and ρ_v.

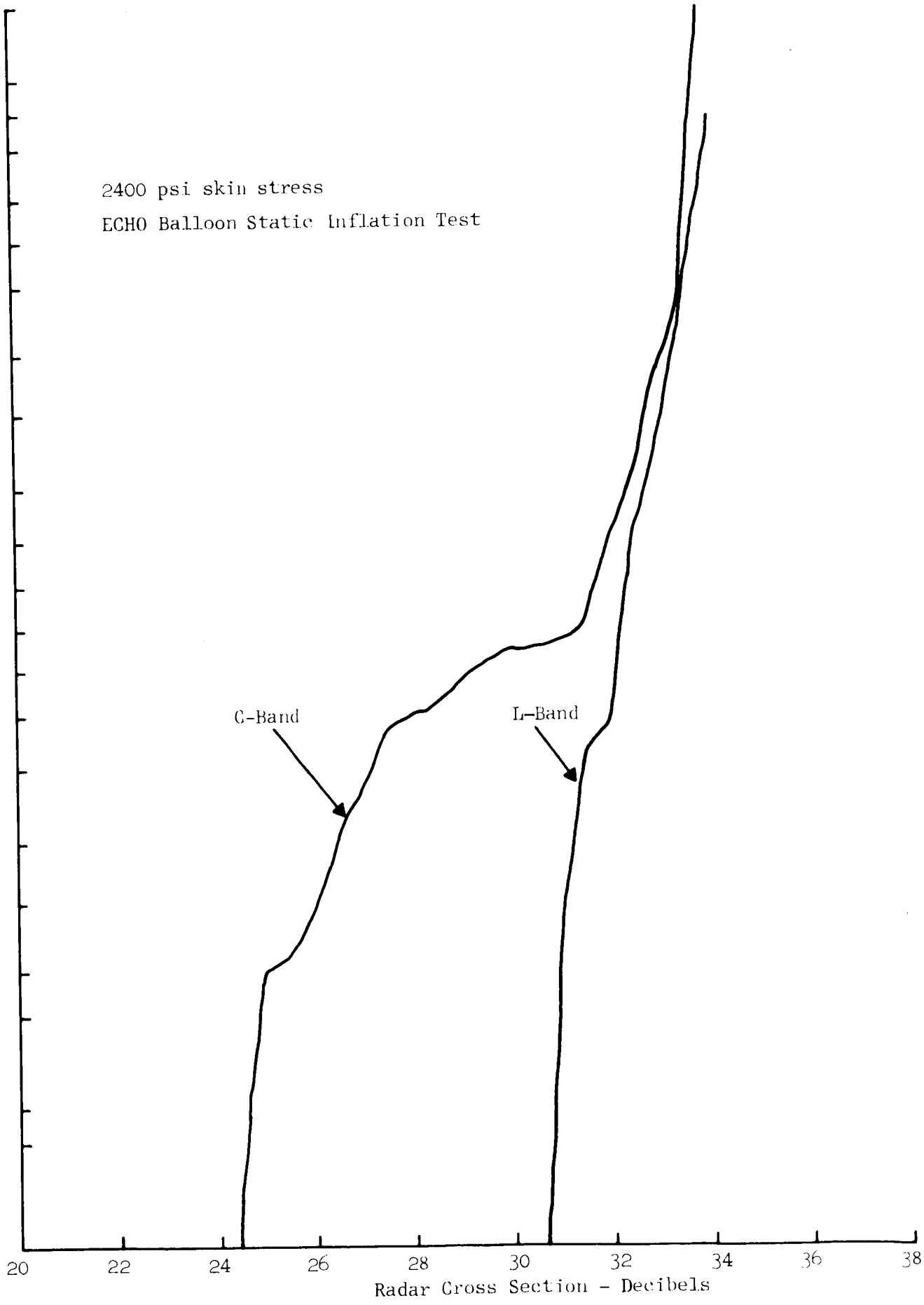
2400 psi skin stress
ECHO Balloon Static Inflation Test
C-Band
L-Band
20
22
24
26
28
30
32
34
36
38
Radar Cross Section - Decibels

Figure 2-10

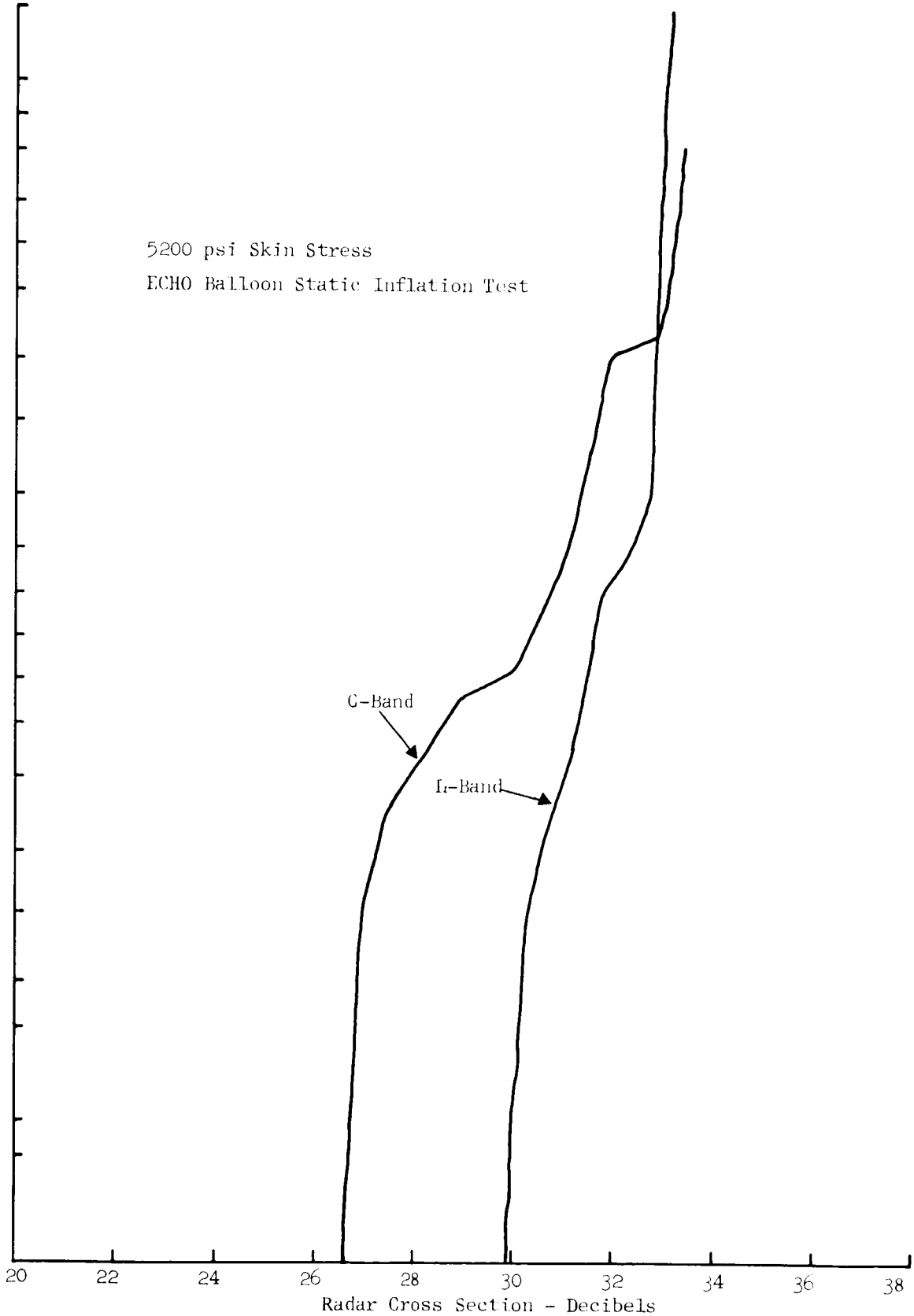
5200 psi Skin Stress
ECHO Balloon Static Inflation Test
C-Band
L-Band
20
22
24
26
28
30
32
34
36
38
Radar Cross Section - Decibels

Figure 2-11

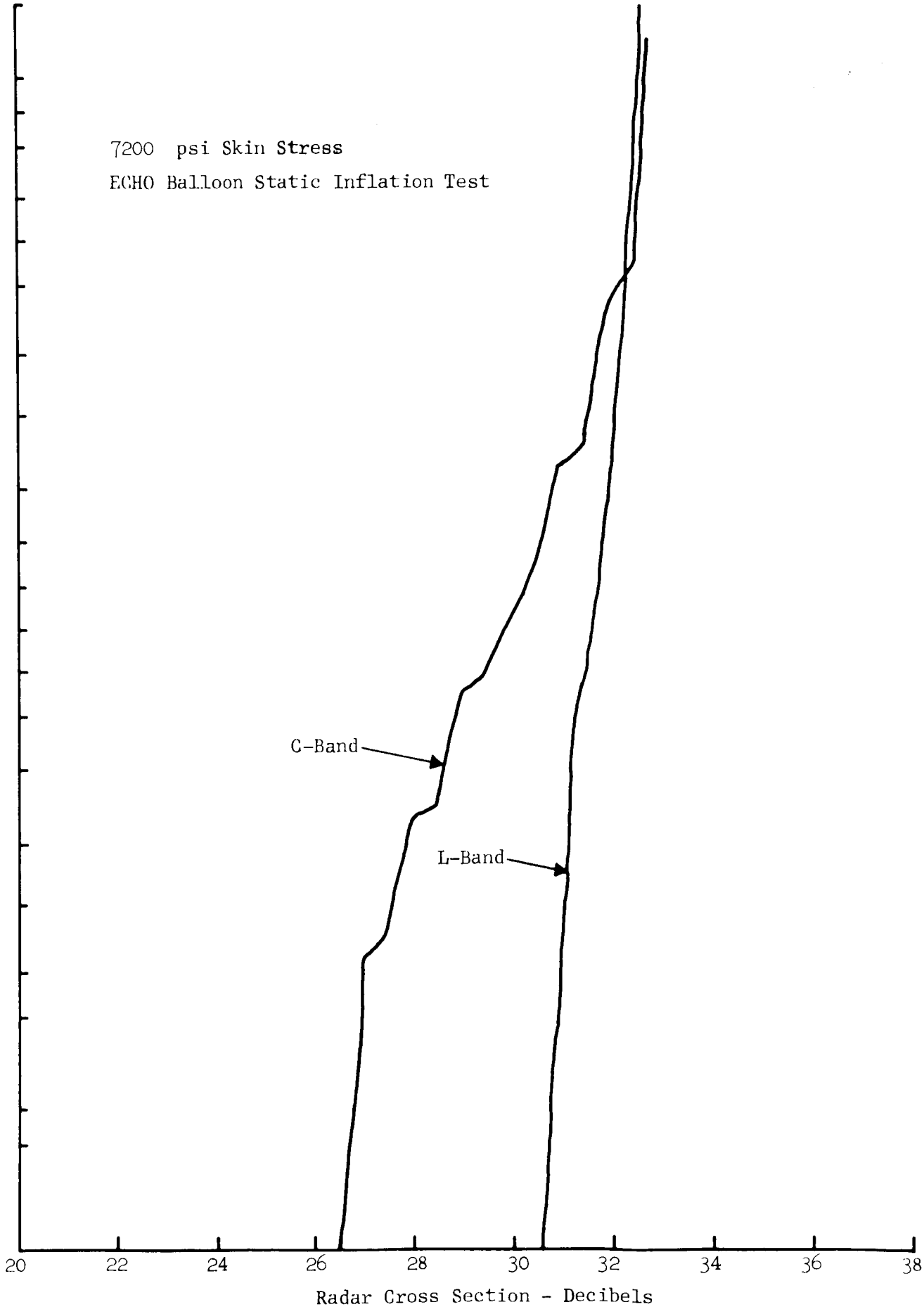
7200 psi Skin Stress
ECHO Balloon Static Inflation Test
C-Band
L-Band
20
22
24
26
28
30
32
34
36
38
Radar Cross Section - Decibels

Figure 2-12

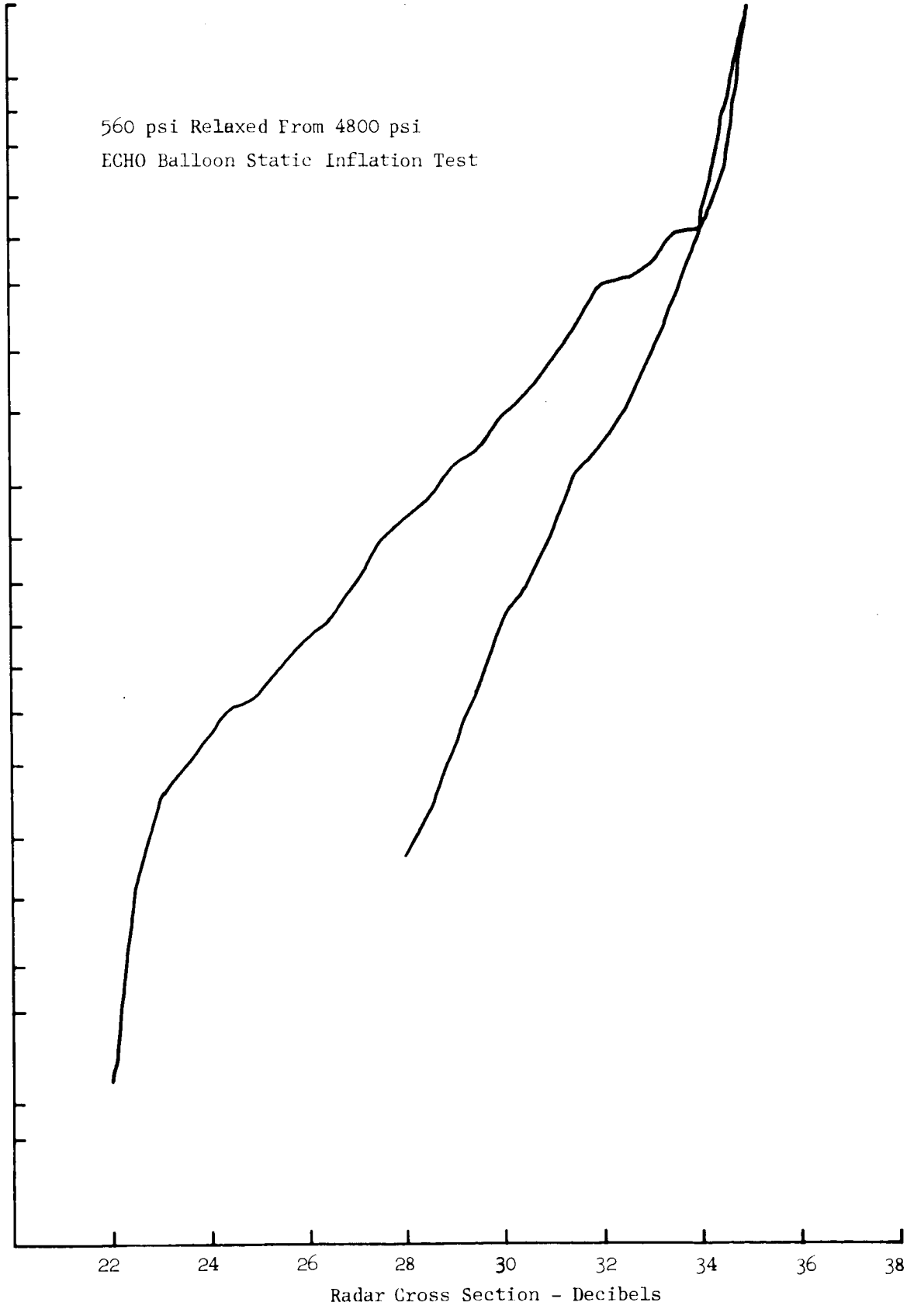
560 psi Relaxed From 4800 psi
ECHO Balloon Static Inflation Test
22
24
26
28
30
32
34
36
38
Radar Cross Section - Decibels

Figure 2-13

For every case the extreme values of C-band data are further apart than are those of the L-band data. This fact is consistent with intuition - at C-band perturbations of the balloon surface are more important than at the longer wavelength of L-band. It is to be noted that the cumulative distributions at C-band are non-linear; nevertheless, approximately linear portions of the graphs exist between about the twentieth and eightieth percentiles and average slopes have been determined for these regions. They are 2.9 db for 2400 psi (Figure 2-10), 2.2 db for 5200 psi (Figure 2-11), 1.4 db for 7120 psi (Figure 2-12) and 3.3 db for 560 psi after relaxation (Figure 2-13).

For the orbital balloon Figure gives cumulative distributions of data for two passes from the Millstone Hill radar site (L-band) and a typical Kwajelein C-band pass. Again, for purposes of comparison, the curves have been plotted so as to match one another at high cross section values. This data has two features which should be noted: first, the fact that the spread of the L-band data is in one case greater than that of the C-band data. This fact is inconsistent with the results for the static data, but is consistent with the "roughness" in the UHF data that has previously been referred to. Second, the excellent agreement of these distributions near the median suggests that (since the L-band data was shifted several db) a calibration error was present in the data. Data simultaneous in both time and location at different frequencies which would be required to put these differences on a firm footing was (as previously reported) not available.

Matching of the slope of the flight test data distributions of Figure 2-14 with the previously presented static inflation test distributions shows that the orbital balloon has radar cross section characteristics which are consistent with ground tested balloons that have been inflated only to low pressure levels, and inconsistent with ground tested balloon that have been stressed to and above 1500 psi.

2.7 Comparison of ECHO I and ECHO II

Computer data tapes of near simultaneous recordings of ECHO I and ECHO II were not available for performing a comparative analysis of the radar returns from both balloons.

During the time that this report was being prepared, analogue data comparing the two satellites was obtained. This data is now discussed briefly:

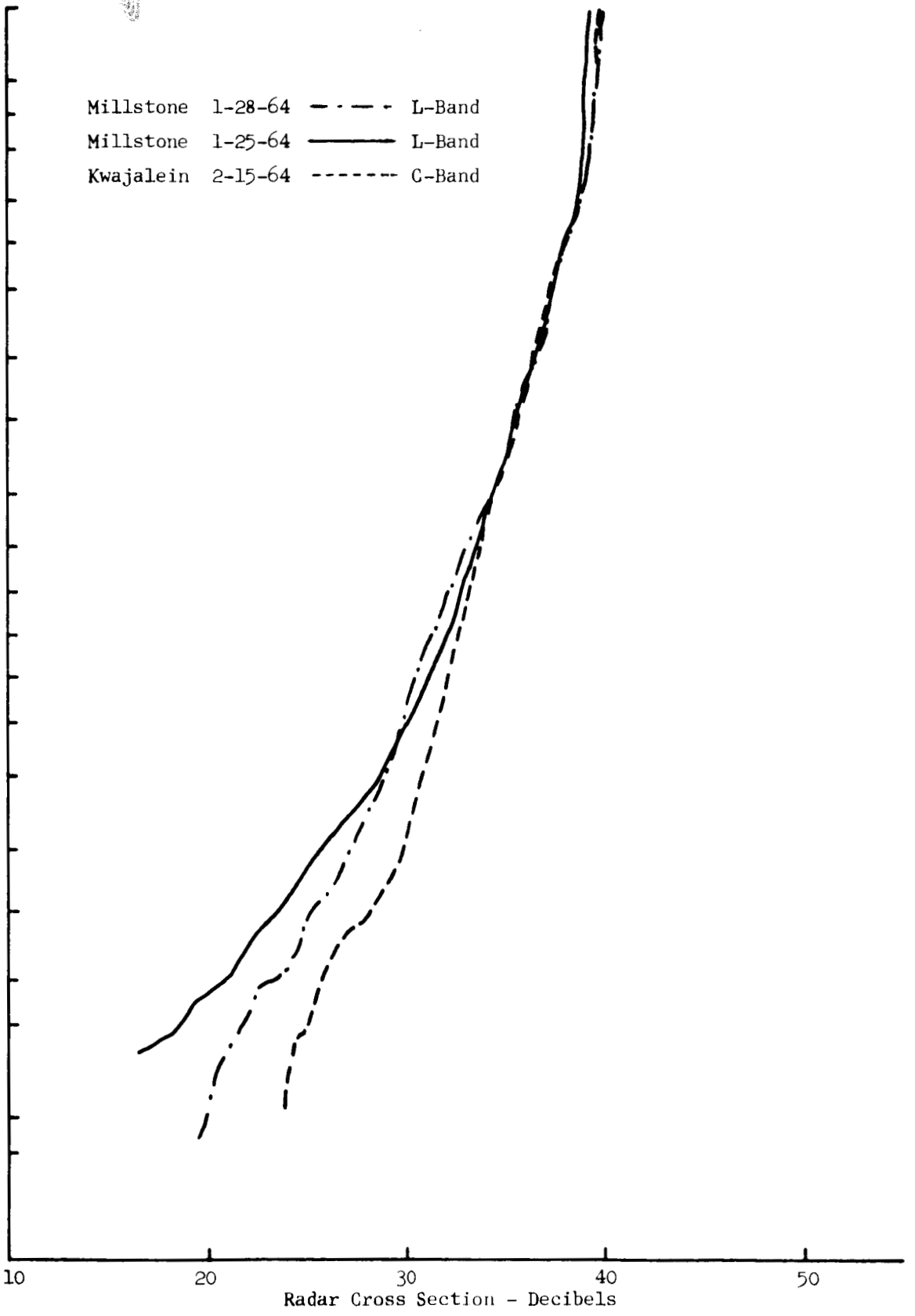
Millstone 1-28-64 L-Band
Millstone 1-25-64 L-Band
Kwajalein 2-15-64 C-Band
10
20
30
40
50
Radar Cross Section - Decibels

Figure 2-14

S-Band: Three AGC records of the Spandar radar were obtained for ECHO I during the period 18 November - 20 November, and three records for ECHO II during the period 17 November - 19 November. These AGC records are not absolutely calibrated. However, the ECHO I data exhibits deeper, and more prolonged nulls than does the ECHO II data.

C-Band: AGC recordings from the FPQ-6 were obtained for ECHO I on 20 November, and for ECHO II on 14 November. Absence of absolute calibration precluded comparison of average cross section value. There is a compression of the AGC calibration for ECHO I as compared to that of ECHO II. When this compression is taken into account, no apparent distinctive exists between the two sets of data.

3.0 BALLOON GEOMETRY

3.1 Anomalies in the Data

The possible effect of ECHO II balloon deformations from a nominal spherical shape on the radar returns received from the balloon was investigated. There is present in some of the data a periodic drop inn the cross section return which endures for several seconds. Upon examination of simultaneous beacon and radar data obtained by RRE, this effect appears to be well correlated with the periodic nature of the beacon data. This simultaneous data is shown in Figure 3-1 and suggests an interesting hypothesis which will be the subject of discussion in Section 3.3 of this report. The best explanation of the drop-out effect seems to be to attribute it to one or more deformed areas on the surface of the balloon which effect the radar return once each rotation. NASA requested Conductron to investigate, specifically, whether wrinkles parallel to the gore seams, large holes, or various other hypothetical deformation would account for the "drop out".

3.2 Wedges

By observing the Malvern radar and beacon data, it is noted that on the gores of the balloon corresponding to the location of the "drop-out" are mounted solar panels and telemetry beacons. Because of the balloon is rotating, this equipment exerts an outward directed force. Suppose that, as a result of this force on the balloon, the shape near these gores appears as in Figure 3-2.

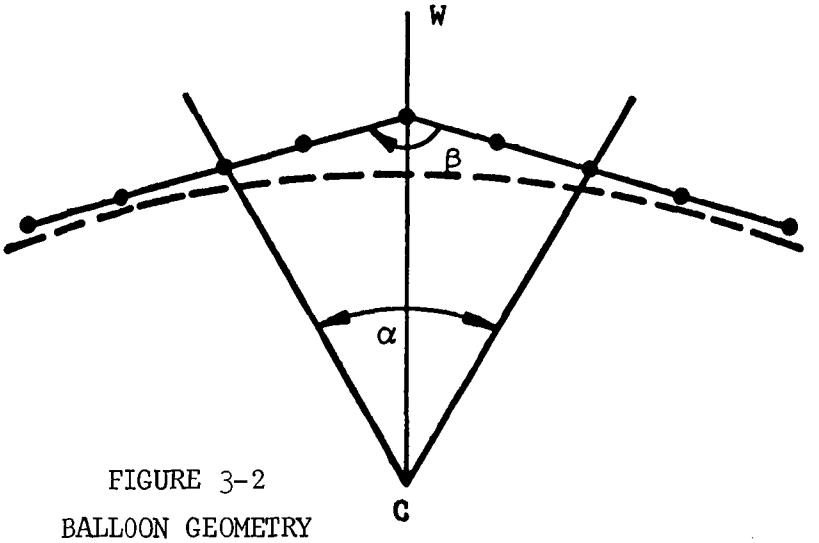

FIGURE 3-2
BALLOON GEOMETRY

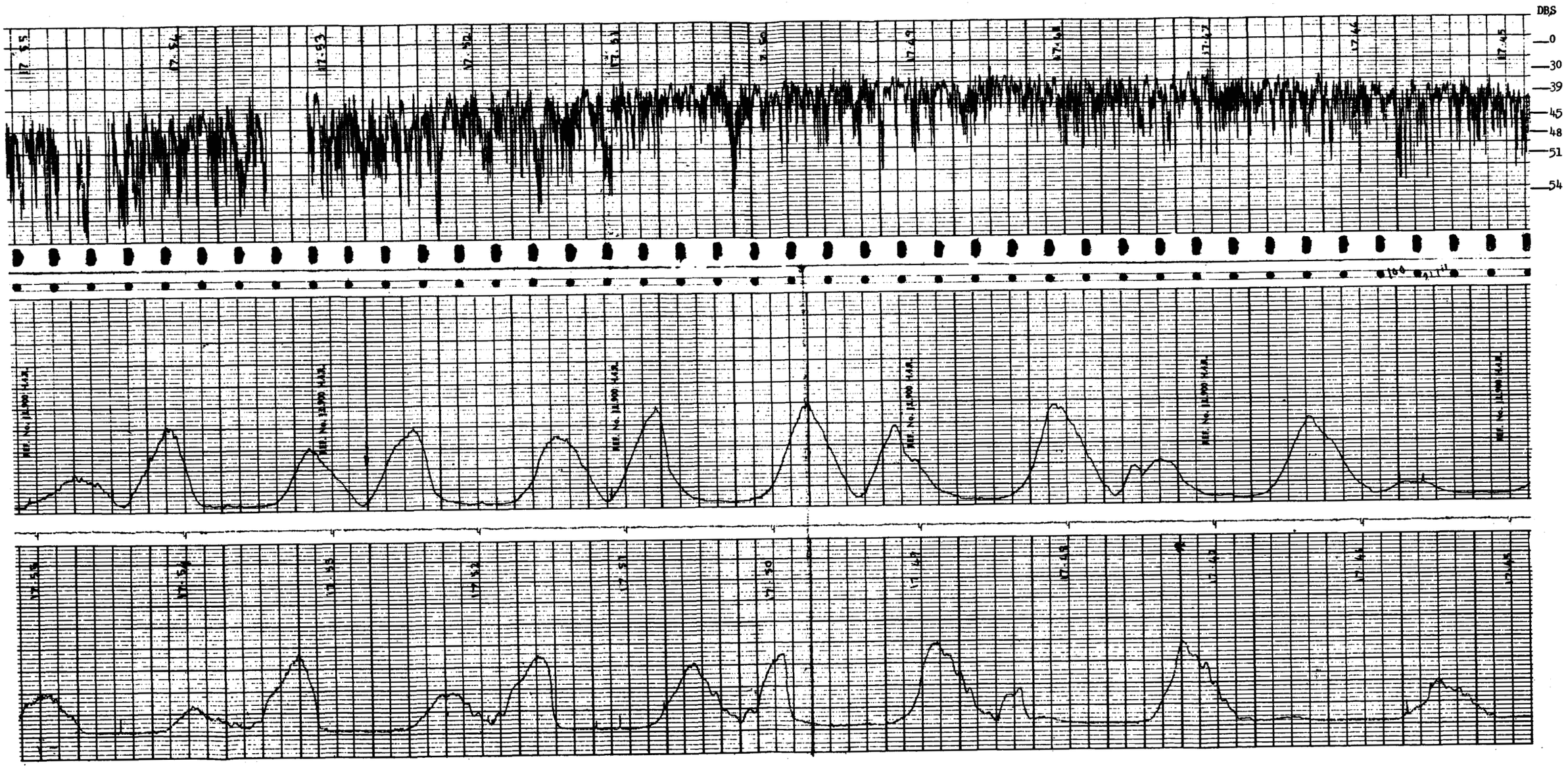

FIGURE 3-1

SIMULTANEOUS RADAR AND BEACON DATA, 28 JANUARY 1964, RRE

In Figure 3-2 the dotted line indicates the sphere contour, C indicates the center of the balloon, and W represents the seam joining thw two reinforced gores on which are mounted the equipment. The resulting cross section, for aspect angles within the angular domain indicated by α would be that of a cylindrical wedge, and considerably lower than that of the nominal balloon cross section. The backscattering cross section of the wedge is approximately

$$\sigma = \frac{R\lambda}{4} \tan^2 \beta/2$$

where λ is the wavelength and β is the wedge angle. Also, the distance $WC = R_o \cos\frac{\alpha}{2}$. For a 10 db drop-out at the Millstone frequency, $\alpha = 10.6^o$, as compared to the actual drop-out interval of 18^o. For this value of α, WC = 67.8 ft., requiring the radius to have been "pulled-out" only .3 feet.

Conversely, for $\alpha = 18^o$, the wedge cross section will be approximately $58m^2$, giving a drop out of 13 db. For this value of α, WC = 68.2 ft., requiring the radius to have been "pulled-out" .7 feet. Thus this hypothesis is consistent with the data observed.

3.3 The Wrinkle Hypothesis

If it is assumed that the wrinkles are parallel to the gore seams, then a drop in signal from the beacon region could be accounted for by a change in curvature of the surface in this region. Since the wrinkles are assumed to be parallel to the gore seams, the radius of curvature in the direction of the gore seams can be assumed to be that of the balloon, namely 67.5 feet. Assuming this radius of curvature in one direction, in order to obtain a signal drop of 10 db, the other radius of curvature would have to be about 6.75 feet. Actually this 6.75 feet radius would be a mean value since the return signal varies approximately $\pm$ 6 db. Therefore, the equivalent radius of curvature in the depressed region could vary between 1.8 feet and 27 feet and be made up of many wrinkles that can present a signature with an equivalent radius range.

3.4 The Hole Hypothesis

The radar cross section of the hole in a sphere when the wavelength is small with respect to all diameters can be computed by evaluating the hole rim contributions by a modification of the Sommerfeld semi-infinite plane solution and then evaluating the geometric optics contribution of the inner surface of the sphere. This analysis is presented in Appendices B and C. For a large hole, at backscattering, these two terms are of the same order of magnitude and by proper arrangement of phase can combine to give a deep null. For the ECHO II balloon, which is not quite a perfect sphere, the above remarks can serve as a rough model. However, it requires a very fortuitous arrangement of geometric parameters and frequencies to provide a backscattering null throughout the balloon history, since the dropouts of varying width have been observed from all radar sites. On this basis alone, the hole theory appears unacceptable. Even more conclusive is the angular spread of the drop-out. The cross section of a hole has a lobe structure of an equivalent radiating aperture, the major lobe having the beam width λ/d, where λ is the wavelength and d the aperture diameter. At radar frequencies it would require an extremely small diameter to account for the angular width of the drop-out (time intervals of greater than 6 seconds, and in this case the hole would make an extremely small contribution to the cross section. On this basis, the hole theory appears to be ruled out. At the request of NASA, further investigation of the possible effect of holes was investigated and is reported in Appendix B.

4.0 SPECIAL STUDIES

4.1 Scope of Study

Two additional hypotheses have been examined in some detail at the request of NASA to explain the drop out in the cross section data discussed in Section 3.0 and have been rejected.

These are:

(a) The presence of an ionized cloud about the balloon due to escaping gas.

(b) Multipath effects, i.e., cancellation and reinforcement of the returned signal by reflected signals from the earth.

A discussion of the two rejected hypotheses is given below followed by a discussion of the "Echo Box" effect reported by some radar sites.

The "wedge" hypothesis, advanced above, is the simplest and most convincing of the explanations for the drop-outs. The numbers derived above were constant with the data (see Figure 4-1). It should be observed in examining Figure 4-1 that the apparent mean radar cross section of 23-24 db is subject to calibration uncertainties of perhaps as much as 6 db.

4.2 Plasma Effects

Since the sublimating material used to inflate the ECHO balloon to its proper shape is vented to the exterior through a system of small holes in the periphery of the balloon, the ionization of this material by the solar radiation flux could conceivably form plasma densities of sufficient magnitude to cause radar perturbations. Based on information supplied by NASA/GSFC this possibility has been studied and rejected as being improbable for the reasons given below.

For a 200-micron internal balloon pressure NASA/GSFC estimates the electron density along a sphere of one cm around the hole to be 10^{10} electrons/cm^3, and this would decrease to 10^7 electrons/cm^3 as the radius of the sphere becomes equal to the balloon radius. The build-up of ionization around the balloon is precluded by the fact that any free charge formed near the satellite must cut lines of force of the earth's magnetic field. At the orbital velocities encountered, the gyration radius of a free electron in the geomagnetic field is small compared to the orbital radius of the balloon so that instead of being

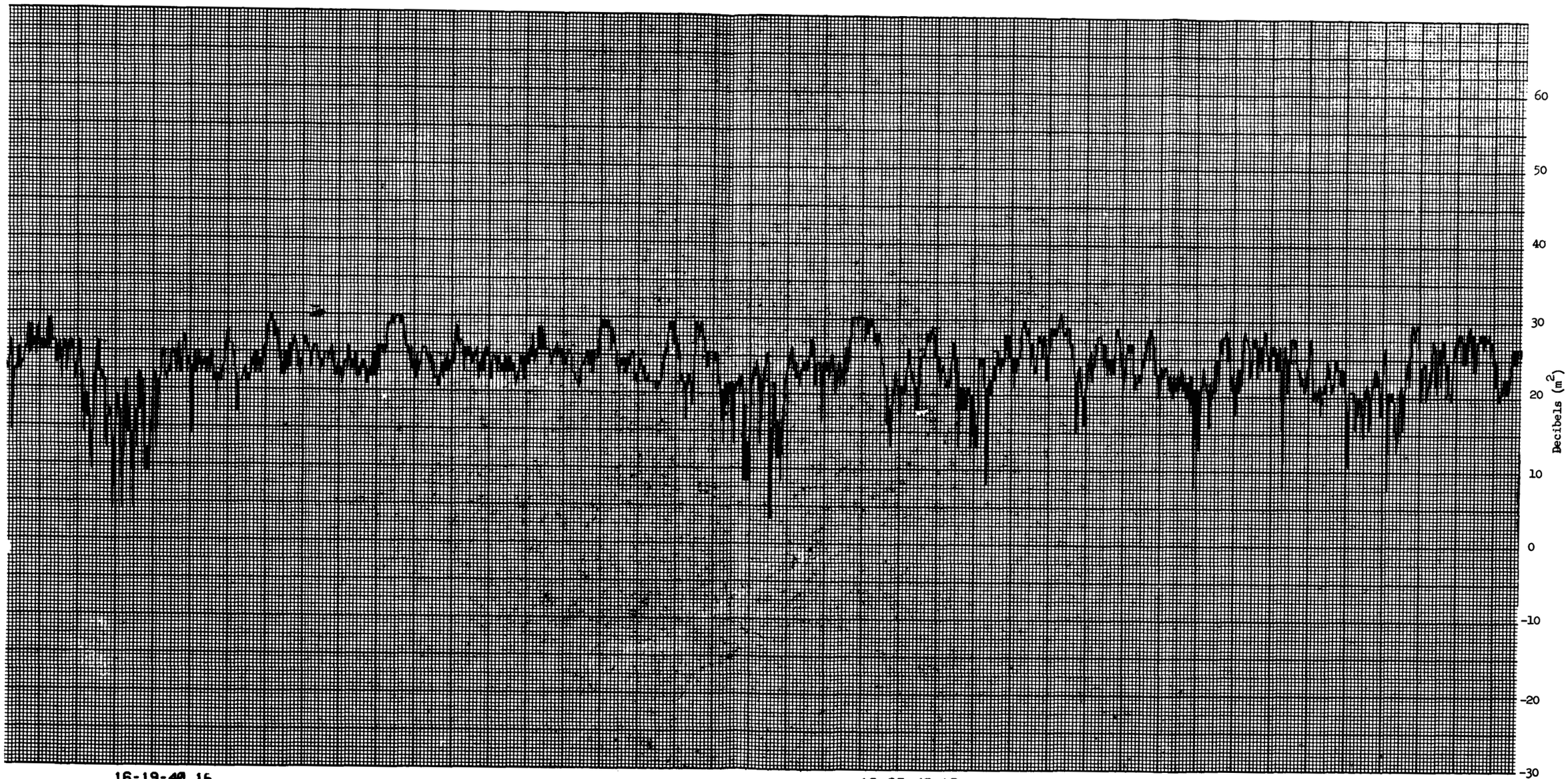

Figure 4-1 TYPICAL ECHO II RADAR CROSS SECTION DATA— 28 January 1964, Millstone Hill Radar Site

carried along in orbit, free charge will diffuse along the magnetic field lines. Consequently, ionization will tend to be swept away from the balloon as it is formed by the combined forces of the magnetic field and the ambipolar diffusion of the ionized gas. This process could be inhibited by a build-up of possitive potential on the balloon; however, in the absence of experimental information it is felt that this process will be unlikely to occur to the extent necessary to account for observational effects.

Since the beacon frequencies of 136 mc are at the lower end of the frequency range of interest, any plasma effects which occur would potentially have their greatest capability for attenuation on the observed beacon pattern. However, due to the relative location of the vent holes and the beacon antennas, calculations indicate that plasma effects will be negligible. The fact that the beacon signals were not affected is corroborative of the absence of plasma.

4.3 Multipath Effects

The energy received by a radar from an object can arrive by more than one path, the direct path from the object and the reflected path from the object to ground to radar. If the range gate of the radar is large and if the increase in path length for the reflected wave is small, then the combination of the two signals will be observed as one signal and the observed signal may not represent the radar return from the object.

If we assume that the earth is a flat, infinite, perfectly reflecting surface, then the reflected signal seen at the antenna would have the same magnitude as the direct signal. If this reflected signal were observed in the side lobe of the antenna pattern, then the signal would be reduced by an amount equal to the side lobe reduction. For the antennas used during these tests, the side lobe was 15 db or more below the main lobe and with the narrow beamwidth antennas used the reflected wave would have to come through the side lobe instead of the main lobe.

This 15 db reduction for the multipath signal is an upper bound and the signal strength will be still further reduced if the earth is assumed to be non-perfectly reflecting. For these reasons it is not thought that the interference pattern seen in the analog records is due to multipath effects, i.e., the multipath signal is not strong enough compared with the direct signal to cause a partial cancellation if they interact out of phase.

Multipathing would be most likely to occur when a radar is pointing at a low elevation angle; however, the, the "drop-out" effect has been observed for high elevation tracking and at all radar sites of ECHO II.

4.4 "ECHO Box" Effect

It has been reported by RRE at Malvern that the S-band radar data obtained exhibits the following anomaly: Subsequent to the reflection of the main pulse, which is of 10μs duration, there is observed an exponentially decaying train of pulses. The explanation that has been supplied with the data for this phenomenon is that an oblong hole (1.5 meters x 0.5 meters) in the balloon has been excited by the incident field, which in turn has excited a mode in the balloon, which in turn is reflected, re-excites the hole, etc., analogous to the familiar "ECHO box".

On the basis of the reported data the explanation that has been offered does not appear to Conductron to be correct. The interval between the end of the main pulse and the "ECHO" is reported to be of the order of 10μs. Taking into account the pulse width, the balloon would then be acting as a 20μs delay line. The clear two-way path of any mode excited in the balloon is 270 feet, corresponding to a free space time of 0.27μs. The mode velocity is therefore .27/20 or 1/90 of free space velocity. Geometric optical approximation shows that the principal mode has a velocity of $\frac{1}{\sqrt{2}}$ of free space velocity. Therefore the "ECHO box" effect would have to be related to a very high order mode, i.e., to a very large number of internal reflections. Furthermore, it would depend upon not only this high order mode being excited, but no lower modes being excited. This is so unlikely it can be considered impossible. This would be equivalent to some high frequency oscillation mode of an cavity being excited, but none of the lower frequency modes.

Somewhat similar trailing effects have been reported by other observers but these have been attributed by the observers to multi-path phenomena associated with low elevation angles or no explanation has been proffered.

5.0 BALLOON ORIENTATION AND SPIN

5.1 Spin Axis and Beacon Orientation

A mathematical procedure was developed involving both machine and hand calculations to obtain the beacon parameters and spin axis orientation of the ECHO II balloon. This calculation utilizes beacon data for the special case in which two distinct maxima of intensity are received from each of the two beacons during each rotation period about the balloon spin axis. The input data for the procedure consists of the angular separation of these peaks for each beacon on each of two separate passes; the location of the balloon relative to the receiving station for each observation; and the orientation in space of the zenith at the receiving station for each observation. The output of the analysis consists of the included angle of the cone of maximum signal intensity from a beacon antenna; the latitude of the beacon antennas relative to the balloon spin axis; and the orientation of the spin axis in space. A check on the validity of this approach is provided by the fact that the method provides an independent estimate of the angle between beacon maxima which is in reasonable agreement with the theoretical prediction of this angle. The calculations involved in determining the results are fairly involved, and they are therefore described in detail in Appendix A to this volume of the Final Report.

5.2 Assumptions Used and Results

The determination of the spin axis orientation and the beacon positions relative to the spin axis is based on beacon data obtained from the Royal Radar Establishment, Malvern, England. An example of such data is given in Figure 3-1. The approximate one-hundred-second period in each of the two beacon recordings along with the apparent presence of an approximate one-hundred-second period in the analog radar data recordings (Figure 6-1 is a typical record received from Millstone Hill.) leads to the conclusion that the balloon is rotating with this approximate period.

The assumptions which provide the basis for the calculation of balloon orientation are as follows:

(a) the balloon has a stable orientation in inertial space;

(b) the motion of the balloon across the sky causes only second order changes in the results during the interval of a single spin period (see Appendix A where this effect is discussed);

(c) smoothing of the distance between successive double maxima of the beacon data to obtain an average angular distance between them can be used.

As discussed in Appendix A, the method of calculation yields numerical results for three different physical parameters but suffers from an inherent disadvantage that one of the three, spin axis orientation, can be determined only up to an ambiguity. The results of the calculation are as follows:

(a) angle between beacon maxima, 153.2^{o}.

(b) displacement of beacon antenna from spin equator, 1.8^{o}.

(c) spin axis orientation, one of the two following orientations.

Declination	Right Ascension
-1.0^{o}	329.2^{o}
$+81.3^{o}$	23.6^{o}

Each of these points determines a vector to the celestial sphere which is either parallel or anti-parallel to the spin axis of the balloon.

6.0 COMMUNICATIONS

6.1 Quantitative Results

Quantitative questions have been examined in connection with the effect of variations in the ECHO II radar cross sections in the functional use of the balloon as a passive communications satellite. The findings depend upon present understanding of the statistical properties of the radar cross section.

On the basis of computations performed below, using typical system parameters, it is concluded that:

(a) Fading rates (in carrier power) are unacceptable for high quality communication at UHF, marginally acceptable at 2000 MC and acceptable at 5000 MC. In practical terms this means that the ECHO II is suitable for frequency modulated transmission at carrier frequencies greater than 2000 MC.

(b) Radar cross section scintillation of the ECHO II introduces noise into the information channel for amplitude modulated signals. For amplitude modulated voice transmission this noise can be expected to significantly degrade quality, whereas for telegraphic or slow data rate communication, the noise can be expected to be negligible.

(c) Although the radar data is monostatic (receiver and transmitter at same location) it can be used to predict bistatic communication performance (receiver and transmitter separated).

For a high quality speech transmission, with a 20-KC bandwidth, the following system parameters have been postulated:

Noise temperature - $1000^{\circ}K$
Signal/Noise Figure - 25 db
Antenna diameter (receiver and transmitting) - 60 ft
Transmitting power - 1 KW
Modulation - F.M.

If σ_m is the minimum balloon cross section required to obtain the 25 db signal/noise figure,

$$\sigma_m \sim 10^3 \lambda^2,$$

where λ is the wavelength of the carrier. For a 40-foot antenna this number would be multiplied by 9/4. This gives the table:

Carrier Frequency	$\frac{\sigma_{min}}{\sigma_o}$ (60-ft antenna)	$\frac{\sigma_{min}}{\sigma_o}$ (40-ft antenna)
300 MC	- 1.2 db	+ 2.3 db
2000 MC	- 17.7 db	- 14.2 db
5000 MC	- 25.6 db	- 22.1 db

Minimal $\frac{\sigma_{min}}{\sigma_o}$ to achieve 25 db signal/noise ratio ($\sigma_o = 1320\ m^2$) at 1 KW transmission.

From this table, the fading rate (percentage of time the balloon cross section is less than σ_{min}) can be computed, assuming that A = 6. (A is defined in 4.2 below):

Carrier Frequency	Fading rate (60 ft antenna)	Fading rate (40 ft antenna)
300 MC	76 percent	90 percent
2000 MC	3 percent	8 percent
5000 MC	.05 percent	.5 percent

The value A = 6 used in these computations is conservative. From data observed, A, in general will be smaller, giving lower fading rates.

6.2 Radar Cross Section Statistics

The data obtained for a run of length T provides a record of the cross section, $\sigma(t)$, as a function of time. The mean cross section σ_o, is defined as:

$$\sigma_o = \frac{1}{T} \int_0^T \sigma(t)\, dt \quad .$$

Let $f = \sigma(t)/\sigma_o$. Regarding f as a random variable, the mean value of f, $\langle f \rangle$, is clearly unity, and the variance of f, $V_f = \langle f^2 \rangle - 1$.

If the cross section is recorded on a db scale, the recorded quantity is 10 log f.

It is assumed that the random variable, 10 log f, is normally distributed with mean m and variance A^2. This assumption is not inconsistent with the observed data.

It is then a simple matter to obtain the following relationships:

$$m = -10 \log \sqrt{\langle f^2 \rangle} = -\frac{\ell n\ 10}{20} A^2 \sim -.115\, A^2.$$

These relationships enable one to find any two of the quantities, m, A, V_f, from the third.

On the basis of data received, both in the flight test and in the static inflation tests, typical values of A are 3 at the lower frequencies and 6 at the higher frequencies, giving corresponding values for m of -1 db and -3 db.

The cumulative probability distribution for f is

$$\Phi\left(\frac{10 \log x - m}{A}\right) \qquad x > 0$$

$$0 \qquad x \leq 0 \quad ,$$

where

$$\Phi(u) = \frac{1}{\sqrt{2\pi}} \int_{-\infty}^{u} e^{-\frac{t^2}{2}}\, dt.$$

6.3 Fading Rate

For a particular receiver sensitivity the minimal acceptable received power is specified. If the power and gain of the transmitting system, the effective aperture of the receiver antenna, and the trajectory of the ECHO II are given, then by using the radar equation,

$$P_r = \frac{P_t G A_r}{16\pi^2 R_t^2 R_r^2} \sigma \quad ,$$

this received power requirement can be translated into a minimal acceptable value of σ, σ_m · σ_m, of course, varies, depending on the variables R_t and R_r, the respective distances from the balloon to the transmitter and receiver. For a particular value of σ_m, the fading rate is the probability that $\sigma < \sigma_m$, or equivalently, that $f < \sigma_m/\sigma_o$, which from section 4.2, is

$$\Phi\left(\frac{10 \log \frac{\sigma_m}{\sigma_o} + .115 A^2}{A}\right) .$$

The fading rate can be interpreted as the percentage of time that the received power is less than the minimal acceptable value.

If, for example, it is desired to have a fading rate < .01, it is necessary that

$$\Phi\left(\frac{10 \text{ lot } \frac{\sigma_m}{\sigma_o} + .115 A^2}{A}\right) < .01, \text{ or}$$

$$- 10 \log \frac{\sigma_m}{\sigma_o} > .115 A^2 + 2.4 A .$$

If A = 5, σ_m must be 15 db below σ_o. When this value is inserted into the radar equation the minimal value of P_t can be determined. If A = 3, σ_m need be only 6 db below σ_o. Therefore, going from A = 5 to A = 3 causes a 9 db reduction in the necessary transmitter power, for a fading rate < .01.

6.4 Signal Modulation by the Balloon

Because the radar data determines the amplitude, but not the phase, of a reflected signal, discussion of balloon modulation has been limited to amplitude modulated signals.

The wave form of an amplitude modulated signal can be represented as

$$1 + s(t)$$

where s(t) is the modulation waveform which is the information carrying signal. If there is no further modulation by the transmission path, the

waveform arriving at the receiver is unchanged and the detected waveform will be

$$s(t) + n(t),$$

where $n(t)$ is the noise of the receiver system. This picture changes when the transmission path modulates the signal.

In particular, after reflection by the balloon, the waveform arriving at the receiver is

$$(1 + s(t)) \quad \frac{\sigma(t)}{\sigma_o} = [1 + s(t)] \sqrt{f}.$$

The modulation waveform is therefore

$$s(t) \sqrt{f} + (\sqrt{f} - 1) = s(t) + (1 + s(t)) (\sqrt{f} - 1)$$

The detected signal is then

$$s(t) + (1 + s(t)) (\sqrt{f} - 1) + n(t).$$

The term $N(t) = (1 + s(t)) (\sqrt{f} - 1)$ is noise which has been added to the information carrying signal $s(t)$. If the signal ensemble is specified, s is a random variable. Then $N(t)$ is a random variable whose distribution can be determined on the basis of the following fact:

If F, G are independent random variables with probability densities, respectively $D_F(x)$, $D_G(x)$, then the probability density for the random variable F G is

$$D_{FG}(x) = \int_{-\infty}^{\infty} D_F(y)\, D_G\left(\frac{x}{y}\right) dy$$

Thus, since in 4.1 we have determined the distributed function for f and hence for $\sqrt{f} - 1$, it is possible to find the distribution function for N. The average noise power is then the expected value

$$\langle N^2 \rangle = \langle (1 + s)^2 (\sqrt{f} - 1)^2 \rangle \quad ,$$

and the signal to noise ratio

$$\frac{\langle S^2 \rangle}{\langle N^2 \rangle} \quad ,$$

is the highest possible signal to noise ratio, even if the system noise is zero.

We have computed this ratio for two different signal ensembles:

(a) s is uniformly distributed over the range $-P \leq x \leq P$, where $0 \leq P \leq 1$, P representing the modulation percentage. In this case

$$\frac{\langle S^2 \rangle}{\langle N^2 \rangle} = \frac{1}{16 A^2} \quad \frac{p^2}{1 + p^2} \times 10^4$$

For A = 5, this ratio is approximately 12 for P = 1 and 6 for $P = \frac{1}{2}$.

For A = 3, the value of the ratio is approximately 33 for P = 1 and 16 for $P = \frac{1}{2}$.

(b) s = 0 and -1 with equal probability (keyed CW transmission). In this case,

$$\frac{\langle S^2 \rangle}{\langle N^2 \rangle} \sim \frac{3}{2} \quad \frac{10^4}{A^2} \quad .$$

Here even for A = 10, the ratio is 150.

6.5 Bistatic Effects

It should be observed that the values of σ obtained during the ECHO II flight tests are monostatic; corresponding to receiver and transmitter being at the same location. On the other hand, for communications purposes, the receiver and transmitter are separated; the appropriate σ is the bistatic

cross section. In earlier work it was determined that for bistatic angles $\leq 30^{\circ}$, and for frequencies > 170 MC, the bistatic cross section can be obtained from the monostatic cross section. In the Static Inflation Tests, the radar cross sections obtained by bistatic measurements were found to correlate with the monostatic radar cross section computed on the basis of photogrammetric measurements, thus verifying the earlier analysis. For lower frequencies and larger bistatic angles it is estimated that the radar cross section statistics, obtained by monostatic radar measurements are applicable to bistatic angles of at least 90°, and for frequencies greater than 100 MC.

7.0 CONCLUSIONS

The radar portion of the flight test experiment monitored the cross section of ECHO II as a function of time. As a result of physical inspection of the analog data and of processing of the available digital data, it is possible to offer at this time conclusions concerning the balloon - its quality as a passive communication satellite, and the degree of success of the earlier theoretical and experimental programs in predicting these properties.

7.1 Physical Description of ECHO II

The following conclusions are advanced:

(a) The balloon inflated to a generally spherical shape having approximately the design radius of 67.5 feet.

(b) The sphere has many minor perturbations in its shape and at least one major deformation, as is evidenced by the marked drop in cross section shown in Figure 4-1. The radar data is consistent with this major deformation being a wedge-like bulge near a beacon. The scintillations of the return obtained by processing the usable data have an average (over 13 runs) standard deviation of 5.73 db at C-band and standard deviations of 4.80, 6.56, and 4.19 db for three L-band runs.

(c) The balloon is spinning with a period varying about 100 seconds. The beacons are located approximately in a plane at an angle of 1.8° with the spin equator.

7.2 Effectiveness as a Communication Satellite

With the data obtained and the radar cross section statistics derivable from this data it is possible to estimate the effectiveness of ECHO II as a communications satellite as is shown in Section 4.0. For typical system parameters relative to high quality audio transmission (20 kc bandwidth), at a carrier frequency of 5000 MC a fading rate of 0.05 percent is predicted to be a reliable communications satellite for frequency modulated signals at frequencies greater than 2000 MC.

7.3 Anomalies

Drop out exhibited in the radar cross section data can be examined in terms of minor geometric perturbations of the balloon surface. Other explanations which have been offered; in particular,

(a) plasma effects
(b) holes in the balloon
(c) multi-pathing

have been examined in quantitative detail and are inconsistent with either the data or with well established physical laws.

7.4 Comparison with Previous Work

Previous work discussed in Volume I of the Final Report consisted of ground testing of small segments of ECHO II material and of theoretical extrapolation as a result of these tests to a full scale balloon and was a valid predictive device for determination of flight performance. Correlation among small segment measurements, full scale static inflation test measurements, theoretical predictions on the basis of photogrammetric measurements, and actual flight test measurements was extremely high.

7.5 Short Duration, Large Amplitude Scintillations

The flight data exhibits one effect which is difficult to explain on the basis of around test results. This is the existence in the time dependent radar cross section patterns of short duration scintillations of up to 15 or 20 db. Because of their short duration (often of the same order as that of typical recording pen recovery speeds, i.e., about 1/8 second) these scintillations have little effect on the radar cross section statistics. These large amplitude scintillations can be seen on Figure 6-1, especially after time 16-20-40.

REFERENCES

1. "Final Report - Phase B," Report No. 0038-B-F, Conductron Corporation.

2. "Six Months Summary Report on ECHO II Data Reduction and Analysis," Report 0038-6-T, Conductron Corporation, 10 August 1964.

3. R. F. Julian, D. P. Hynek, "Cross Section Measurements of the ECHO II Satellite by the Millstone L-Band Radar," Group Report 1964-16, Lincoln Laboratory, 7 April 1964.

4. H. Cramer, "Mathematical Methods of Statistics," Princeton University Press, 1957.

8.0 GLOSSARY OF TECHNICAL TERMS

8.1 Statistics

Mean: The average or arithmetic mean of a set of values is obtained by dividing the sum of the values by the number of values.

Median: The median of a set of values is that value which divides the set so that an equal number of items occurs on either side of that value.

Standard Deviation: The standard deviation gives an indication of the spread of a set of values such as RCS and is defined mathematically as:

$$\left[\sum_{i=1}^{n} (X_i - \bar{X})^2 \right]^{1/2}$$

where X_i are the values, n the number of values, and $\bar{X}$ the mean of the set of values.

Geometric Mean: The geometric mean of a set of n values is the n^{th} root of the product of the values and is defined mathematically as:

$\sqrt[n]{X_1 \cdot X_2 \ldots X_n}$, where X_i are the values.

Variance: The variance of a set of values is the square of the standard deviation.

Frequency Distribution: The frequency distribution of a set of values or observations is a table giving for each value the corresponding number of observations. The probability function of a set of values or observations is similar to a frequency

distribution and is a table giving for each value the corresponding number of observations divided by the total number of observations.

Histogram: A histogram is a graphical representation of a frequency distribution. Rectangles are formed which have the interval used to segregate the observations as the base and frequency of observations in the internal as height. Equal areas represent equal frequencies.

Normal Distribution: The standard normal or gaussian distribution is defined as follows: the probability that the quantity Y is less than or equal to X (Prob $(Y \leq X)$) is defined as:

$$\int_{-\infty}^{X} \exp\left(\frac{-\mu^2}{2}\right) d\mu,$$

which has a mean of zero and a standard deviation of 1.

Log-Normal Distribution: The quantity X is said to have a log-normal distribution if log X is normal or gaussian distributed; that is, if X is of the form e^Y, where Y is normal.

Chi-Square (X^2) Test: This is a statistical test used to determine how closely a distribution with a given mean and standard deviation is approximated by a normal or gaussian distribution with the same mean and standard deviation.

Auto-Correlation: The auto-correlation of a function, f(t), is defined as:

$$\lim_{T\to\infty} \frac{1}{T} \int_{-T/2}^{T/2} f(t)\, f(t+\tau)\, dt,$$

and is a function of the lag τ. If for a lag τ the value of the auto-correlation function is positive and large relative to the value for $\tau = 0$, this indicates the function, $f(t)$, is periodic with period τ.

Power Spectrum: The power spectrum of a function, $f(t)$, is the Fourier transform of the auto-correlation and is a measure of the contribution to the variance of the function by given frequency components.

8.2 Radar

Radar Cross Section: The radar cross section of an object is the ratio of the total reflected electromagnetic energy which is being emitted by a radar. The radar cross section depends on the relative orientations of the object and the radar and also whether the radar transmitter and receiver are at the same location. A simplified form of the radar equation is:

$$P = \frac{K\sigma}{R^4},$$

where,

P = received power in watts, W,
K = radar coefficient in NM^4 W/M^2,
σ = radar cross section in square meters, M^2,

R = range in nautical miles, NM.

Monostatic Cross Section: The cross section of an object when the transmitting and receiving antennas of the radar are at the same location is called the monostatic cross section.

Bistatic Cross Section: The cross section of an object when the transmitting and receiving antennas of the radar are physically separated is called the bistatic cross section.

Gain: The antenna gain is a measure of the power radiated in a particular direction by a directive antenna to the power which would have been radiated in the same direction by an omni-directional antenna with 100 percent efficiency.

Polarization: The direction of polarization of an antenna is defined as the direction of the electric field vector. Most radar antennas are linearly polarized; that is, the direction of the electric field vector is either vertical or horizontal. The polarization may also be elliptical or circular if the direction of the electric field vector varies with time.

Scintillation: In practice the returned radar signal from a target in motion is almost never constant. Variations in the returned signal may be caused by large variations in the radar cross section or by small perturbations of radar cross section, meteorological conditions, the lobe structure of the antenna pattern, or equipment instabilities. Variations in returned

signal due to the last four causes are called scintillation.

Signal to Noise Ratio: The ratio of the power returned from the target to the power received from all other sources, such as receiver noise and background noise picked up by the receiving antenna, is called the signal-to-noise ratio.

Fading Rate: The fading rate is the percentage of time that the received power is less than the minimum acceptable value.

Frequency (or wavelength) Bands:

VHF -- 30 MC to 300 MC (1 m to 10m)
UHF -- 300 MC to 1000 MC (1 m to 15 m)
L-band -- 1000 MC to 2000 MC (15 cm to 30 cm)
S-band -- 2000 MC to 4000 MC (7.5 cm to 15 cm)
C-band -- 4000 MC to 8000 MC (7.5 cm to --)
X-band -- 8000 MC to 12,500 MC (2.4 cm to 3.75cm)

Specular Point: The specular point on a reflecting body, for a monostatic radar, has its surface normal vector pointing directly at the radar; for a bistatic radar, the surface normal vector of the specular point bisects the angle made by the transmitter and receiver at the surface of the body.

Rayleigh Scattering: Rayleigh scattering is a type of reflection where the dimensions of the reflecting object are small compared to the wavelength of the incident electromagnetic energy, $(2\pi a/\lambda \ll 1)$, where a is the characteristic dimension of the object and λ is the radar wavelength. The phenomenon is named after Lord Rayleigh,

and the reflecting objects are called Rayleigh scatterers.

$db > m^2$ — This symbol stands for decibels relative to a square meter. If A is the area of an object in square meters, then $10 \log_{10} A$ is the area in decibels above a square meter.

Gyration Radius: The gyration radius of an electron is the radius, measured perpendicular to the magnetic field lines, of the spiral which describes the path of the electron while moving through the magnetic field:

$$R = \frac{mv}{eB}$$

APPENDIX A

SATELLITE ORIENTATION

Introduction

The problems to be considered in this report are the determination of the location of the two beacon antennas of ECHO II relative to the spin axis of the balloon, and the orientation of that spin axis in space. In solving for these properties, still another quantity must be found - the beam spread angle of the two beacons (assumed to be identical). The information utilized in solving for these quantities comes from a record of the signal intensity received versus time for each beacon at a fixed point on the earth's surface.

Method

I-A. Input Data

The precise antenna pattern of the beacons is not known. However, a reasonable assumption is that the pattern is cylindrically symmetric about the direction of the monopole antenna[1]. A cross section of the antenna pattern on any plane which includes the antenna will then appear as in Figure 1. The angle β between the maxima of the two lobes on this cross section is what we call the Antenna Spread Angle. An observer viewing the balloon from a distance will receive the strongest signal from this beacon whenever he is on the conical surface whose axis of symmetry is along the monopole antenna and whose angle from the axis is $\beta/2$.

If the satellite were fixed in space, but spinning, the signal received by an observer would appear similar in shape to that shown in Figure 2, where $t_3 - t_1$ is the spin period, provided the beacon antenna at its point of closest approach to the observer makes an angle of less than $\beta/2$. If this angle of closest approach is greater than $\beta/2$, only a single maximum will occur during each spin period. The present calculation uses information which is present only in records of the type portrayed in Figure 2, and thus only observations which give this shape are considered here.

---

1. See Footnote 1.

Let us consider a large spherical surface concentric with the balloon, whose north-south axis lies along the balloon spin axis. If this surface rotates with the same angular velocity as the balloon, the direction of maximum signal strength from each beacon can be represented as a stationary circle on the surface - namely, the intersection with the spherical surface of a conical surface whose apex is the center of the sphere, whose axis of symmetry lies along the antenna, and whose central angle is $\beta/2$. The straight line connecting the observer and the satellite intercepts the spherical surface at some point along a circle of constant latitude, tracing this complete circle once each revolution of the balloon about its spin axis. The latitude of this Observer Circle is determined by the direction of the observer relative to the spin axis. Figure 3 shows how this spherical surface, with the Observer Circle and Beam Maximum Circle, might look to someone situated directly over the north pole of the surface, for an orientation capable of providing the observer with a beacon signal like that of Figure 2.

The points of intersection of the Observer Circle with the Beam Maximum Circle correspond to the times t_1 and t_2 of Figure 2. The angular distance α along the Observer Circle between these two points is the angle rotated by the balloon in the time interval $t_2 - t_1$. Since the spin period is $t_3 - t_1$,

$$\frac{\alpha}{2\pi} = \frac{t_2 - t_1}{t_3 - t_1} \qquad (1)$$

It is this angle α which serves as the input for our solution.[2]

Since we have four unknowns - the two quantities required to specify the direction of the spin axis, plus the Antenna Spread Angle and the angle from spin axis to the beacon - four quantities such as α are required to determine the solution. Since there are two beacons on the balloon, virtually

2. See Footnote 2.

identical, but distinguishable on account of frequency, we may, if the orientation is right, obtain two values of α, α_{11} for beacon 1 and α_{21}, for beacon 2, from a single pass. Another pass, with a different orientation between observer and spin axis, provides us with two more values, α_{12} and α_{22}. However, we now must relate these four values of α to one another. α_{11} and α_{21} share a common Observer Circle, with their Beam Maximum Circles diametrically opposed. The same is true of α_{12} and α_{22}, but with a different Observer Circle. Finally, if the direction of the satellite from the observer for each observation is known, these two points determine the length and direction in absolute celestial coordinates of an arc of a great circle connecting the observer circle of pass 1 with that of pass 2.

I-B. Method of Calculation

Since our input is the angular distance α of Figure 3, we need to see how this quantity is related to the size of the Observer Circle and of the Beam Maximum Circle, and their relative positions. Let us then take two known circles on the surface of a sphere, and calculate the angle α determined by their intersections. The Observer Circle "0", with its center on the vertical axis, subtends an angle θ_o (i.e., is at the latitude $\frac{\pi}{2} - \theta_o$). The Beam Maximum Circle "B" has its center on a line which is displaced by an angular distance δ from the vertical axis, and subtends an angle $\frac{\beta}{2}$. Figure 4 shows the projection of these circles onto the plane containing the centers of both circles and the center of the spherical surface upon which they are drawn.

If the vertical axis is chosen to be the z direction, then the two circles intersect when their z components are equal. The Observer Circle is in the plane of constant z, whose value is

$$z_o = \cos \theta_o \qquad (2)$$

For the Beam Maximum Circle, let us define a position angle φ_B (see Figure 3) measured at the center of the circle, with its zero position occurring when the radius vector lies in the plane of Figure 4. The z component of circle B is thus

$$z_B = \cos\delta \cos\frac{\beta}{2} + \sin\delta \sin\frac{\beta}{2} \cos\varphi_B \tag{3}$$

When the two circles intersect, $z_B = z_o$, and this equation determines a particular value of φ_B, which we call φ_1:

$$\cos\varphi_1 = \frac{\cos\theta_o - \cos\delta \cos\frac{\beta}{2}}{\sin\delta \sin\frac{\beta}{2}} \tag{4}$$

The angular distance between the two points of intersection, measured at the center of circle 0, is α. The two circles have radii

$$\begin{aligned} r_o &= \sin\theta_o \\ r_B &= \sin\frac{\beta}{2} \end{aligned} \tag{5}$$

respectively (See Figure 4). The linear distance between the two points of intersection is $2\, r_1 \sin\varphi_1$ or $2\, r_0 \sin\frac{\alpha}{2}$. Setting these two expressions equal, we find

$$\sin\frac{\alpha}{2} = \frac{r_1}{r_0}\sin\varphi_1 = \frac{\sin\frac{\beta}{2}}{\sin\theta_0}\sin\varphi_1 \tag{6}$$

Thus

$$\cos\alpha = 1 - 2\sin^2\frac{\alpha}{2} = 1 - 2\frac{\sin^2\frac{\beta}{2}}{\sin^2\theta_0}\left[1 - \cos^2\varphi_1\right] \tag{7}$$

and by combining equations (4) and (7), we obtain

$$\cos\alpha = \frac{2\cos^2\frac{\beta}{2} + \cos^2\delta\cos^2\theta_0 - \sin^2\delta + \cos^2\theta_0 - 4\cos\theta_0\cos\delta\cos\frac{\beta}{2}}{\sin^2\delta\sin^2\theta_0} \tag{8}$$

In order to make the calculation, we must have four values of α, labeled α_{11}, α_{21}, α_{12}, α_{22} as defined in Section I-A. Each of the Beam Maximum Circles subtends the same angle $\frac{\beta}{2}$, but there are two values of δ: δ_1 for

beacon 1 and δ_2 for beacon 2. Since we know, however, that the beacon antennas are diametrically opposed,

$$\delta_2 = \pi - \delta_1 \tag{9}$$

Finally, we have two Observer Circles θ_1 and θ_2. Thus we begin with four equations similar to Equation 8. Utilizing the relationships (9), these are

$$\cos \alpha_{11} = \frac{2 \cos^2 \frac{\beta}{2} + \cos^2 \delta_1 \cos^2 \theta_1 - \sin^2 \delta_1 + \cos^2 \theta_1 - 4 \cos \delta_1 \cos \frac{\beta}{2} \cos \theta_1}{\sin^2 \delta_1 \sin^2 \theta_1} \tag{10a}$$

$$\cos \alpha_{12} = \frac{2 \cos^2 \frac{\beta}{2} + \cos^2 \delta_1 \cos^2 \theta_2 - \sin^2 \delta_1 + \cos^2 \theta_2 - 4 \cos \delta_1 \cos \frac{\beta}{2} \cos \theta_2}{\sin^2 \delta_1 \sin^2 \theta_2} \tag{10b}$$

$$\cos \alpha_{21} = \frac{2 \cos^2 \frac{\beta}{2} + \cos^2 \delta_1 \cos^2 \theta_1 - \sin^2 \delta_1 + \cos^2 \theta_1 + 4 \cos \delta_1 \cos \frac{\beta}{2} \cos \theta_1}{\sin^2 \delta_1 \sin^2 \theta_1} \tag{10c}$$

$$\cos \alpha_{22} = \frac{2 \cos^2 \frac{\beta}{2} + \cos^2 \delta_1 \cos^2 \theta_2 - \sin^2 \delta_1 + \cos^2 \theta_2 + 4 \cos \delta_1 \cos \frac{\beta}{2} \cos \theta_2}{\sin^2 \delta_1 \sin^2 \theta_2} \tag{10d}$$

One other piece of data required is the change in viewing aspect between the two passes. This quantity is needed in order to fix the orientation in space of the spin axis of the balloon. The two lines from the observer to the satellite are stationary in the absolute coordinate system, and since they intersect at the center of the balloon, define a plane. The portion of this plane between the two observer lines intersects the spherical surface concentric with the satellite in an arc of a great circle. If the latitudes of the two Observer Circles are known, then the length γ of this arc enables us to calculate the spherical angle between this arc and the arc connecting the spin axis with one of the observer lines. This spherical angle, ζ, is shown in Figure 5. From spherical trigonometry,

$$\cos \zeta = \frac{\cos \theta_2 - \cos \gamma \cos \theta_1}{\sin \gamma \sin \theta_1} \tag{11}$$

We therefore have five unknown quantities, β, δ_1, θ_1, θ_2, and ζ, and five input quantities: α_{11}, α_{12}, α_{21}, α_{22}, and γ. Our system of equations (10a), (10b), (10c), (10d), and (11) is thus sufficient to provide a solution.

I-C. Equations

To simplify the appearance of our equations, let us eliminate the trigonometric functions by defining

$x_1 = \cos \theta_1$

$x_2 = \cos \theta_2$

$w = \cos \zeta$

$y = \cos \frac{\beta}{2}$

$z = \cos \delta_1$

$A_{11} = \cos \alpha_{11}$

$A_{12} = \cos \alpha_{12}$

$A_{21} = \cos \alpha_{21}$

$A_{22} = \cos \alpha_{22}$

$G = \cos \gamma$

Our initial equations (10a) through (10d) and (11) become

$$A_{11} = \frac{x_1^2 (1 + z^2) + (2 y^2 + z^2 - 1) - 4 yzx_1}{(1 - z^2) (1 - x_1^2)} \tag{12a}$$

$$A_{12} = \frac{x_2^2 (1 + z^2) + (2 y^2 + z^2 - 1) - 4 yzx_2}{(1 - z^2) (1 - x_2^2)} \tag{12b}$$

$$A_{21} = \frac{x_1^2 (1 + z^2) + (2 y^2 + z^2 - 1) + 4 yzx_1}{(1 - z^2) (1 - x_1^2)} \tag{12c}$$

$$A_{22} = \frac{x_2^2 (1 + z^2) + (2 y^2 + z^2 - 1) + 4 yzx_2}{(1 - z^2) (1 - x_2^2)} \tag{12d}$$

$$w = \frac{x_2 - G x_1}{\sqrt{1 - G^2} \sqrt{1 - x_1^2}} \tag{12e}$$

The first four of these equations must be solved as a set to determine x_1, x_2, y, and z. The last equation (12e), however, may be solved separately for w after x_1 and x_2 have been obtained. The four equation set (12a) through (12d) becomes easier to work with if we define the new input quantities

$$\begin{aligned} C_1 &= \tfrac{1}{2}\,[A_{11} + A_{21}] \\ C_2 &= \tfrac{1}{2}\,[A_{12} + A_{22}] \\ D_1 &= \tfrac{1}{2}\,[A_{21} - A_{11}] \\ D_2 &= \tfrac{1}{2}\,[A_{22} - A_{12}] \end{aligned} \tag{13}$$

With these definitions, we have

$$C_1 = \frac{(1 + z^2)\, x_1^{\,2} + (2\, y^2 + z^2 - 1)}{(1 - z^2)\,(1 - x_1^{\,2})} \tag{14a}$$

$$C_2 = \frac{(1 + z^2)\, x_2^{\,2} + (2\, y^2 + z^2 - 1)}{(1 - z^2)\,(1 - x_2^{\,2})} \tag{14b}$$

$$D_1 = \frac{4\, y\, z\, x_1}{(1 - z^2)\,(1 - x_1^{\,2})} \tag{14c}$$

$$D_2 = \frac{4\, y\, z\, x_2}{(1 - z^2)\,(1 - x_2^{\,2})} \tag{14d}$$

Equation (14a) can be reworked to give

$$x_1 = \left[\frac{C_1\,(1 - z^2) + (1 - z^2 - 2\, y^2)}{C_1\,(1 - z^2) + (1 + z^2)} \right]^{\frac{1}{2}} \tag{15}$$

while from equation (14c), we obtain

$$x_1 = \frac{D_1\,(1 - z^2)\,(z^2 + y^2)}{2\, yz\, [C_1\,(1 - z^2) + (1 + z^2)]} \tag{16}$$

Squaring equations (15) and (16), and setting them equal, we have

$$C_1 (1 - z^2) + (1 - z^2 - 2 y^2) = \frac{D_1^2 (1 - z^2)^2 (z^2 + y^2)^2}{4 y^2 z^2 [C_1 (1 - z^2) + (1 + z^2)]} \qquad (17)$$

Similarly, from equations (14b) and (14d), we get

$$C_2 (1 - z^2) + (1 - z^2 - 2 y^2) = \frac{D_2^2 (1 - z^2)^2 (z^2 + y^2)^2}{4 y^2 z^2 [C_2 (1 - z^2) + (1 + z^2)]} \qquad (18)$$

Equations (17) and (18) are now two equations in two unknowns; x_1 and x_2 have been eliminated. We may further eliminate y to obtain a single equation in z by the following procedure.

Let $v = 1 - z^2 = \sin^2 \delta_1$. Now equations (17) and (18) may be written as

$$\frac{1}{D_1^2} [C_1 v + v - 2 y^2] [C_1 v - v + 2] = \frac{v^2 [1 + y^2 - v]}{4 y^2 (1 - v)} \qquad (19a)$$

$$\frac{1}{D_2^2} [C_2 v + v - 2 y^2] [C_2 v - v + 2] = \frac{v^2 [1 + y^2 - v]}{4 y^2 (1 - v)} \qquad (19b)$$

Subtracting (19b) from (19a), and solving for y^2, we obtain

$$y^2 = \frac{[D_2^2 (C_1^2 - 1) - D_1^2 (C_2^2 - 1)] v + 2 [D_2^2 (C_1 + 1) - D_1^2 (C_2 + 1)]}{[D_2^2 (C_1 - 1) - D_1^2 (C_2 - 1)] v + 2 [D_2^2 - D_1^2]} \frac{v}{2} \qquad (20)$$

To keep the algebra from getting completely out of hand, we define the following four quantities:

$$a = D_2^2 (C_1^2 - 1) - D_1^2 (C_2^2 - 1)$$

$$b = D_2^2 (C_1 + 1) - D_1^2 (C_2 + 1)$$

$$c = D_2^2 (C_1 - 1) - D_1^2 (C_2 - 1)$$

$$d = D_2^2 - D_1^2$$

Now equation (20) becomes

$$y^2 = \left(\frac{av + 2b}{cv + 2d}\right)\left(\frac{v}{2}\right) \tag{21}$$

After substituting this value of y^2 back into equation (19a), and doing a large amount of algebraic manipulation, we obtain a quartic equation in v:

$$Av^4 + Bv^3 + Cv^2 + Dv + E = 0 \tag{22}$$

where the coefficients A, B, C, D, and E are purely functions of the input parameters -

$$A = -2ac\,(C_1^2 - 1) + 2a^2\,(C_1 - 1) + 1/4\,[a\,(4c - a) - 4c^2]\,D_1^2 \tag{23a}$$

$$B = 2\,[ac - 2ad - 2bc]\,(C_1^2 - 1) + 2a\,(4b-a)\,(C_1 -1) - 4ac\,(C_1+1) + 4a^2 + [2c\,(c + b - 2d) + a\,(2d - c - b)]\,D_1^2 \tag{23b}$$

$$C = 4\,[ad + b\,(c - 2d)\,]\,(C_1^2-1) + 8b\,(b-a)\,(C_1 - 1) + 4\,[ac - 2bc - 2ad]\,(C_1 + 1) + 4a\,(4b - a) + [2d\,(4c - 2d - a + 2b) - c^2 - 2bc - b^2]\,D_1^2 \tag{23c}$$

$$D = 8\,bd\,(C_1^2 - 1) - 8b^2\,(C_1 - 1) + 8\,[ad + bc - 2bd]\,(C_1 + 1) + 16b\,(b - a) + 4\,[d\,(2d - c - b)\,]\,D_1^2 \tag{23d}$$

$$E = 16\,bd\,(C_1 + 1) - 16b^2 - 4d^2\,D_1^2 \tag{23e}$$

From the four input quantities α_{11}, α_{12}, α_{21}, and α_{22}, a program for the IBM 1620 computer calculates these five coefficients. A root finding program for the same computer then obtains the possible values of v (i.e., solutions of equation 22). There are four such solutions, but only values of v between zero and one are allowable, from the definition of v. The value (or values) satisfying this condition are then plugged back into equation 21 to obtain a value of y. These values are then used with equation (15) or (16) to obtain x_1, and with the analogous equation to find x_2.

From the value of y and z we obtain directly the antenna spread angle β and the angular distance δ_1 from the spin axis to the beacon. From the quantities x_1 and x_2 we may find the orientation of the spin axis in space.

I-D. Orientation

The celestial coordinate system is defined relative to the earth. If we assume a large spherical surface to be centered on the earth, spatial orientations may be designated as the intersection on this sphere of the radius vector which is parallel to the given direction. The extension along the earth's spin axis of its north pole intersects this sphere to form the celestial north pole, and the celestial equatorial plane is coincident with the earth's equatorial plane. Let us imagine a set of longitude semi-circles and latitude circles drawn upon this sphere. Then the radius vector from the earth to the sun at the vernal equinox intersects the sphere at the point of zero declination and zero right ascension. The latitude circles, labeled as on earth from zero at the equator to 90° at the pole, are loci of constant declination; conventionally, north declinations are positive and south declinations are negative. The longitude semi-circles are loci of constant right ascension; the values increase from zero to 360° as one progresses eastward (counter-clockwise as viewed from the north pole) from the zero position.

The local observer's coordinate system is defined by his zenith and the local north. Positions are given in this coordinate system as an angle of elevation and an angle of azimuth. Elevation is measured positive upward from the horizon, with 90° elevation being directly overhead. Azimuth angles are measured from the local north clockwise about the zenith as an axis; for example, directly east is 90° azimuth, south is 180°, and west, 270°.

Transformation from the observer's coordinate system into celestial coordinate system can be made by taking into account the observer's longitude and latitude, the time of day, and the time of year of the observation.

These factors may be incorporated into a transformation matrix which multiplies the vector representing the direction of observation. The resulting vector represents the direction of observation in the celestial coordinate system. By transforming both observation directions into vectors in the celestial coordinate system, a common reference system for the two observations is obtained. The angle between these two vectors is the angle γ of equation (11).

The quantities x_1 and x_2 are the cosines of the angles between the spin axis of the satellite and the first and second observation vectors, respectively. If the observation vectors are expressed as $(a_1\vec{i} + b_1\vec{j} + c_1\vec{k})$ and $(a_2\vec{i} + b_2\vec{j} + c_2\vec{k})$, and the spin axis as $(S_1\vec{i} + S_2\vec{j} + S_3\vec{k})$ in the celestial coordinate system (suitably defined for cartesian coordinates), then

$$a_1S_1 + b_1S_2 + c_1S_3 = x_1 \tag{24a}$$

$$a_2S_1 + b_2S_2 + c_2S_3 = x_2 \tag{24b}$$

and, since $\vec{S}$ is a unit vector,

$$S_1^2 + S_2^2 + S_3^2 = 1 \tag{25}$$

These three equations suffice to solve for the three unknowns S_1, S_2, and S_3, which then define the orientation of the spin axis.

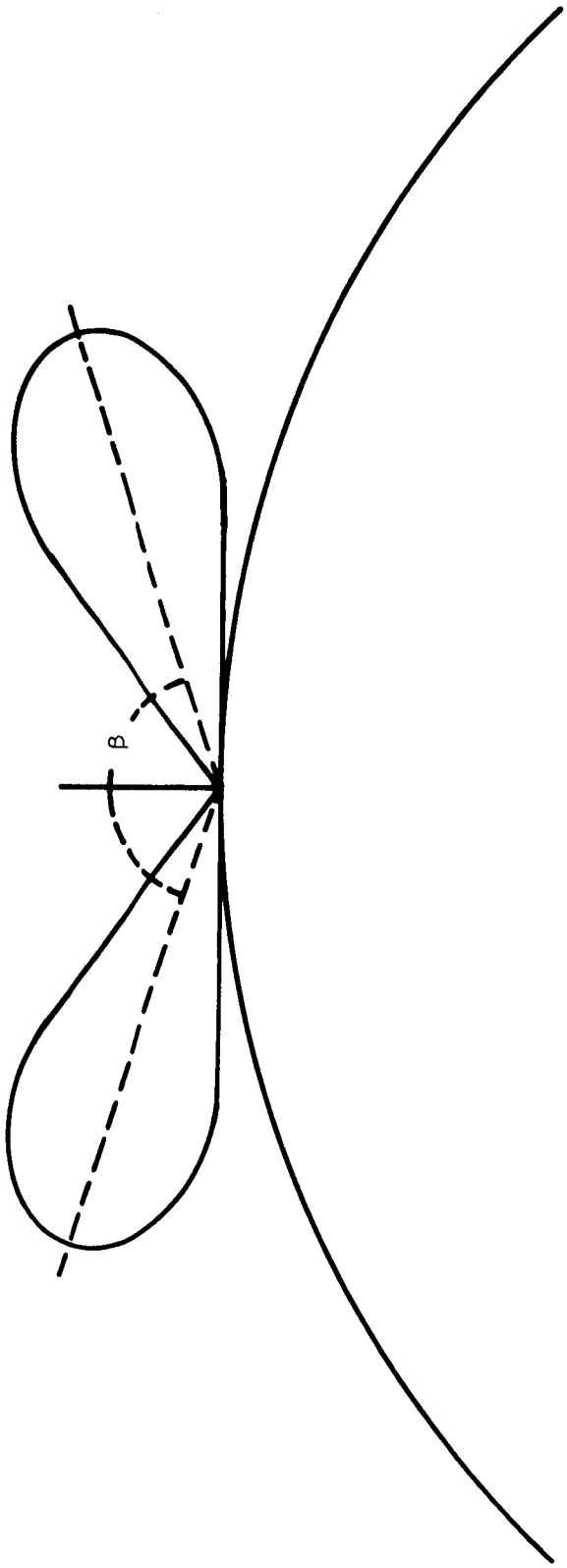

FIGURE 1

FIGURE 2

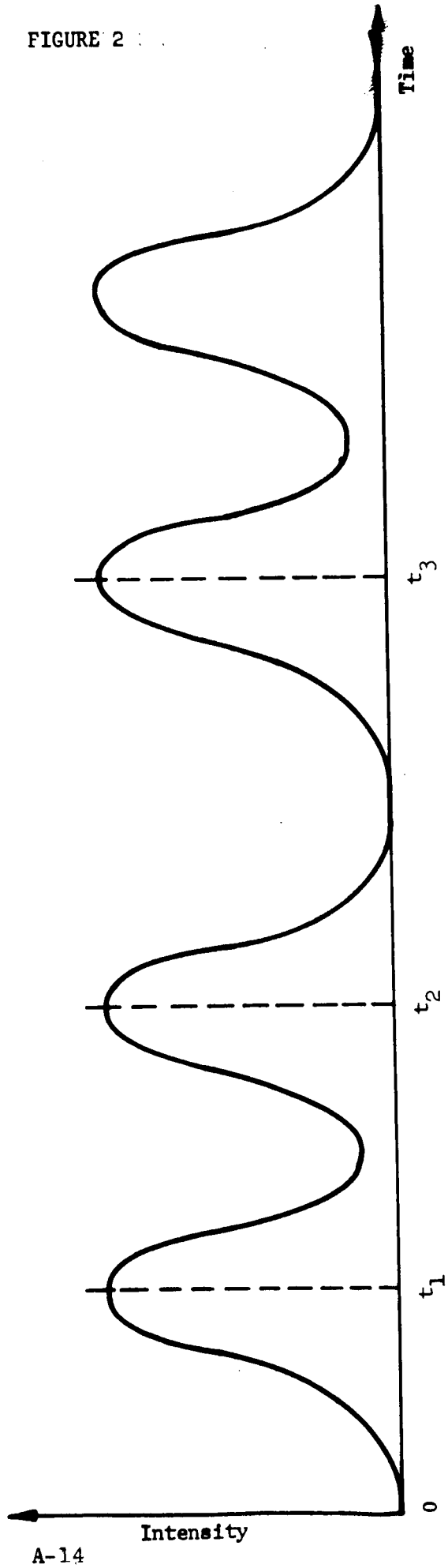

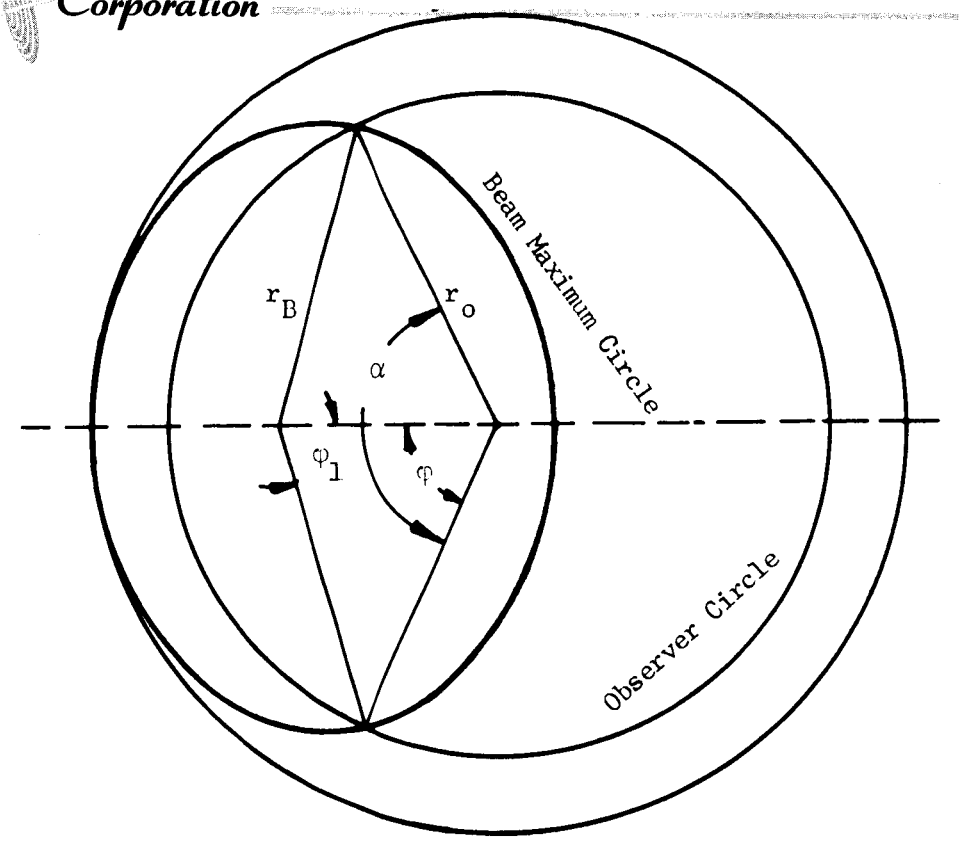

FIGURE 3

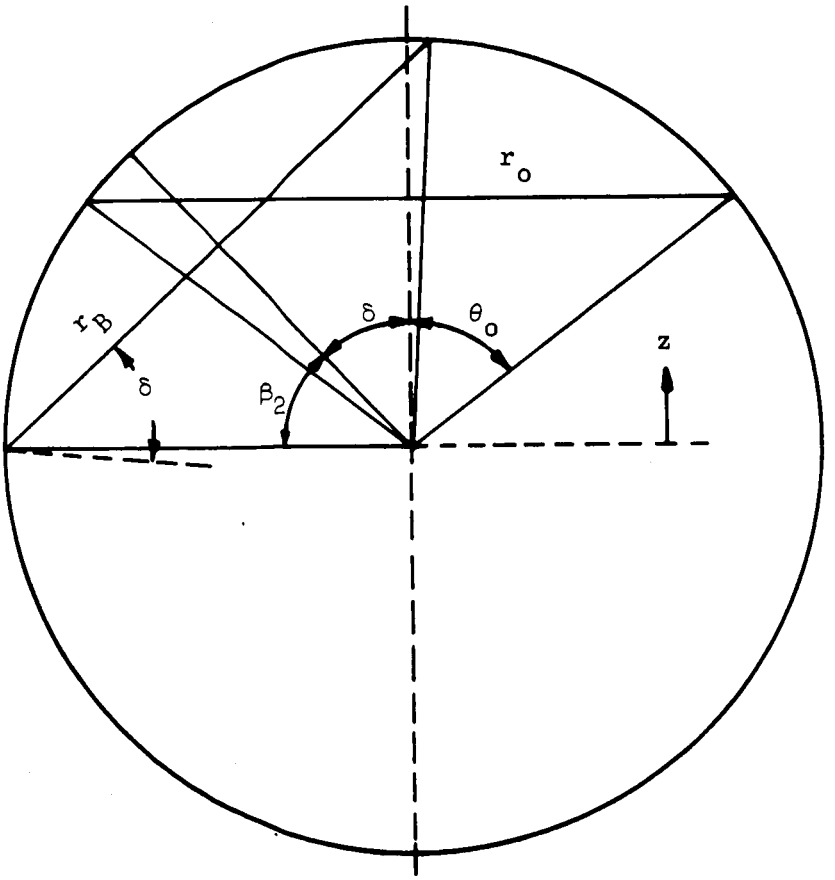

FIGURE 4

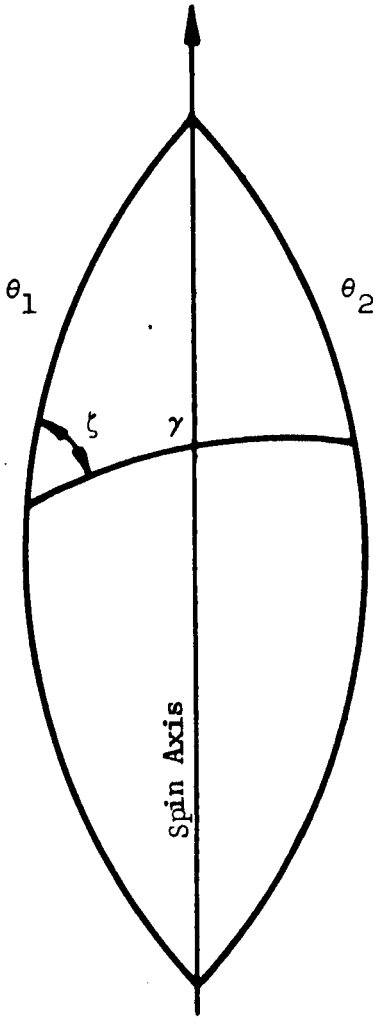

FIGURE 5

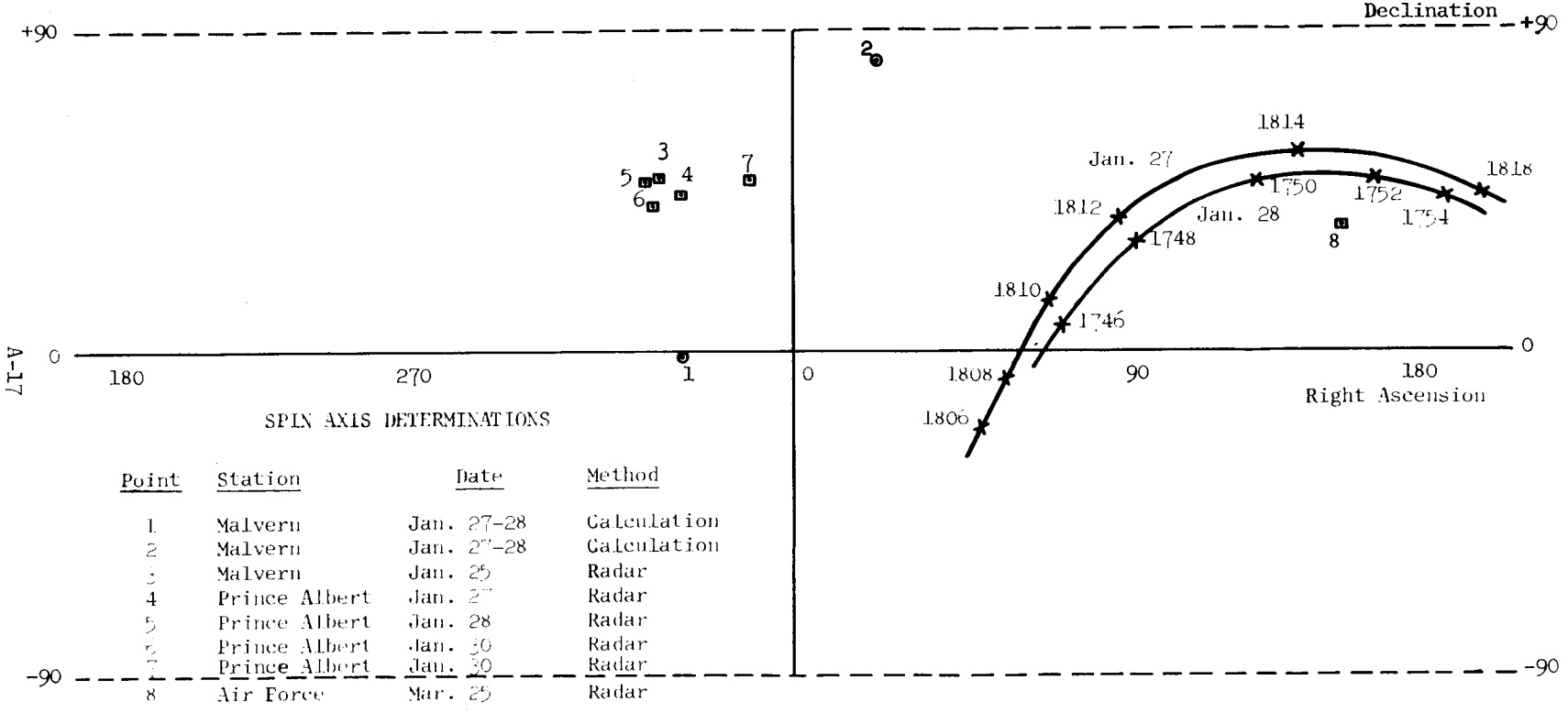

SPIN AXIS DETERMINATIONS

Point	Station	Date	Method
1	Malvern	Jan. 27-28	Calculation
2	Malvern	Jan. 27-28	Calculation
3	Malvern	Jan. 25	Radar
4	Prince Albert	Jan. 27	Radar
5	Prince Albert	Jan. 28	Radar
6	Prince Albert	Jan. 30	Radar
7	Prince Albert	Jan. 30	Radar
8	Air Force	Mar. 25	Radar

Figure 4 Spin Axis Determinations And Malvern Flight Paths

II Results

The information taken from the records of beacon signal strength is the ratio expressed by equation (1). On the available beacon records, the signal peaks are fairly irregular, so that the proper choice of t_1, t_2, and t_3 is not readily apparent.

The observations used in the analysis were made from Malvern, England which has the coordinates:

$$52^{\circ}08' \ 04.07'' \quad N,$$
$$02^{\circ}19' \ 57.23'' \quad W.$$

The times, directions of the satellite from the receiving station, and the measured peak-to-peak angles are,

Date	Time	Elevation	Azimuth	Beacon 1	Beacon 2
Jan 27, 1964	1808	26.65°	153.83°	153.2°	153.2°
Jan 28, 1964	1752	20.37°	33.95°	146.8°	140.0°

Thus we have,

$$\alpha_{11} = 153.2^{\circ},$$
$$\alpha_{12} = 146.8^{\circ},$$
$$\alpha_{21} = 153.2^{\circ},$$
$$\alpha_{22} = 140.0^{\circ}.$$

We note that this causes the quantity D_1 (see equation 13) to be zero. With this quantity zero, the algebraic manipulation of equations (16) to (23) no longer applies. However, a fairly simple reworking of equation (14) allows a solution to be found as follows. From (14c), we have $x_1 = 0$, indicating that the spin axis was perpendicular to the first line of observation. The remaining equations, (14a), (14b), and (14d) were solved for x_2, y, and z with the following results:

$$x_1 = 0.000,$$

$$x_2 = 0.660,$$

$$y = 0.232,$$

$$z = 0.031.$$

From the values of y and z, the antenna spread angle is determined,

$$\beta = 2 \cos^{-1} (.232) = 153.2^{o},$$

and the beacon antennas are located at an angle,

$$\delta_1 = \cos^{-1} (.031) = 88.2^{o},$$

from the spin axis, or 1.8^{o} from the spin equator. The angles between the spin axis and the viewing directions were found to be,

$$\theta_1 = 90.0^{o},$$

$$\theta_2 = 48.7^{o}.$$

Equations (24a) and (24b) define two circles in the celestial coordinate system. These circles have two intersections, which turn out to be the directions,

-1.0^{o} declination, 329.2^{o} right ascension,

and

81.3^{o} declination, 23.6^{o} right ascension.

III Discussion

Several observers have noted that occasionally the radar signal reflected off the ECHO II balloon satellite seems to become very smooth for a few seconds, then returns to its normal character. A group of five such occasions have been reported for the period from 27 January to 30 January 1964. When the direction of view of the radar for each occasion is plotted in the celestial coordinate system, it is noted that all the vectors lie quite close to one another. The smoothing out of the signal is assumed to be caused by the radar looking up the spin axis of the satellite. If this occurs, then for a short period the portion of the satellite serving as a reflector does not change. If this explanation is true, then the spin axis was somewhere in a region centered about a declination of 45^{o} and a right ascension of 325^{o} during the period 27-30 January.

A rather interesting effect was noted in the Malvern recording of the beacon data for January 25, 1964. At about 2051 hours on that date, the beacon signal (in the one channel producing a readable signal at that time) departed from its characteristic two-humped appearance to produce, instead, three consecutive humps, followed by a return to the two-humped regime. The first and second humps (of the three) appear to be in proper progression with the pairs of humps preceding them, while the second and third humps are in the proper paired relationship for the pairs following them. Thus this three-peaked region appears to be the intersection of two distinct sets of data. The best explanation for this occurrence is that the spin axis, at that instant, pointed approximately at the receiving station. The fact that the same station shows a smoothing out of the radar return at that same time provides further verification of this explanation. The direction of the satellite from Malvern at this time was 49.80^{o} declination, and 319.87^{o} right ascension.

Figure 6 is a plot in celestial coordinates of the paths followed by ECHO II as seen from Malvern for the two passes used as input data in the

calculations. Also indicated are the viewing vectors for six times when the radar data smoothed out, and the two spin axis orientations calculated in Section II. Points 1 and 2 are the calculated portions. Point 3 is the direction of view from Malvern on January 25, discussed above. Points 4, 5, 6, and 7 are from radar returns from the Prince Albert, Canada, station on January 27, 28, and 30 (two points). Point 8 is an Air Force indication from late March.

It should not be too surprising that the points calculated in Section II fail to agree closely with the radar indications of the spin axis orientation. The beacon signal records were such that it was difficult to estimate the times t_1, t_2, and t_3 closer than one or two seconds. But each second is 3.6^o rotation about the spin axis, so that errors of between 4^o and 7^o in the α's are not unlikely. Since the differences in these angles are only 7^o to 14^o, the resulting answers can only be approximate. For example, it would not be difficult to interpret the records as giving $\alpha_{11} = \alpha_{12} = \alpha_{21} = \alpha_{22}$, with the value somewhere between 140^o and 160^o. In this case, the orientation calculation would have shown a point at about 42^o declination and 327^o right ascension, which is quite close to the other points.

The antenna parameters, δ_1 and β, appear to be fairly insensitive to errors in the values of the α's. The antenna spread angle β is almost certainly $\beta = 150^o \pm 10^o$, and very likely $\beta = 152^o \pm 5^o$. The values of z seem always to be quite close to zero, so that we may reasonably assume the beacon to lie within 5^o of the spin equator. It is this latter condition which causes trouble in the calculation of the orientation of the spin axis, especially if the viewing vectors themselves come close to the spin equator of the satellite.

FOOTNOTES

1. A calculation (Reference 1) performed at Conductron has found that even if the surface of the balloon is warped, so that the antenna does not point radially away from the center of the satellite, the antenna pattern will still be cylindrically symmetrical about this radial line, but with less of a null on or near the radial direction.

2. For simplicity, the effects of the motion across the sky of the satellite have been neglected. This motion is not large during the interval of a single spin period. The effects of motion in the plane perpendicular to the spin axis should be only second order, since this motion will, to first order, increase or decrease both the quantities $t_2 - t_1$, and $t_3 - t_1$ by the same factor, which cancels out of equation (1). Motion in the direction of the spin axis causes the Observer Circle to become a spiral. If the ratio of equation (1) remains fairly nearly constant over several periods of revolution, we may conclude distance between adjacent terms of this spiral is small, and it is a good approximation to a circle for any one period. Such a condition appears to hold for the observations which are used in this calculation.

REFERENCE

1. J. Clark, "Radiation Pattern of a Tilted Monopole", 30 March 1964, D-0620-208-M, Appendix A to Monthly Progress Report No. 2, ECHO II, Flight Test Data Reduction and Analysis, 038-2-P, 22 February 1964 through 22 March 1964, Conductron Corporation.

APPENDIX B

EFFECT OF PUNCTURES ON THE RADAR CROSS SECTION OF ECHO II

B.1 Introduction

The radar data collected thus far on the ECHO II satellite exhibits deep fading in signal level during an orbital pass. In an effort to explain this fading, some observers have speculated that a large hole was punched in the surface of the balloon during the ejection sequence.

In order to evaluate this hypothesis, Conductron Corporation initiated a theoretical analysis of the effect of a puncture on the radar cross section of ECHO II. The results of this study are presented in this Appendix. These results indicate that it is unlikely that the presence of a puncture would perturb the radar return enough to account for the observed fading.

B.2 Scattering From A Conducting Spherical Shell With A Circular Hole

The purpose of this discussion is to give an approximate method of solution to the problem of the scattering of electromagnetic waves from a sphere with a circular hole. The essence of the method is to treat the sphere and the rim of the hole separately, and to add their contributions to the scattered field in phase. For this procedure to be valid, we must require that both the sphere and the hole be large compared with the wavelength of the illuminating radiation, i.e.,

$$ka \gg 1, \quad ka' \gg 1,$$

where a is the radius of the sphere, a' is the radius of the rim of the hole and $k = 2\pi/\lambda$.

In what follows, the case of a puncture in one side of the sphere is worked out in detail. Other cases involving multiple holes can be treated by combining the component returns derived below with the proper phase.

B.2.1 Nose-On Backscattering

In this case, the incident radiation is perpendicular to the plane determined by the rim of the hole (See Figure B-1).

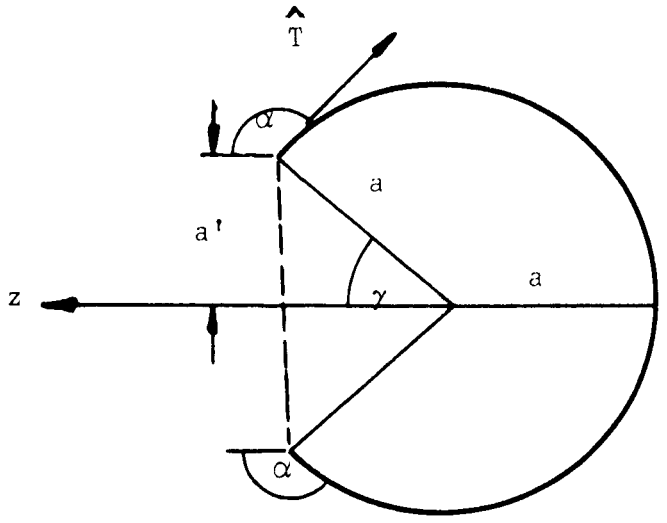

Figure B-1

Balloon Cross Section Showing Incidence Along Axis of Hole

The sphere will contribute to the scattered field primarily by the specular reflection from the back of the sphere opposite the mouth of the hole.

The specular return can be obtained from physical optics and in the far zone (Reference 1) is,

$$\vec{E}^{s} = -\vec{E}^{inc} \left(\frac{a}{2r}\right) e^{ikr + 2ika} , \qquad (1)$$

$$\vec{H}^{s} = \vec{H}^{inc} \left(\frac{a}{2r}\right) e^{ikr + 2ika} , \qquad (2)$$

where, in the usual case, the origin is taken at the center of the sphere. The negative sign results from the shift in phase that the electric vector undergoes upon a reflection from a metallic boundary.

The main part of this discussion will consist of a derivation of the field diffracted by the rim of the hole. The contribution from the rim is obtained from the Sommerfeld solution of the diffraction of electromagnetic waves from a half plane (See Appendix C), by considering each element of the rim as a small element of half plane, computing the field diffracted by this element, and then adding up all such contributions.

In the case of backscattering, the half plane answer given by Sommerfeld is,

$$\vec{E}^{\text{diffracted}}_{\parallel} = \frac{e^{i(kr + \pi/4)}}{2\sqrt{2\pi\, kr}} \left(1 - 1/\cos\alpha\right) \vec{E}^{\text{inc}}_{\parallel} \quad , \tag{3}$$

where $\vec{E}^{\text{inc}}_{\parallel}$ is the component of the incident E vector which is parallel to the edge; and,

$$\vec{H}^{\text{diffracted}}_{\parallel} = \frac{e^{i(kr + \pi/4)}}{2\sqrt{2\pi\, kr}} \left(1 + 1/\cos\alpha\right) \vec{H}^{\text{inc}}_{\parallel} \quad , \tag{4}$$

where $\vec{H}^{\text{inc}}_{\parallel}$ is the component of the incident H vector which is parallel to the edge. The angle between the edge and the direction of propagation is α and r is the distance from the edge. (Figure B-2)

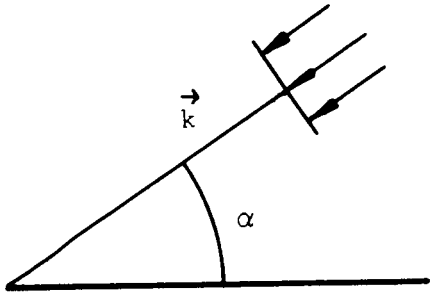

Figure B-2
Edge Geometry

The $e^{ikr}/\sqrt{kr}$ dependence shows these fields are those of an infinite line source. This fact is helpful in evaluating the contribution from a differential element of half plane. We recall that a line source is obtained by integrating a point source,

$$\frac{e^{ikR}}{R} \text{, where } R = \sqrt{x^2 + y^2 + z^2} = \sqrt{r^2 + z^2} \quad ,$$

over a line of infinite length. Assuming k is large we may use the stationary phase formula

$$\int g(x)\, e^{ikf(x)}\, dx \sim g(x_o) \sqrt{\frac{2\pi i}{kf''(x_o)}}\, e^{ikf(x_o)} \quad , \tag{5}$$

where

$$f'(x_o) = 0 \quad ,$$

$$f''(x_o) \neq 0 \quad ,$$

and evaluate the integral of a point source over an infinite line, i.e.,

$$\int_{-\infty}^{\infty} \frac{e^{ik\sqrt{r^2 + z^2}}}{\sqrt{r^2 + z^2}} dz \approx \sqrt{\frac{2\pi i}{kr}} e^{ikr} = \frac{\sqrt{2\pi}}{\sqrt{kr}} e^{i(kr + \pi/4)} \quad .$$

Thus, we obtain the Sommerfeld answer by integrating a certain distribution of a point source,

$$C \frac{e^{ikR}}{R} \quad ,$$

where C is a constant over the edge of the half plane. This yields,

$$\int_{-\infty}^{\infty} C \frac{e^{ikR}}{R} dz \approx C \frac{\sqrt{2\pi}}{\sqrt{kr}} e^{i(kr + \pi/4)} \quad .$$

In the parallel E polarization case,

$$C = C_{\parallel} = \frac{1}{4\pi} (1 - 1/\cos \alpha) \quad , \tag{6}$$

and in the orthogonal case,

$$C = C_{\perp} = \frac{1}{4\pi} (1 + 1/\cos \alpha) \quad . \tag{7}$$

On the other hand, an infinitesimal line source corresponds to integrating a point source over a differential length dL; since dL is small this gives just the length of the interval dL multiplied by the integrand evaluated somewhere in the range of integration, which we may take to be an end point.

$$\int_0^{dL} \frac{e^{ikR}}{R} dz \approx dL \left. \frac{e^{ikR}}{R} \right|_{z = 0} = dL \frac{e^{ikr}}{r} \quad .$$

Thus, we see that the field diffracted from a differential element of half-space is of the form,

$$\frac{dL}{4\pi} \frac{e^{ikr}}{r} \quad (1 \pm 1/\cos \alpha) \quad . \tag{8}$$

Let us set up a polar coordinate system in the plane determined by the rim as shown in Figure B-3.

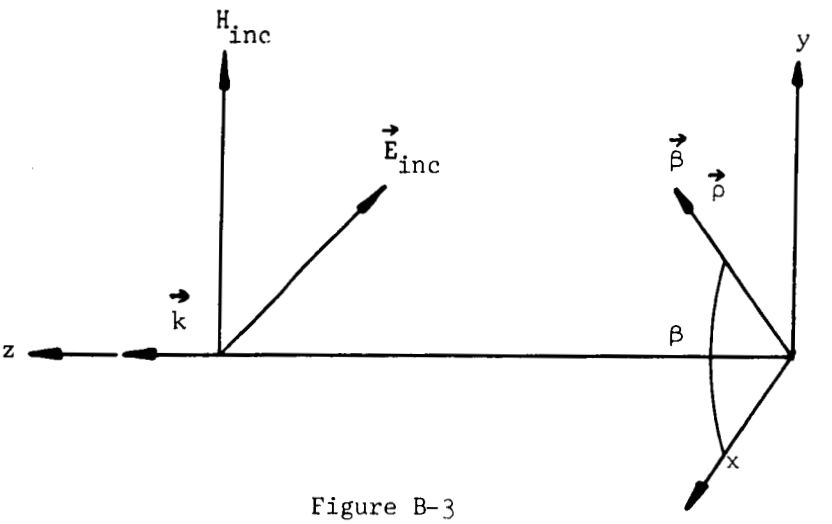

Figure B-3
Geometry for Axial Incidence

In this figure,

$$\vec{\beta} = \vec{i}_x \sin \beta - \vec{i}_y \cos \beta \quad , \tag{9}$$

is a unit vector tangent to the rim of the hole at the angle β and,

$$\vec{\rho} = -\vec{i}_x \cos \beta - \vec{i}_y \sin \beta \quad , \tag{10}$$

is a unit vector perpendicular to the rim.

The element of length of the rim a' $d\beta$ gives rise to a diffracted field $dE(\beta)$ which is contained in the plane perpendicular to the propagation vector $\vec{k}$, that is the plane determined by the rim.

How much of each type of diffracted field is present depends on the polarization of the incident radiation and on the constants $C_{\parallel}$ and $C_{\perp}$.

The components of $\vec{E}^{inc}$ and $\vec{H}^{inc}$ which are parallel to $\vec{\beta}$ are,

$$\vec{E}^{inc}_{\parallel} = (\vec{E}^{inc} \cdot \hat{\beta})\,\hat{\beta} \quad , \tag{11}$$

and

$$\vec{H}^{inc}_{\parallel} = (\vec{H}^{inc} \cdot \hat{\beta})\,\hat{\beta} \quad . \tag{12}$$

We define $\vec{E}^{inc}_{\perp}$ to be the component of the incident electric field which corresponds to $\vec{H}^{inc}_{\parallel}$ and defines $\vec{E}^{diff}_{\perp}$ to be the component of the diffracted electric field corresponding to $\vec{H}^{diff}_{\parallel}$. Since,

$$\vec{E}^{inc} \times \vec{H}^{inc} = \vec{-k} \quad , \tag{13}$$

and

$$\vec{E}^{diff} \times \vec{H}^{diff} = \vec{k}, \tag{14}$$

it follows that,

$$\vec{E}^{inc} = -(\vec{H}^{inc} \times \vec{k}), \quad \vec{H}^{inc} = \vec{E}^{inc} \times \vec{k} \quad , \tag{15}$$

$$\vec{E}^{diff} = \vec{H}^{diff} \times \vec{k} \quad ,$$

and, in particular,

$$\vec{E}^{inc}_{\perp} = -(\vec{H}^{inc}_{\parallel} \times \vec{k}) = \vec{k} \times \vec{H}^{inc}_{\parallel} = (\vec{k} \times \vec{\beta})(\vec{H}^{inc} \cdot \vec{\beta})$$

$$= (\vec{k} \times \vec{\beta})(\vec{E}^{inc} \times \vec{k}) \cdot \vec{\beta} \quad , \tag{16}$$

and,

$$\vec{E}^{diff}_{\perp} = \vec{H}^{diff}_{\parallel} \times \vec{k} = \vec{-k} \times \vec{H}^{diff}_{\parallel} \quad . \tag{17}$$

Now,

$$\vec{E}^{diff} = \vec{E}^{diff}_{\parallel} + \vec{E}^{diff}_{\perp} \quad , \tag{18}$$

where,

$$\vec{E}^{diff}_{\parallel} = \frac{e^{ikr}}{r} \int \vec{E}^{inc}_{\parallel}\, C_{\parallel}\, dL \quad , \tag{19}$$

and,

$$\vec{E}_{\perp}^{diff} = \vec{-k} \times \vec{H}_{\parallel}^{diff} = \vec{-k} \times \frac{e^{ikr}}{r} \int \vec{C}_{\perp} \vec{H}_{\parallel}^{inc} \, dL \qquad (20)$$

$$= \frac{e^{ikr}}{r} \int C_{\perp} (\vec{-k} \times \vec{H}_{\parallel}^{inc}) \, dL$$

$$= \frac{e^{ikr}}{r} \int C_{\perp} \vec{E}_{\perp}^{inc} \, dL$$

$$= \frac{-e^{ikr}}{r} \int C_{\perp} (\vec{E}^{inc} \times \vec{k}) \cdot \vec{\beta} \, (\vec{k} \times \vec{\beta}) \, dL$$

Hence,

$$\vec{E}^{diff} = \frac{e^{ikr}}{r} \int \left\{ C_{\parallel} (\vec{E}_{inc} \cdot \vec{\beta}) \vec{\beta} - C_{\perp} (\vec{E}_{inc} \times \vec{k}) \cdot \vec{\beta} \, (\vec{k} \times \vec{\beta}) \right\} dL \qquad (21)$$

Substituting for $C_{\parallel}$ and $C_{\perp}$ their values given in (6) and (7) and for dL, its equivalent $\alpha'\, d\beta$, we get,

$$E^{diff} = \frac{a' e^{ikr}}{4\pi r} \int \left\{ (1 - \frac{1}{\cos \alpha})(\vec{E}_{inc} \cdot \vec{\beta}) \vec{\beta} - (1 + \frac{1}{\cos \alpha})(\vec{E}_{inc} \times \vec{k}) \cdot \vec{\beta} \, (\vec{k} \times \vec{\beta}) \right\} d\beta \, . \qquad (22)$$

For the nose-on case, $\vec{k} = \vec{i}_z$, and, without loss of generality we may take $\vec{E}^{inc} = -\vec{i}_x$. In this case, α is constant and is equal to $\pi/2 + \gamma$. Substituting for $\vec{\beta}$ and $\vec{\rho}$ from (9) and (10), Equation (22) can easily be evaluated giving,

$$\vec{E}^{diff} = \frac{a' e^{ikr} \vec{i}_x}{2r \cos \alpha} = \frac{a' e^{ikr}}{2r \sin \gamma} \vec{E}_{inc} \, . \qquad (23)$$

Then, adding to this result the specular return from the back of the sphere, the total scattered field nose-on is,

$$\vec{E}^{s} = -\left(\frac{a}{2r} e^{ikr} - \frac{a'}{2r} \frac{e^{ikr}}{\sin \gamma} e^{2i\delta}\right) \vec{E}^{inc} \, , \qquad (24)$$

where δ, the difference in phase between the specular point and the rim of the hole, is determined from the formula,

$$\delta = \vec{k} \cdot \vec{D} \quad ,$$

D being the distance between the contributors.

Since the propagation vector $\vec{k}$ is in the z direction, a glance at Figure A-1 shows,

$$\delta = k\,(a + a \cos \gamma) \quad .$$

Finally using $a' = a \sin \gamma$, we find for the scattered field,

$$\vec{E}^{s} = \frac{-a}{2r}\, e^{ikr} \left[1 + e^{2ika\,(1 + \cos \gamma)} \right] \vec{E}^{inc} \quad , \tag{25}$$

and thus, the nose-on radar cross section is,

$$\sigma = 2\pi a^{2} \left[1 + \cos 2\ ka\,(1 + \cos \gamma) \right] \tag{26}$$

From this expression it is evident that (for axial incidence) phase interference can occur, giving rise to fading. The presence (or absence) of this fading is quite sensitive to the frequency of the illuminating radar, and to the relative distances between contributors.

If, for example, we consider a sphere radius a = 70', a hole radius a' = 10', and an L band frequency (say 1300 mc). We see that ka' is of the order of 560 and ka' is of the order of 80. Thus the two contributions go in and out of phase very rapidly. For fading to occur over an extended period of time, we will see that the balloon must retain an aspect stability such that $2\,ka' \sin \theta \ll \frac{\pi}{4}$, or $\theta \ll \frac{1}{3}^{o}$, and that the relative distances stay constant to a precision of less than a $\frac{1}{4}$ wave length, i.e., 2". For higher frequencies the angle is smaller and the precision requirement on the relative distances is even finer.

B.2.2 Off-Nose-On Backscattering

As before, the field is obtained by integrating the contributions,

$$C_{\parallel} \frac{e^{i\vec{k} \cdot \vec{R}}}{R} \quad ,$$

and

$$C_{\perp} \frac{e^{i\vec{k} \cdot \vec{R}}}{R} \quad ,$$

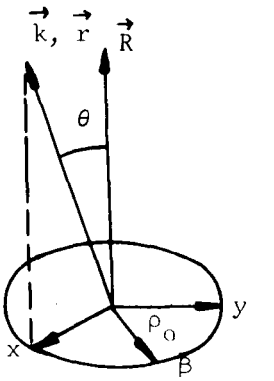

Figure B-4
Geometry for Off-Axis Incidence

Now, however, the wave vector $\vec{k}$ is not perpendicular to the plane defined by the rim, and several alterations in our method are necessary.

A. The contributors from the arc elements $a' \, d\beta$ will not add in phase. Let $\vec{R} = \vec{r} + \vec{\rho}$, where $\vec{r}$ is the distance to the receiver from the center of the hole ($\vec{r}$ is parallel to $\vec{k}$) and $\vec{\rho}$ is the distance from the center of the hole to the rim,

$$\vec{\rho} = a' \cos \beta \, \vec{i}_x + a' \sin \beta \, \vec{i}_y \quad .$$

Let the x-axis be determined by the projection of $\vec{k}$ on the plane defined by the rim, and measure the angle β from the x-axis. The propagation vector, $\vec{k}$, makes an angle θ with the perpendicular to the plane of the rim,

$$\vec{k} = (\vec{i}_x \sin \theta + \vec{i}_z \cos \theta) \, k \quad .$$

The incident radiation is in the direction $-\vec{k}$. Thus,

$$\frac{e^{i\vec{k} \cdot \vec{R}}}{R} = \frac{e^{ikr} \, e^{i\vec{k} \cdot \vec{\rho}}}{R} \approx \frac{e^{ikr}}{r} \, e^{i\vec{k} \cdot \vec{\rho}} \quad ,$$

in the far field, where,

$$|\vec{r}| \gg |\vec{\rho}| \quad .$$

B. The angle α, which appears in $C_{\parallel}$ and $C_{\perp}$ is now a function of β, (See Figure B-1) and,

$$\cos \alpha = \vec{k} \cdot \vec{T} \quad , \tag{27}$$

where $\vec{T}$ is a unit vector in the tangent plane to the sphere, perpendicular to the rim,

$$\vec{T} = \cos \gamma \cos \beta \, \vec{i}_x + \cos \gamma \sin \beta \, \vec{i}_y - \sin \gamma \, \vec{i}_z \quad , \tag{28}$$

yielding,

$$\cos \alpha = \cos \theta \cos \gamma \cos \beta - \cos \theta \sin \gamma \quad . \tag{29}$$

C. The backscattered diffracted field vectors must be contained in a plane perpendicular to the propagation vector $\vec{k}$. As before, for each element of the rim, the $\vec{E}^{diff}$ field will consist of two components, one arising from $\vec{E}^{inc}_{\parallel}$ and one from $\vec{H}^{inc}_{\parallel}$. These quantities are as defined in Equations (11) and (12), and, in fact, all the relations (13) - (18) hold in both nose-on and off-nose-on as cases. Equation (19), however, yields an $\vec{E}^{diff}_{\parallel}$ which is in the plane of the hole, and in the off-nose-on case, since this plane is not perpendicular to $\vec{k}$, we take the projection of this component on such a plane. (The $\vec{E}^{diff}$ component is in the $\vec{k} \times \vec{\beta}$ direction in either case; see Equation (20)).

We define $\vec{\beta}_o$, the projection of $\vec{\beta}$ on the plane perpendicular to $\vec{k}$, as follows:

$$\vec{\beta}_o = \vec{\beta} - (\vec{\beta} \cdot \vec{k}) \vec{k} = |\vec{\beta}_o| \, \vec{\beta}_o = [1 - (\vec{k} \cdot \vec{\beta})^2]^{1/2} \vec{\beta}_o \quad . \tag{30}$$

Then, replacing (19) by

$$\vec{E}^{diff}_{\parallel} = \frac{e^{ikr}}{r} \int e^{i\vec{k}\cdot\vec{\rho}} (\vec{E}^{inc}\cdot\vec{\beta}_o)\vec{\beta}_o \, dL$$

$$= \frac{e^{ikr}}{r} \int e^{i\vec{k}\cdot\vec{\rho}} [(\vec{E}^{inc}\cdot\vec{\beta})\vec{\beta}]\cdot\vec{\beta}_o\vec{\beta}_o \, dL$$

$$= \frac{e^{ikr}}{r} \int e^{i\vec{k}\cdot\vec{\rho}} (\vec{E}^{inc}\cdot\vec{\beta})(\vec{\beta}\cdot\vec{\beta}_o)\vec{\beta}_o \, dL \quad , \qquad (31)$$

we can write again,

$$\vec{E}^{diff} = \vec{E}^{diff}_{\parallel} + \vec{E}^{diff}_{\perp} \quad .$$

With these modifications, the derivation of the expression for $\vec{E}^{diff}$ follows closely the one for Equation (22) in the nose-on case, and yields,

$$\vec{E}^{diff} = \frac{a' e^{ikr}}{4\pi r} \int_0^{2\pi} e^{i\vec{k}\cdot\vec{\rho}} \left(1 - \frac{1}{\cos\alpha}\right) (\vec{E}_{inc}\cdot\vec{\beta})(\vec{\beta}\cdot\vec{\beta}_o)\vec{\beta}_o$$

$$- \left(1 + \frac{1}{\cos\alpha}\right) (\vec{E}_{inc} \times \vec{k})\cdot\vec{\beta}\,(\vec{k}\times\vec{\beta}) \, d\beta \quad . \qquad (32)$$

Some slight manipulation yields the further simplification,

$$\vec{E}^{diff} = \frac{a' e^{ikr}}{4\pi r} \int_0^{2\pi} e^{i\vec{k}\cdot\vec{\rho}} \left(1 - \frac{1}{\cos\alpha}\right) (\vec{E}^{inc}\cdot\vec{\beta}_o)\vec{\beta}_o$$

$$- \left(1 + \frac{1}{\cos\alpha}\right) (\vec{E}_{inc} \times \vec{k})\cdot\vec{\beta}_o\,(\vec{k}\times\vec{\beta}_o) \, d\beta \quad , \qquad (33)$$

which is Equation (22) with $\vec{\beta}$ replaced by $\vec{\beta}_o$.

This integral is difficult to evaluate exactly. However, since the wavelength is short, and in particular $ka' \gg 1$, we ex pect the major contributions will come from the places where the phase is stationary. Since,

$$\vec{k}\cdot\vec{\rho} = ka' \sin\theta\cos\beta \quad ,$$

$$\frac{d}{d\beta}(\vec{k}\cdot\vec{\rho}) = -ka \sin\theta \sin\beta \quad ,$$

there will be two stationary phase points, one at $\beta = 0$, the other at $\beta = \pi$. Thus, evaluating $\vec{k}\cdot\vec{\rho}$, and,

$$\frac{d^2(\vec{k}\cdot\vec{\rho})}{d\beta^2} = -ka' \sin\theta\cos\beta$$

at each of these points, we can approximate the integral by,

$$\vec{E}^{diff} \approx \frac{a' e^{ikr}}{4\pi r}\left[\sqrt{\frac{2\pi i}{-ka' \sin\theta}}\; e^{ika' \sin\theta}\,\vec{G}(0) + \sqrt{\frac{2\pi i}{ka' \sin\theta}}\; e^{-ika' \sin\theta}\,\vec{G}(\pi)\right] \tag{34}$$

$$= \frac{e^{ikr}}{4\pi r}\sqrt{\frac{2\pi a \sin\gamma}{k \sin\theta}}\left[e^{[ika \sin\theta \sin\gamma - i\pi/4]}\,\vec{G}(0) + e^{[-ika \sin\theta \sin\gamma + i\pi/4]}\,\vec{G}(\pi)\right],$$

where

$$\vec{G}(\beta) = \left(1 - \frac{1}{\cos\alpha}\right)(\vec{E}^{inc} \cdot \vec{\beta})\,\vec{\beta} - \left(1 + \frac{1}{\cos\alpha}\right)(\vec{E}^{inc} \times \vec{k}) \cdot \vec{\beta}(\vec{k} \times \vec{\beta}). \tag{35}$$

At $\beta = 0$, $\vec{\beta} = -\vec{i}_y$, $\cos\alpha = \sin(\theta - \gamma)$, and at $\beta = \pi$, $\vec{\beta} = \vec{i}_y$, $\cos\alpha = -\sin(\theta + \gamma)$. Further, if we designate the angle between the y-axis and the incident electric field, by ω_o, we may write,

$$\vec{E}^{inc} = \sin\omega_o \cos\theta\,\vec{i}_x + \cos\omega_o\,\vec{i}_y - \sin\omega_o \sin\theta\,\vec{i}_z.$$

Then,

$$\vec{G}(0) = \left(1 - \frac{1}{\sin(\theta - \gamma)}\right)\cos\omega_o\,\vec{i}_y - \left(1 + \frac{1}{\sin(\theta - \gamma)}\right)\sin\omega_o(\cos\theta\,\vec{i}_x - \sin\theta\,\vec{i}_z),$$

and,

$$\vec{G}(\pi) = \left(1 + \frac{1}{\sin(\theta + \gamma)}\right)\cos\omega_o\,\vec{i}_y - \left(1 - \frac{1}{\sin(\theta + \gamma)}\right)\sin\omega_o(\cos\theta\,\vec{i}_x - \sin\theta\,\vec{i}_z).$$

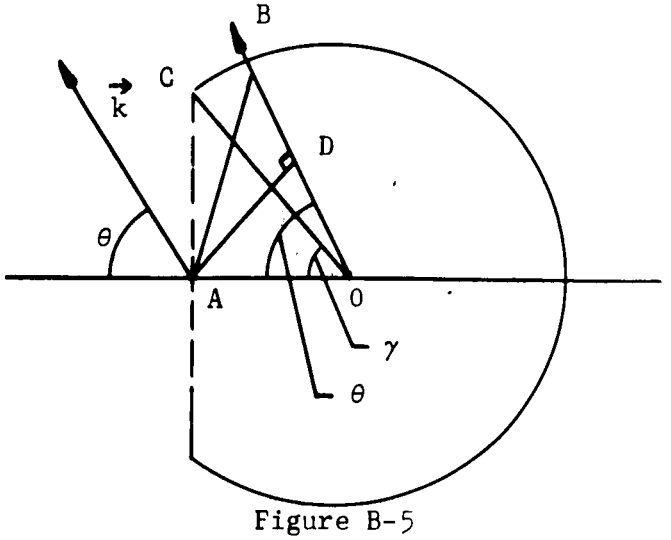

Figure B-5
Balloon Cross Section Showing Off-Axis Incidence

When $\theta > \gamma$, there will be a specular reflection from the sphere at the point whose radius vector is parallel to $\vec{k}$. This radius vector makes an angle θ with the z-axis. Reference to Figure B-5 shows that the projection on the propagation vector of the distance AB from the specular point to the center of the rim is,

$$\begin{aligned} BD &= OB - OD = a - OA \cos\theta \\ &= a - OC \cos\gamma \cos\theta \\ &= a\,(1 - \cos\gamma \cos\theta) \quad . \end{aligned}$$

Thus, for $\theta > \gamma$, the field scattered from both the hole and the sphere is,

$$\vec{E}^s = \frac{-a}{2r}\, e^{ikr}\, e^{i2ka\,(1 - \cos\gamma\cos\theta)}\, \vec{E}_{inc} + \vec{E}^{diff}_{rim} \quad .$$

If $\theta < \gamma$, no specular return from the outside of the sphere is possible. However, there will be a specular return from the point on the back of the sphere whose normal makes an angle θ with the z_1 axis. The projection of the propagation vector of the distance between the center of the hole and the specular point is,

$$a\,(1 + \cos\gamma\cos\theta) \quad ,$$

so that the field in this case is,

$$\vec{E}^s = \frac{-a}{2r}\, e^{ikr}\, e^{i2a\,(1 + \cos\gamma\cos\theta)}\, \vec{E}_{inc} + \vec{E}^{diff}_{rim} \quad .$$

Written out in full detail, the components of the scattered field are,

$$E^s_x = \frac{-e^{ikr}}{r}\, |\vec{E}_{inc}|\, \sin\omega_o \cos\theta \left\{ \frac{a}{2}\, e^{i2ka\,(1 \pm \cos\gamma\cos\theta)} \right.$$

$$+ \frac{1}{4\pi} \sqrt{\frac{2\pi a \sin\gamma}{k \sin\theta}}\, \left[\left(1 - \frac{1}{\sin(\gamma - \theta)}\right) e^{ika \sin\gamma \sin\theta - i\pi/4} \right.$$

$$\left. \left. + \left(1 - \frac{1}{\sin(\gamma + \theta)}\right) e^{-ika \sin\gamma \sin\theta + i\pi/4} \right] \right\}$$

$$E^s_y = \frac{e^{ikr}}{r}\, |\vec{E}_{inc}|\, \cos\omega_o \left\{ -\frac{a}{2}\, e^{i2ka\,(1 \pm \cos\gamma\cos\theta)} \right. +$$

$$+ \frac{1}{4\pi} \sqrt{\frac{2\pi a \sin\gamma}{k \sin\theta}} \left[\left(1 + \frac{1}{\sin(\gamma - \theta)}\right) e^{ika \sin\gamma \sin\theta - i\pi/4} \right.$$

$$\left. + \left(1 + \frac{1}{\sin(\gamma + \theta)}\right) e^{-ika \sin\gamma \sin\theta + i\pi/4} \right] \Bigg\} \quad ,$$

and

$$E_z^s = \frac{e^{ikr}}{r} \left| \vec{E}_{inc} \right| \sin\omega_o \sin\theta \left\{ \frac{a}{2} e^{i2ka(1 \pm \cos\gamma \cos\theta)} \right.$$

$$+ \frac{1}{4\pi} \sqrt{\frac{2\pi a \sin\gamma}{k \sin\theta}} \left[\left(1 + \frac{1}{\sin(\gamma - \theta)}\right) e^{ika \sin\gamma \sin\theta - i\pi/4} \right.$$

$$\left. \left. + \left(1 - \frac{1}{\sin(\gamma + \theta)}\right) e^{-ika \sin\gamma \sin\theta + i\pi/4} \right] \right\} \quad ,$$

where the - sign applies for $\theta > \gamma$ and the + sign applies for $\theta < \gamma$.

We note that each of these expressions contains a term independent of frequency, and a term proportional to $\frac{1}{\sqrt{k}}$. At radar frequencies the former term will dominate. Hence, no phase interference would occur off axis, and as a result we find that a smooth circular hole would give rise to no fading except at axial incidence.

B.3 Scattering from a Conducting Spherical Shell with a Jagged Hole

The above considerations deal with the radar return from a perfectly circular hole in a sphere. In real life, a puncture in the ECHO II balloon would undoubtedly have a somewhat jagged periphery, and it is of interest to determine how this jaggedness might modify the return.

In the material presented below, a jagged hole is studied using (1) a half-plane model, and (2) a wire model. The half-plane model has somewhat higher fidelity, while the wire model is much easier for computational purposes. The main shortcoming of the wire model is its failure to predict the behavior of the cross polarized component. This is the minor component at and near axial incidence.

B.3.1 Half-Plane Model

We now consider the case where the rim of the hole is jagged, that is, comprised of a number of line segments of different lengths and different orientations. It is required that the segments which compose the rim join

continuously, although the tangent to the rim may be discontinuous. We may write down an expression for the diffracted field which is a slight generalization of Equation (33),

$$\vec{E}_{diff} = \frac{e^{ikr}}{4\pi r} \int e^{i\vec{k} \cdot \vec{\rho}(\beta)} \left\{ \left(1 - \frac{1}{\cos \alpha}\right) \left(\vec{E}_{inc} \cdot \vec{\beta}_o\right) \vec{\beta}_o \right.$$

$$\left. - \left(1 + \frac{1}{\cos \alpha}\right) \left(\vec{E}_{inc} \wedge \vec{k} \cdot \vec{\beta}_o\right) \vec{k} \wedge \vec{\beta}_o \right\} \frac{\partial L}{\partial \beta} \, d\beta \quad ,$$

where β is a parameter specifying the position on the rim. In view of our model for the rim we see that there is a physical optics type contribution from the places where the segments join together, and so we have,

$$E_{diff} = \frac{e^{ikr}}{4\pi r} \sum_{n=1}^{N} \int e^{i\vec{k} \cdot \vec{\rho}_n} \frac{\partial L}{\partial \beta_n} \, d\beta_n$$

$$\left\{ \left(1 - \frac{1}{\cos \alpha}\right) \left(\vec{E}_{inc} \cdot \vec{\beta}_{o_n}\right) \vec{\beta}_{o_n} - \left(1 + \frac{1}{\cos \alpha}\right) \left(\vec{E}_{inc} \wedge \vec{k} \cdot \vec{\beta}_{o_n}\right) \vec{k} \wedge \vec{\beta}_{o_n} \right\},$$

where the sum goes over the N line segments, with β_{on} being the projection of the tangent vector of the nth segment on the plane perpendicular to $\vec{k}$. $\vec{\rho}(\beta)$ is a vector from the origin to the point on the rim specified by the value of the parameter β.

The curve specifying the rim is comprised of a number of straight line segments, which in general will not lie in a plane, and hence, scattering will occur as from an array of randomly oriented line segments. We may place an upper bound on the magnitude of such scattering as follows. The major contribution to the sum will be from the line segments from which specular return is possible, that is, those segments in the sum where the phase is stationary.*

For the case of backscattering, the specular segments will be those whose edges lie in a plane perpendicular to the wave vector $\vec{k}$. Since the problem is to determine how large a scattered field the rim can produce, we may consider the case where the entire rim lies in a plane perpendicular to $\vec{k}$. In this case, the line

* A generalization of the stationary phase technique for approximating the sum is not possible, since the second and all higher derivatives of the phase with respect to the parameter β vanish.

segments scatter in phase. Since for the specular case $e^{ik\cdot\rho} = 1$, we may perform the β integration and write the diffracted field as,

$$E_{diff} = \frac{e^{ikr}}{4\pi r} \sum_{n=1}^{N} \left\{ \left(1 - \frac{1}{\cos\alpha}\right) A_n \vec{\beta}_{n_o} - \left(1 + \frac{1}{\cos\alpha}\right) B_n \vec{k} \wedge \vec{\beta}_o \right\} \ell_n,$$

where $A_n = (\vec{E}_{inc} \cdot \vec{\beta}_{o_n})$,

$B_n = (\vec{E}_{inc} \wedge \vec{k}) \cdot \vec{\beta}_{o_n}$,

ℓ_n = the length of the nth segment so that $\sum_{n=1}^{N} \ell_n = L$, the perimeter of the hole.

We may now easily bound the magnitude of this field:

$$\left|\vec{E}_{diff}\right| \leq \left|\frac{e^{ikr}}{4\pi r}\right| \sum_{n=1}^{N} \left\{ \left|1 - \frac{1}{\cos\alpha}\right| \left|A_n\right| + \left|1 + \frac{1}{\cos\alpha}\right| \left|B_n\right| \right\} \ell_n,$$

but since $\left|A_n\right| \leq \left|\vec{E}_{inc}\right|$, $\left|B_n\right| \leq \left|\vec{E}_{inc}\right|$,

$$\left|\vec{E}_{diff}\right| \leq \frac{1}{4\pi r} \left|\vec{E}_{inc}\right| \frac{2}{\cos\alpha} \sum_{n=1}^{N} \ell_n = \frac{2L \left|\vec{E}_{inc}\right|}{4\pi r \cos\alpha} .$$

We have tacitly assumed the angle α which the incident radiation makes with the tangent plane of the rim is constant; that is,we have replaced cos α by an average value, which we may take to be equal to the cos α = sin δ of the circular hole of Parts B.2 and B.3.

We found that the field diffracted from the rim of a circular hole for nose-on incidence is (Equation 23),

$$\vec{E}_{diff} = \frac{e^{ikr}}{2r \cos\alpha} \vec{E}_{inc} .$$

For purposes of comparison, we may write the magnitude of this field as (since $L = 2\pi a'$),

$$\vec{E}_{diff} = \frac{L \vec{E}_{inc}}{4\pi r \cos\alpha} .$$

Thus, we see that the field diffracted by a jagged rim can be no greater than the field diffracted by an equivalent circular rim of perimeter 2L (radius a = L/π).

In general, only some of the line segments will lie in a plane of constant phase. However, these may be expected to dominate the return. The field scattered from these specular segments is,

$$\vec{E}_{diff} = \frac{e^{ikr}}{4\pi r} \sum_{n=1}^{N'} \left\{ \left(1 - \frac{1}{\cos\alpha}\right) A_n \vec{\beta}_n - \left(1 + \frac{1}{\cos\alpha}\right) B_n \vec{k} \wedge \vec{\beta}_n \right\} \ell_n \ .$$

The magnitude of this field may be estimated just as before with the result that the perimeter L is replaced by L', the sum of the lengths of the dominant scatterers.

It is instructive to write out the explicit form of the field scattered from one such dominant scatterer.

Let $\vec{E}_{inc} = \cos\theta\ \vec{\beta} + \sin\theta\ (\vec{k} \wedge \beta)$,

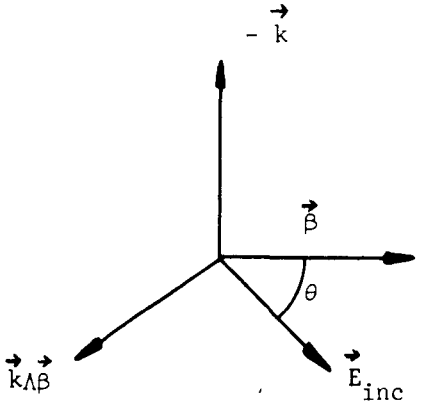

Figure B-6

$$\vec{E}_{diff} = \frac{\ell e^{ikr}}{4\pi r} \left\{ \left(1 - \frac{1}{\cos\alpha}\right) \cos\theta\ \vec{\beta} - \left(1 + \frac{1}{\cos\alpha}\right) \sin\theta\ (\vec{k} \wedge \vec{\beta}) \right\} \ .$$

Such a segment gives rise to a cross section,

$$\sigma = \frac{\ell^2}{4\pi} \left\{ \left(1 - \frac{1}{\cos\alpha}\right)^2 \cos^2\theta + \left(1 + \frac{1}{\cos\alpha}\right)^2 \sin^2\theta \right\} \quad .$$

When we average over polarizations, we obtain,

$$\bar{\sigma} = \frac{1}{2\pi} \int_0^{2\pi} \sigma(\theta)\, d\theta$$

$$= \frac{\ell^2}{4\pi} \left\{ 1 + \frac{1}{\cos^2\alpha} \right\}$$

Often, an effective cross section is defined for which the component of the diffracted field colinear with the antenna polarization is favored. In our case, the effective cross section is,

$$\sigma_e = \frac{8}{3} \frac{\ell^2}{4\pi} \left\{ \left(1 - \frac{1}{\cos\alpha}\right)^2 \cos^4\theta - \left(1 + \frac{1}{\cos\alpha}\right)^2 \sin^4\theta \right\} \quad .$$

B.3.2 Average Over Edge Segment Orientation

We may compute an average dominant field due to the edge segments in the plane of constant phase, by averaging over all orientations of the line segments in this plane.

Writing the dominant field as,

$$E_{diff} = \frac{e^{ikr}}{4\pi r} \sum_{n=1}^{N'} \left\{ A'_n \vec{\beta}_n - B'_n \vec{k} \wedge \vec{\beta}_n \right\} l_n \quad ,$$

where

$$A'_n = (\vec{E}_{inc} \cdot \vec{\beta}_n) \left(1 + \frac{1}{\cos\alpha}\right) \quad ,$$

$$B'_n = (\vec{E}_{inc} \wedge \vec{k} \cdot \vec{\beta}_n) \left(1 - \frac{1}{\cos\alpha}\right) \quad ,$$

then $(4\pi r)^2 \ (E_{diff})^2$ is the double sum,

$$\sum_{m,n} \Big\{ A'_n \, A'_m \, \vec{\beta}_n \cdot \vec{\beta}_m - A'_n \, B'_m \, \vec{\beta}_n \cdot \vec{k} \wedge \vec{\beta}_m$$

$$- B'_n \, A'_m \, \vec{k} \wedge \vec{\beta}_n \cdot \vec{\beta}_m + B'_n \, B'_m \, \vec{k} \wedge \vec{\beta}_n \cdot \vec{k} \wedge \vec{\beta}_m \Big\} \cdot e^{2ikr} \, \ell_m \, \ell_n \, .$$

A general term in this double sum will look like,

$$\left\{ C_1 \cos\theta \, \vec{\beta}_m - C_2 \sin\theta \, (\vec{k} \wedge \vec{\beta}_m) \right\} \quad \ell_m \, | E_{inc} |$$

$$\cdot \left\{ C_1 \cos(\theta + \delta) \, \vec{\beta}_n - C_2 \sin(\theta + \delta) \, \vec{k} \wedge \vec{\beta}_n \right\} \quad \ell_n \, | E_{inc} |,$$

where

$$C_1 = 1 + \frac{1}{\cos\alpha} \, ,$$

$$C_2 = 1 - \frac{1}{\cos\alpha} \, ,$$

and δ is the angle between the two segments.

Then since,

$$\vec{\beta}_m \cdot \vec{\beta}_n = \cos\delta,$$

$$\vec{k} \wedge \vec{\beta}_m \cdot \vec{\beta}_n = \sin\delta,$$

$$\vec{k} \wedge \vec{\beta}_n \cdot \vec{\beta}_m = - \sin\delta,$$

$$\vec{k} \wedge \vec{\beta}_n \cdot \vec{k} \wedge \vec{\beta}_n = \cos\delta.$$

We find after expanding $\cos(\theta + \delta)$ and $\sin(\theta + \delta)$, that the product reduces to

$$\cos\theta \, \sin\theta \, \sin\delta \, \cos\delta \, (C_2^2 - C_1^2) + \cos^2\delta \, (C_1^2 \cos^2\theta + C_2^2 \sin^2\theta)$$

$$+ C_1 \, C_2 \, \sin^2\delta.$$

A number of averaging processes are available. First, we may average over the antenna polarization angle θ. This yields the result,

$$\frac{1}{2}\ (C_1^2 + C_2^2)\ \cos^2\delta + C_1\ C_2\ \sin^2\delta.$$

Next we may average over the mutual orientations of the segments by considering the angle δ to be a continuous variable and integrating from 0 to 2π. This gives,

$$\frac{1}{4}\ (C_1^2 + C_2^2) + \frac{1}{2}\ C_1\ C_2 = \frac{1}{4}\ (C_1 + C_2)^2 = 1.$$

thus the gross behavior of the diffraction from the rim is determined by the length of the edge segments,

$$\left|\overline{E_{diff}}\right|^2 = \frac{\left|E_{inc}\right|^2}{(4\pi r)^2} \sum_{n,m} \ell_n\ \ell_m.$$

If we assume that the lengths of the edge segments obey a Rayleigh distribution,

$$\rho\ (l) = \frac{2\ell N}{\langle \ell^2 \rangle}\ \exp\left\{\frac{-\ell^2}{\langle \ell^2 \rangle}\right\} \qquad \ell > 0,$$

then we may replace the double sum by the double integral,

$$\frac{4N^2}{\langle \ell^2 \rangle^2} \iint_{x,y\ \ o} x^2\ y^2\ \exp\left\{\frac{x^2 + y^2}{\langle \ell^2 \rangle}\right\}\ dxdy.$$

Changing to polar coordinates we have,

$$\frac{4N^2}{\langle \ell^2 \rangle} \int_0^{\pi/2} \int_0^{\infty} \rho^5\ \cos^2\phi\ \sin^2\phi\ e^{-\rho^2/\langle \ell^2 \rangle}\ d\rho d\phi$$

$$= \frac{N^2}{4\langle \ell^2 \rangle^2}\ \pi \int_0^{\infty} \rho^5\ e^{-\rho^2/\langle \ell^2 \rangle}\ d\rho = \frac{N^2\pi}{4}\ \langle \ell^2 \rangle.$$

Thus, the cross section, averaged over antenna polarization, segment orientation and segment length is,

$$\sigma = \frac{1}{16} \quad N^2 \quad \langle \ell^2 \rangle .$$

As might be expected, it is a function of the number of segments N, and the mean squared length of each segment, $\langle \ell^2 \rangle$.

B.3.3 Wire Model

In a sphere with an almost circular jagged hole, we assume that the hole consists of straight edges which scatter like a collection of wires. This section considers two cases: wires which are long with respect to wavelength, and wires which are short with respect to wavelength.

For the long wire case, Chu's result (Ref. 4) is used as the starting point of the analysis.

$$\sigma = \frac{4 \pi \ell^2 \sin^2 \theta \ (\frac{\sin x}{x})^2}{(\frac{\pi}{2})^2 + (\ell n \ \lambda/\gamma \pi \ a \sin\theta)^2} ,$$

where

2ℓ = length of wire,

θ = angle between direction of incidence and wire,

ϕ = angle between incident electric field and plane, formed by wire and incident direction.

$$x = \frac{2\pi \ell^2}{\lambda} \cos\theta .$$

It is usual to simplify this formula by letting $\lambda/a = 85$ and $\sin\theta \approx 1$. These are justified by the relative insensitivity of σ to a (see Reference 1, page 47), and by the physical properties of the hole we are considering. This simplification makes the denominator π^2, so that,

$$\sigma = \frac{4}{\pi} \ \ell^2 \ \sin^2\theta \ (\frac{\sin x}{x})^2 \ \cos^4\phi .$$

We are interested in backscattering when the direction of incidence is perpendicular to the plane of the circle which most closely fits the hole. As a

first simplification, we can assume that all the edges of the hole lie in the plane of this circle. Since incidence is normal, in this case, all the scattering will add in phase, and the total cross section from N contributors, each with cross section σ_i, will be

$$\sigma = \left[\sum_{i=1}^{N} \sqrt{\sigma_i} \right]^2 .$$

Each σ_i will be of the form,

$$\sigma_i = \frac{4}{\pi} \ell_i^2 \cos^4 \phi_i ,$$

since $\theta = 90^\circ$ for all contributors.

Since the edges may be assumed to be arranged in a somewhat random manner, we will compute the sum by averaging, over all possible values, the contribution from each one. The angle ϕ_i is allowed to range over 0 to 2π, and the length from L_1 to L_2. Then

$$\sigma = \left[\frac{2}{\sqrt{\pi}} \sum_{i=1}^{N} \ell_i \cos^2 \phi_i \right]^2$$

$$= \frac{2}{\sqrt{\pi}} N \langle \ell \rangle \langle \cos^2 \phi \rangle ,$$

where the notation $\langle \ \rangle$ implies average value.

$$\langle \cos^2 \phi \rangle = \frac{1}{2\pi} \int_0^{2\pi} \cos^2 \phi \, d\phi = \frac{1}{2} ,$$

$$\langle \ell \rangle = \frac{1}{2} \left(\frac{1}{L_2 - L_1} \right) \int_{L_1}^{L_2} \ell \, d\ell = \frac{1}{4} (L_1 + L_2) ,$$

and

$$\sigma = \left[\frac{2}{\sqrt{\pi}} \; N \; \langle \ell \rangle \; \frac{1}{2} \right]^2 = \frac{N^2 \langle \ell \rangle^2}{\pi} \quad .$$

Letting $L = 2 \langle \ell \rangle$, be the average length of edge, we may relate L and N through a jaggedness factor c, which is the ratio of the perimeter of the torn

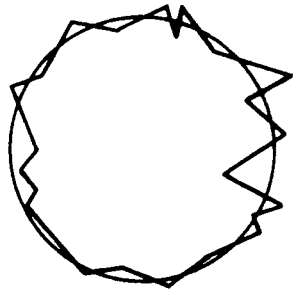

Figure B-7

hole to the circumference of the associated circle. This factor is always greater than one, and may reasonably be assumed to be between 1.2 and 2.

Using $c = \frac{N L}{2\pi R}$, we can now write,

$$\sigma = \frac{N^2 \langle \ell \rangle^2}{\pi} = \frac{4 N^2 L^2}{\pi} = \frac{4}{\pi} \; [2\pi \; Rc]^2 = 16\pi \; R^2 \; c^2.$$

We can show that this is smaller than πa^2, cross section of the smooth hole (Section B.2), whenever $c < \frac{a}{4R}$. For the particular sphere in which we are interested, $a = \frac{135}{2}$ feet, R = 10 ft. and $\frac{a}{4R} = 1.7$.

In the case that the edges of the hole do not all lie in a plane, but are nevertheless, arranged so that there is a most closely fitting circle, we consider backscattering in a direction normal to the plane of this circle. We use a long wire approximation, as in the previous case, where individual contributions will not add in phase. We use random phase addition, whereby,

$$\sigma = \sum_{i=1}^{N} \sigma_i \ ,$$

and

$$\sigma_i = \frac{4}{\pi} \ell_i^2 \sin^2 \theta_i \left(\frac{\sin x_i}{x_i} \right)^2 \cos^4 \phi_i .$$

In this case, it is necessary to average over θ_i and x_i as well as over ℓ_i and ϕ_i. We assume that the θ_i will take on, with equal likelihood, values between $\pi/2$ and α, where α is the angle between the direction of incidence and the tangent to the sphere perpendicular to the rim of the associated circular hole. (See Figure B-8).

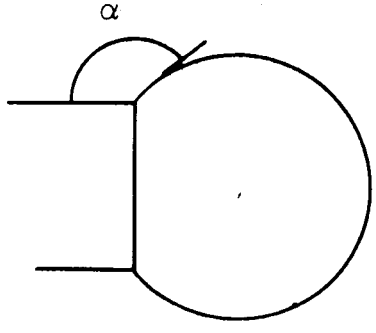

Figure B-8

Then we let,

$$\theta_i = \frac{\pi}{2} + \frac{(\alpha - \pi/2)\, i}{N} ,$$

and

$$x_i = \frac{4\pi \ell_i}{\lambda} \cos\theta_i = \frac{4\pi \ell_i}{\lambda} \sin(\pi/2 - \alpha)\, i ,$$

for $i = 0, 1, \ldots, N-1$.

The factor $\left(\frac{\sin x_i}{x_i}\right)^2$ appearing in the expression for σ is shown graphically in Figure B-9. Since the decrease in the maximum of this function between the first and second lobe is 15 db, we shall consider negligible any contributions which come from other than the first lobe, and then,

$$\sigma = \sum_{L=1}^{N_1} \sigma_i ,$$

where N_1 is the number of terms for which $x_i < 3.14$ radians.

Averaging, as before, over ϕ_i and ℓ_i, we obtain,

$$\langle \cos^4 \phi_i \rangle = \frac{3}{8} ,$$

$$\langle \ell^2 \rangle = \frac{L_2^3 - L_1^3}{3(L_2 - L_1)} .$$

If we assume that $L_2 - L_1 << L_1$,

$$\langle \ell^2 \rangle \approx \left(\frac{L_1 + L_2}{2}\right)^2 = L^2.$$

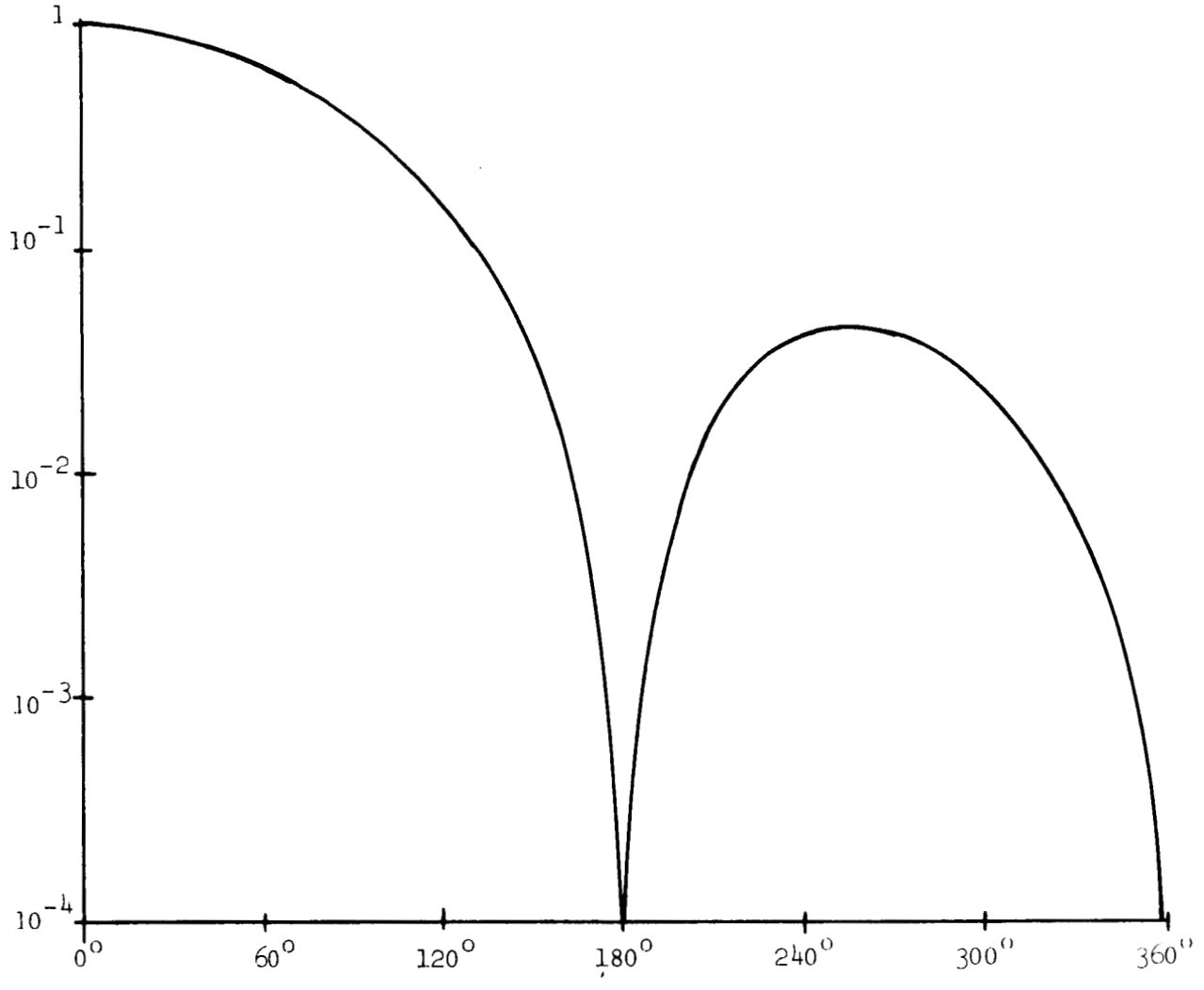

Figure B-9

Then,

$$\langle \sigma_i \rangle = \frac{3}{2\pi} \sin^2 \theta_i \left(\frac{\sin x_i}{x_i} \right)^2 L^2 ,$$

and,

$$\sigma = \frac{3}{2\pi} L^2 \sum_{i=1}^{N_1} \sin^2 \theta_i \left(\frac{\sin x_i}{x_i} \right)^2 \leq \frac{3}{2\pi} L^2 N_1 \leq \frac{3}{2\pi} L^2 N \leq \frac{3}{2\pi} L^2 N^2$$

$$= \frac{3}{2\pi} (2\pi R c)^2 = 6 \pi R^2 c^2 .$$

As before, the condition that the cross section of the jagged hole be less than that of the smooth hole can be reduced to an inequality on c. In this case c must be less than 2.75, which is assured by the earlier assumption that $1.2 \leq c \leq 2$.

For short wires, where wire length to wavelength ratio is less than .8, we can use the result of J. Weber (Reference 5). When modified for backscattering, the cross section of a single wire is,

$$\sigma = \frac{240}{\pi} \left(\frac{\lambda \cos \psi}{Z_{in}} \right)^2 \left[\frac{1}{\sin K\ell \sin\theta} \right]^2 \left[\frac{\cos (K\ell \cos\theta)}{\sin^2 \theta} \right.$$

$$(\sin K\ell \cos (K\ell \cos\theta) - \cos \theta \cos K\ell \sin (K\ell \cos \theta))$$

$$\left. - \frac{\cos K\ell}{2} \left(\frac{\sin (2K\ell \cos\theta)}{2 \cos\theta} + K\ell \right) \right]^2 ,$$

which for $\theta = \pi/2$ becomes,

$$\sigma = \frac{240}{\pi} \left(\frac{\lambda \cos \psi}{Z_{in}} \right)^2 (1 - K\ell \cot K\ell)^2 ,$$

where,

ℓ - is the half length of the wire,

Z_{in} - is the input impedance of the wire, for which the value 7.10^2 was used (Reference 6),

ψ - is the angle between the incident field and the wire axis.

For the same range of θ as described in the long wire case,

$$\frac{\sigma}{\lambda^2} < 1,$$

whenever $2\ell/\lambda < 1$. Thus a maximum is attained only around $\frac{2\ell}{\lambda} = .5$ and elsewhere,

$$\frac{\sigma}{\lambda^2} \leq .2.$$

Assuming N small wires, each with this cross section, added in random phase, we get for the cross section of the hole consisting of these wires,

$$\sigma \leq N \lambda^2 ,$$

in the very worst case in which all the wires are one half wavelength.

Here again, as in the long wire case, the cross section can be shown to be less than that of the smooth hole, which is πa^2, and

$$N\lambda^2 = \frac{2\pi R c}{L} \lambda^2 = 2\pi Rc \frac{\lambda}{L} \lambda = \frac{\pi R c}{\frac{L}{2\lambda}} \lambda = \frac{\pi R c}{\left(\frac{\ell}{\lambda}\right)} \lambda$$

$$< \frac{\pi R c}{.1} \lambda < 600 \pi \lambda .$$

Since $a = 135$, $600\pi\lambda < \pi a^2$ whenever $\lambda < \frac{a^2}{600} = 304$ ft.

SUMMARY OF APPENDIX

Appendix B examines the hypothesis that fading observed in the radar return from the ECHO II balloon is caused by a hole punched in its surface. Hence, the radar cross sections of a spherical metal shell with an exactly circular hole, and a spherical shell with a jagged, roughly circular hole, are examined in detail to determine if they could cause a "drop-out" as observed in the cross section records.

The conclusions of this study are summarized as follows:

1. For orientations such that the a line from the radar to the balloon center does not intercept the hole, the normal sphere return ($\sigma = \pi a^2$) should be recorded.
2. For orientations where this line intercepts the hole, the contribution from the back wall of the shell dominates, unless the line lies along the centerline of the hole. In that case the diffracted field from the edge of the hole becomes comparable to the return from the back wall.
3. Thus, when viewed along the axis of the hole, the balloon radar return may drop, if dimensions are such that destructive interference occurs between specular and edge-diffracted contributions. This is very unlikely because of the dimensional precision required. Furthermore, even if it occurred, the signal drop would be of very short duration.
4. If the edges of the hole are jagged, the level of the edge-diffracted return is still lower, making fading even less likely.
5. In conclusion, if the balloon maintains its nominal spherical shape but has a hole punched in it, it is quite unlikely that such a hole will give rise to regular fading of the radar return.

APPENDIX C

SOMMERFELD EDGE DIFFRACTION

In this appendix, we give the applicable scattered fields from the diffraction of a straight edge as derived by Sommerfeld*. Figure C-1 gives a drawing of the half plane and the coordinates. ϕ and α are measured with respect to the surface and are the field angle and angle of incidence respectively. The region of interest to us is divided into two regions; region I where there exists both an incident and reflected wave along with the diffracted wave and region II where there exists just the incident and diffracted wave. The line C_i represents the dividing line between these regions. Special consideration must be given to the field along this line.

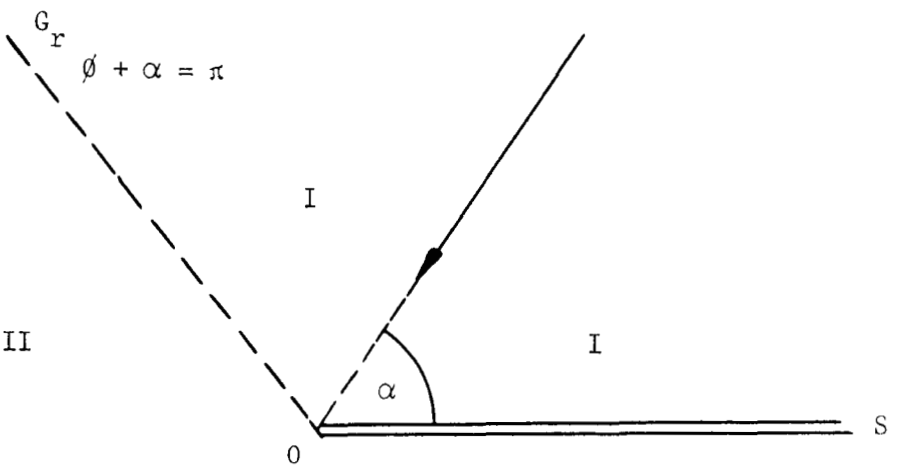

Figure C-1

The sommerfeld solution is basically a scalar solution, but can be interpreted as a vector solution when the electric or magnetic field is parallel to the edge. The total field is given by,

$$U = U(r, \phi - \alpha) \pm U(r, \phi + \alpha), \qquad \text{(C-1)}$$

---

* Sommerfeld, A.,"Optics, Lectures on Theoretical Physics", Vol. IV.

where the upper sign refers to the case where the electric field is parallel to the edge and the lower sign corresponds to the magnetic field being parallel to the edge. With Sommerfeld we define,

$$\begin{aligned} \psi_a &= \phi - \alpha, \\ \psi_b &= \phi + \alpha, \\ \rho_a &= 2\sqrt{\frac{kr}{\pi}} \cos \psi_a/2, \\ \rho_b &= 2\sqrt{\frac{kr}{\pi}} \cos \psi_b/2. \end{aligned} \tag{C-2}$$

Thus, we are interested in the value of the function $U(r,\psi)$ in the various regions. This function is a contour integral. Asymptotic solutions for it are available and it is these that we shall use. In addition, we will specialize immediately to the case of interest, namely, backscattering. Now, $\phi = \alpha$ so,

$$\begin{aligned} \psi_a &= 0, \\ \psi_b &= 2\alpha, \\ \rho_a &= 2\sqrt{\frac{kr}{\pi}}, \\ \rho_b &= 2\sqrt{\frac{kr}{\pi}} \cos \alpha. \end{aligned} \tag{C-3}$$

The line G_r now corresponds to $\alpha = \pi/2$. In addition, we are concerned only with the far field where $kr \gg 1$.

In <u>region I</u>, $\alpha < \frac{\pi}{2}$ and ρ_a and ρ_b are both positive. Thus, we want solution b of Sommerfeld, namely,

$$U = U_o - \frac{e^{i(kr + \pi/4)}}{2\sqrt{2\pi\, kr}\cos \psi/2} + \ldots. \tag{C-4}$$

where $U_o = e^{-ikr\cos\psi}$. Thus the total field is,

$$U = e^{-ikr} \mp e^{-ikr\cos 2\alpha} - \frac{e^{i(kr + \pi/4)}}{2\sqrt{2\pi\, kr}} \left[1 \mp \frac{1}{\cos\alpha}\right]. \quad (C\text{-}5)$$

Near the line $\alpha = \frac{\pi}{2}$, the quantity ρ_a is still $\gg 1$, but the quantity ρ_b approaches zero. For the first term since ρ is large and positive, we have,

$$U(r,0) = e^{-ikr} - \frac{e^{i(kr + \pi/4)}}{2\sqrt{2\pi\, kr}}, \quad (C\text{-}6)$$

and for the second term we define $\alpha = \pi/2 - \delta$ where δ is very small. Thus, $\cos 2\alpha \tilde{\sim} -1$ and $\cos\alpha \tilde{\sim} \sin\delta$, so

$$U\ (r,\ 2(\tfrac{\pi}{2} - \delta)) = \frac{e^{-ikr}}{2}\left\{1 + (1-i)\,2\sqrt{\frac{kr}{\pi}}\sin\delta + \ldots\right\}, \quad (C\text{-}7)$$

and the total field is,

$$U = e^{-ikr} \mp \frac{e^{+ikr}}{2} - \frac{e^{i(kr + \pi/4)}}{2\sqrt{2\pi\, kr}} \mp e^{-ikr}\,(1-i)\sqrt{\frac{kr}{\pi}}\sin\delta. \quad (c\text{-}8)$$

In <u>region II</u>, the parameters are,

$$\alpha > \pi/2,$$

$$\rho_a = 2\sqrt{\frac{kr}{\pi}},$$

$$\rho_b = 2\sqrt{\frac{kr}{\pi}}\cos\alpha < 0,$$

$$U(r,0) = e^{-ikr} - \frac{e^{i(kr + \pi/4)}}{2\sqrt{2\pi\, kr}},$$

$$U(r,2\alpha) = \frac{1}{2\sqrt{2\pi\, kr}\cos\alpha}\, e^{i(kr + \pi/4)},$$

and the total field is given by,

$$U = e^{-ikr} - \frac{e^{i(kr + \pi/4)}}{2\sqrt{2\pi\, kr}} \left[1 \pm \frac{1}{\cos\alpha}\right] .$$

REFERENCES FOR

APPENDICES B AND C

1. Crispin, Jr., J. W., Goodrich, R. F., and Siegel, K. M., "A Theoretical Method for the Calculation of the Radar Cross Section of Aircraft and Missiles", The University of Michigan Radiation Laboratory, Report No. 2591-1-H.

2. Sommerfeld, A., "Optics, Lectures on Theoretical Physics," Vol. IV.

3. D. M. Raybin,"Electromagnetic Scattering Waves by a Finite Plasma", CTPC-1-1520-010-F, 30 December 1963. UNCL.

4. J. H. Van Vleck, F. Bloch, and M. Hamermesh, "Theory of Radar Reflection from Wires or Thin Metallic Strips", Journal of Applied Physics, Vol. 18, March 1947, pp. 274-291.

5. J. Weber, "Scattering of Electromagnetic Waves by Wire and Plates", Proceedings of the IRE, Jan. 1955, pp. 82-89.

6. S. A. Schelkunoff,"Advanced Antenna Theory", John Wiley and Sons, 1952.